

Electronic Thesis and Dissertation Repository

2-24-2023 2:30 PM

Simplified Modeling of Bonded Prestressed High Strength Concrete Girders during Fire Exposure

Yi Mao, *The University of Western Ontario*

Supervisor: Youssef, Maged, *The University of Western Ontario*

A thesis submitted in partial fulfillment of the requirements for the Master of Engineering Science degree in Civil and Environmental Engineering

© Yi Mao 2023

Follow this and additional works at: <https://ir.lib.uwo.ca/etd>



Part of the [Structural Engineering Commons](#)

Recommended Citation

Mao, Yi, "Simplified Modeling of Bonded Prestressed High Strength Concrete Girders during Fire Exposure" (2023). *Electronic Thesis and Dissertation Repository*. 9141.
<https://ir.lib.uwo.ca/etd/9141>

This Dissertation/Thesis is brought to you for free and open access by Scholarship@Western. It has been accepted for inclusion in Electronic Thesis and Dissertation Repository by an authorized administrator of Scholarship@Western. For more information, please contact wlsadmin@uwo.ca.

Abstract

Engineers need design tools to overcome the complexities associated with structural analysis during fire exposure to evaluate the behaviour of structures exposed to fire and estimate their structural fire resistance. These complexities include the uneven distribution of temperature within the structural elements and the deterioration in material properties.

The current study introduces the first simplified numerical model to evaluate the flexural behaviour of bonded prestressed high-strength concrete (HSC) sections exposed to fire. The model starts by predicting the temperature distribution within a structural element using 2-D finite difference analysis. It then uses one-dimensional sectional analysis to estimate the section behaviour, which is based on force equilibrium and strain compatibility and accounts for concrete spalling and the changes in the material properties with the fire temperature. The numerical model is validated using experimental work by others.

The model is developed based on standard fire exposure. To generalize the model and make it valid for natural fire exposure, equations are developed to transfer any natural fire to a standard fire with an equivalent duration. The equivalent standard fire produces a similar internal temperature distribution within an HSC prestressed section as that by the natural fire. The equivalent duration analysis is the first to consider different cross-section shapes and account for the explosive spalling phenomenon.

A parametric study was then conducted on prestressed concrete sections of different shapes. For each section, the structural performance is evaluated in terms of the moment-curvature diagram. Simplified equations are then developed, using non-linear regression analysis, to estimate the moment-curvature diagram of the considered sections when they are exposed to a standard fire of a specific duration.

Keywords

High Strength Concrete, Prestressed Beams, Fire, Structural Performance, Numerical Model, Natural Fire, Equivalent Duration, Bridge Girders, Fire Resistance.

Summary for Lay Audience

Concrete as a construction material, is performing well on load bearing and fire resisting, but when a fire event lasts more than a few hours, high temperature would decompose part of concrete exposed to fire and the concrete would lose most of its strength. Structural engineers have responsibilities to design a concrete structure to withstand the fire long enough for people to escape and provide support for the rescue effort. A reliable method is using computer software to simulate the structure behavior under fire attack, so that engineers can estimate how much load a structure can support and how long the structure can survive when it is under fire exposure. This research is focusing on prestressed high strength concrete girder, which is normally used as a critical structural member for heavy loads and long span locations, how well it can resist fire is crucial for the fire safety of the whole structure system. This thesis provides a theoretical analysis for the prestressed concrete girder exposed to fire and provides a method with computer program to calculate the girder's behavior and capacity during fire incident. This research fills in some blanks of current structural analysis/design practice, and provides a tool to estimate the performance of prestress girders under fire exposure.

Co-Authorship Statement

All numerical and analytical work presented in this thesis was performed by Yi Mao. Work was reviewed by Dr. Maged Youssef and Dr. Salah El-Fitiany. Part of chapter 3 of this thesis has been submitted as a conference paper co-authored by Yi Mao, Maged A. Youssef, and Salah El-Fitiany. Two Journal papers based on the thesis are being drafted.

Acknowledgments

I would like to express my greatest gratitude to my advisor, Prof. Maged Youssef, Western University, for his continued support, encouragement, and guidance during the course of my studies. I would like to convey my sincere thanks for his encouragement and perseverance which made my graduate studies very rewarding.

I would like to thank Dr. Salah El-Fitiany, as he paved a solid foundation for my research and provided great assistance with the details of my work. I would like to thank Prof. Youssef's research team members, Robert Kuehnen, Malek Lazhari, and Amer Sabsabi. Their continuous help extended the boundary of my knowledge.

Additionally, I would like to thank all the faculty members and staff at the Civil and Environmental Engineering department at Western University for their help and support during the difficult pandemic period.

Table of Contents

Abstract	ii
Keywords	ii
Summary for Lay Audience	iii
Co-Authorship Statement.....	iv
Acknowledgments.....	v
Table of Contents	vi
List of Tables	ix
List of Figures	x
List of Abbreviations, Symbols, and Notations	xiii
Chapter 1 Introduction and Outline of the Thesis.....	1
1.1 Introduction	1
1.2 Research objective	2
1.3 Thesis Outline	2
1.3.1 Chapter 1: Introduction	2
1.3.2 Chapter 2: Literature Review.....	2
1.3.3 Chapter 3: Simplified Modeling of Prestressed Concrete Girders during Fire Exposure	2
1.3.4 Chapter 4: Equivalent standard Fire Duration for Prestressed Concrete Girders Exposed to Natural Fire	3
1.3.5 Chapter 5: Girder design parameters study.....	3
1.3.6 Chapter 6: Summary, Conclusions, and future research.....	3
1.4 Reference.....	4
Chapter 2 Literature Review	5
2.0 Introduction	5
2.1 Code Provisions on Structural Fire Resistance	5
2.2 Fire Temperature.....	6
2.2.1 Standard Fire.....	6
2.2.2 Natural Fire and Equivalent Design Fire	7
2.2.3 Concrete Thermal Properties	9
2.2.4 Concrete Surface Temperature	11

2.2.5 Temperature distribution.....	12
2.3 High-Strength Concrete Mechanical Properties Under Elevated Temperatures....	13
2.3.4 Strain at elevated temperatures	17
2.3.4 Compressive failure strain	19
2.3.5 Spalling of High-Strength Concrete under Fire	19
2.4 Reinforcing Steel Properties at Elevated Temperature	22
2.4.1 Strand Mechanical Properties	22
2.4.2 Properties of regular steel bars at elevated temperatures.....	23
2.5 Moment-curvature of prestressed Beam section	24
2.6 Conclusions	26
2.7 Reference.....	27
Chapter 3 Simplified Modeling of Prestressed Concrete Girders during Fire Exposure	30
3.0 Introduction	30
3.1 Modeling Approach	32
3.2 Transient Thermal Analysis	34
3.2.1 Thermal properties of HSC.....	34
3.2.2 Concrete surface temperature	34
3.2.3 Spalling of HSC in this numerical model	34
3.2.4 Heat transfer calculations.....	35
3.3 Mechanical Analysis	37
3.3.1 Material constitutive models.....	38
3.3.2 Shear capacity	44
3.3.3 Flexural behaviour	44
3.3.4 Stresses and Forces	47
3.3.5 Moment-curvature Relationship	49
3.4 Validation.....	51
3.5 Summary and Conclusions.....	55
3.6 Reference.....	56
Chapter 4: Equivalent standard Fire Duration for Prestressed Concrete Girders Exposed to	
Natural Fire	58
4.0 Abstract	58

4.1 Introduction	58
4.2 Natural Fire Curves	60
4.3 Thermal Gradient in a Concrete Section	62
4.4 Equivalent exposure time	62
4.5 Simplified equation for the time equivalence estimation.....	65
4.6 Influence of section size	67
4.7 Application of time equivalent method for non-rectangular sections.....	70
4.8 Summary and Conclusions.....	75
4.9 Reference.....	77
Chapter 5 Structural fire performance of HSC prestressed sections.....	79
5.1 Introduction	79
5.2 Parametric study.....	79
5.2.1 Influence of the concrete strength of the girder	81
5.2.2 Influence of concrete strength of the girder and the topping slab.....	82
5.2.3 Influence of section shape.....	84
5.2.4 Moment-curvature diagrams	85
5.3 Proposed expressions of the capacity adjustment factor.....	86
5.5 Summary and Conclusions.....	88
5.6 Reference.....	89
Chapter 6 Summary and Conclusions.....	90
6.1 Literature Review.....	90
6.2 Simplified Modeling of Prestressed Concrete Girders during Fire Exposure.....	90
6.3 Equivalent standard Fire Duration for Prestressed Concrete Girders Exposed to Natural Fire	91
6.4 Structural behaviour of prestressed HC sections exposed to fire.....	91
6.5 Limitations of this research.....	92
6.6 Recommendations for Future Work.....	92
Curriculum Vitae	93

List of Tables

Table 2.1 Reduction of strength at elevated temperature (EN 1992-1-2, 2002).....	14
Table 2.2 Parameters affect the HSC spalling	21
Table 3.1 Stress-strain data for HSC considering $f_{c20'}=75\text{MPa}$	42
Table 3.2 Stress-strain data for reinforcing steel considering $f_y= 400\text{ MPa}$	43
Table 4.1 Natural fire parameters for the considered cases	61
Table 4.2 Natural fire parameters for beam width evaluation	68
Table 5.1 Structural design of girder sections	80
Table 5.2 Parametric study layout	81
Table 5.3 Yield and ultimate moments of G1 considering different concrete strengths	82
Table 5.4 Coefficients to determine the moment capacity deterioration	87

List of Figures

Figure 2.1 Comparison of standard fire time-temperature curves	7
Figure 2.2 Comparison of natural fire and standard fire.....	7
Figure 2.3 Design fire temperature profile examples	8
Figure 2.4 Concrete Thermal Conductivity and Specific Heat.....	10
Figure 2.5 Value of k_1 for Equation 2.3 (Wickström, 1986)	11
Figure 2.6 Comparison of HSC strength models at elevated temperatures	15
Figure 2.7 modulus of elasticity at elevated temperatures.....	16
Figure 2.8 HSC stress-strain curves at elevated temperatures	17
Figure 2.9 Free thermal expansion strain of HSC.....	18
Figure 2.10 Concrete strain components	18
Figure 2.11 Illustration of the HSC spalling mechanism (Kodur, 2000).....	20
Figure 2.12 Simplified model to account for explosive spalling (Shin, 2011).....	22
Figure 2.13 Comparison of Euro Code model and testing curves of strand stress-strain relationship.....	23
Figure 2.14 Ideal moment-curvature curve of a prestressed beam	25
Figure 3.1 Overall procedure to evaluate a prestress girder's fire performance.....	33
Figure 3.2 Section before and after spalling	35
Figure 3.3 Heat transfer analysis for CPCI-1200 girder with a topping slab	37
Figure 3.4 Concrete ultimate strain at elevated temperatures.....	39
Figure 3.5 Stress-strain model for 7-wire-strand at elevated temperatures	40
Figure 3.6 Examples of HSC and reinforcing steel constitutive model charts	41
Figure 3.7 The simplified 1-D model and associated strains.....	45

Figure 3.8 Strain components in the 1D model at elevated temperatures	46
Figure 3.9 Constructing the moment-curvature diagram of a section	48
Figure 3.10 Calculation of the deflections from the section curvatures	50
Figure 3.11 Structural details and loading of beam H1	51
Figure 3.12 Test setup (Kumar 2021).....	52
Figure 3.13 Fire temperature record inside the heating chamber	52
Figure 3.14 Experiment record and model predicted temperature comparison.....	53
Figure 3.15 Moment-Curvature diagrams of the section of beam H1 at different fire durations.....	53
Figure 3.16 Curvature and deflection of beam H1	55
Figure 4.1 Standard and natural fire curves	59
Figure 4.2 Natural fire curves	61
Figure 4.3 Flow chart to calculate AITP time equivalence (t_e).....	63
Figure 4.4 Errors in estimating temperatures using a standard fire with a duration of t_e	64
Figure 4.5 Error in predicting AITP profile using a standard fire.	65
Figure 4.6 Accuracy of t_e prediction using Equation 4.4.....	66
Figure 4.7 Error from using equation 4.4 at different t_e values	67
Figure 4.8 Natural fire curves to examine the effect of beam width	68
Figure 4.9 Effect of the section width on t_e	69
Figure 4.10 Sections of the considered CPCI girders	70
Figure 4.11 Equivalent standard fire exposure time (t_e) of CPCI girders.....	71
Figure 4.12 Mean error resulting from using t_e for CPCI girders	73
Figure 4.13 Comparison between the equivalent time predicted by the equation versus that by the numerical study	74

Figure 5.1 Girder sections for the parametric study	80
Figure 5.2 $M-\Psi$ curves at ambient temperature	80
Figure 5.3 Comparison of M_{yT} and M_{uT} of G1 with different concrete strength.....	82
Figure 5.4 Yield and ultimate moments of section G2 at different fire durations	83
Figure 5.5 Yield and ultimate moments for sections G1, G2, G3, and G4 ($f_c' = 75$ MPa).....	84
Figure 5.6 $M-\Psi$ curves at elevated temperatures for Section G2.....	85
Figure 5.7 Idealized moment-curvature curves	86

List of Abbreviations, Symbols, and Notations

avg_tmp1	layer average temperature calculated as a mathematical mean ($^{\circ}\text{C}$)
avg_tmp2	layer average temperature calculated to achieve the mean f'_{cT} ($^{\circ}\text{C}$)
avg_tmp3	layer average temperature calculated to achieve the mean E_{cT} ($^{\circ}\text{C}$)
A	cross-section area of the beam section (mm^2)
A_c	cross-section area of concrete (mm^2)
A_k	load effect resulting from fire (N)
A_p	area of prestress strands (mm^2)
A_s	area of tension steel (mm^2)
A_v	effective shear area (mm^2)
B	beam width (mm)
b_w	web width (mm)
C	specific heat ($\text{J}\cdot\text{kg}^{-1}\cdot\text{K}^{-1}$)
c_l	concrete specific heat ($\text{J}\cdot\text{kg}^{-1}\cdot\text{K}^{-1}$)
c_p	volumetric specific heat ($\text{J}\cdot\text{m}^{-3}\cdot\text{K}^{-1}$)
D	depth of the beam (mm)
d_i	distance to layer i measured from the bottom (mm)
d_v	effective shear depth (mm)
D	specified dead load (N or N/m)
E	eccentricity of the strand from the section centroid (mm)
E_c	tangent elastic modulus of concrete at ambient temperature (MPa)
E_{ci}	initial elastic modulus of concrete at ambient temperature (MPa)

E_{cT}	tangent elastic modulus of concrete at T°C (MPa)
E_{ciT}	initial elastic modulus of concrete at T°C (MPa)
E_p	tangent elastic modulus of the strands at ambient temperature (MPa)
E_{pT}	tangent elastic modulus of the strands at T°C (MPa)
E_s	tangent elastic modulus of steel at ambient temperature (MPa)
E_{sT}	tangent elastic modulus of steel at T°C (MPa)
E_{cT}^{SC}	secant modulus of concrete at T°C (MPa)
E_{pT}^{SC}	secant modulus of the strands at T°C (MPa)
E_{sT}^{SC}	secant modulus of steel at T°C (MPa)
f_c	concrete compressive stress at ambient temperature (MPa)
f_{cT}	concrete compressive stress at T°C (MPa)
f_{ct}	concrete tensile strength at ambient temperature (MPa)
f_{ctT}	concrete tensile strength at T°C (MPa)
f_p	strand stress at ambient temperature (MPa)
f_{pT}	strand stress at T°C (MPa)
f_{py}	strand yield stress at ambient temperature (MPa)
f_{pyT}	strand yield stress at T°C (MPa)
f_{pu}	strand ultimate stress at ambient temperature (MPa)
f_{puT}	strand ultimate stress at T°C (MPa)
f_s	steel stress at ambient temperature (MPa)
f_{sT}	steel stress at T°C (MPa)
f_{syo}	steel yield stress at ambient temperature (MPa)

f_{syT}	steel yield stress at T°C (MPa)
f'_c	concrete compressive strength at ambient temperature (MPa)
f'_{cT}	concrete compressive strength at T°C (MPa)
H	a factor used in the high-strength concrete stress-strain model
k_t	thermal conductivity ($\text{W}\cdot\text{m}^{-1}\cdot\text{K}^{-1}$)
k_{ET}	a factor for calculating steel elastic modulus at T°C
k_{pT}	a factor for calculating steel proportional strain at T°C
k_{yT}	a factor for calculating steel yield stress at T°C
L	specified live load (N or N/m)
M_r	moment resistance of a beam section (N·m)
M_y	yield moment of a beam section (N·m)
M_{yT}	yield moment of a beam section at T°C (N·m)
M_u	ultimate moment of a beam section (N·m)
M_{uT}	ultimate moment of a beam section at T°C (N·m)
M_z	zero curvature moment of a beam section (N·m)
M_{zT}	zero curvature moment of a beam section at T°C (N·m)
N	normal force (N)
N_c	compression force in the concrete in a beam section (N)
N_p	tension force in the steel bars in a beam section (N)
N_s	Tension force in the strands in a beam section (N)
P_e	effective prestress force (N)
S	spacing of stirrups (mm)

S	specified snow load (N)
t	time (minutes)
t^*	compartment fire equivalent time (hr)
t_e	equivalent time of a standard fire exposure (min)
t_{final}	overall fire duration of a natural fire (min)
t_{max}	time of the maximum temperature of a natural fire (min)
T	fire temperature ($^{\circ}\text{C}$)
T_{av}	the average concrete temperature at a given section height ($^{\circ}\text{C}$)
T_f	the temperature of the standard fire ($^{\circ}\text{C}$)
T_{max}	maximum temperature of a natural fire ($^{\circ}\text{C}$)
T_o	ambient temperature (20°C)
T_w	concrete surface temperature ($^{\circ}\text{C}$)
u	a common variable represents temperature in the developed program
V_a	the volume fraction of aggregates
V_{cT}	concrete shear resistance at $T^{\circ}\text{C}$ (N)
V_{rT}	shear resistance of a section at $T^{\circ}\text{C}$ (N)
V_{sT}	shear resistance provided by the steel bars at $T^{\circ}\text{C}$ (N)
V_{pT}	shear resistance provided by prestressing at $T^{\circ}\text{C}$ (N)
X	distance between the considered section and the nearest support (mm)
y_i	distance from the center of layer i to the centroid of the section (mm)
α_i	the slope of the tangent line at section i (rad)
α_y	an adjustment factor for the yield moment of a section

α_u	an adjustment factor for the ultimate moment of a section
α_z	an adjustment factor for zero curvature moment of a section
β_i	the angle between the tangent line at section i and the cord from i to $i+1$ (rad)
β_y	an adjustment factor for the yield curvature of a section
β_u	An adjustment factor for the ultimate curvature of a section
Γ	compartment fire time adjustment factor
Δ	deflection of beam (mm)
$\Delta\varepsilon_p$	initial prestress strain of strand (mm/mm)
ε_{cen}	total strain at the centroid of section (mm/mm)
ε_{cr}	concrete long-term creep strain (mm/mm)
ε_{ck}	concrete cracking strain (mm/mm)
ε_{cmT}	concrete mechanical strain at T°C (mm/mm)
ε_{cth}	concrete free thermal strain (mm/mm)
ε_{cuT}	concrete ultimate strain at T°C (mm/mm)
$\varepsilon_{f,T}$	instantaneous stress-related strain at T°C (mm/mm)
ε_{Lth}	equivalent linear thermal strain (mm/mm)
ε_{pth}	the free thermal strain of the strands (mm/mm)
ε_{pT}	effective strand strain at T°C (mm/mm)
ε_s	steel strain (mm/mm)
ε_{sp}	steel proportional strain (mm/mm)
ε_{st}	concrete thermal induced strain (mm/mm)
ε_{sth}	steel free thermal strain (mm/mm)

ε_{sT}	steel strain at T°C (mm/mm)
ε_{tot}	total strain (mm/mm)
ε_{tr}	concrete transient thermal strain (mm/mm)
η_w	the ratio between the temperature of the concrete surface and the fire
ρ	density (kg/m ³)
ρ_l	normal concrete density (kg/m ³)
φ_b	beam size adjustment factor
Ψ	section curvature (rad/m)
Ψ_y	section yield curvature at ambient temperature (rad/m)
Ψ_{yT}	section yield curvature at T°C (rad/m)
Ψ_u	section ultimate curvature at ambient temperature (rad/m)
Ψ_{yT}	section ultimate curvature at T°C (rad/m)
ACI	American Concrete Institute
AITP	average internal temperature profile
ASCE	American Society of Civil Engineers
CSA	Canadian Standards Association
CPCI	Canadian Precast Prestressed Concrete Institute
FTS	free thermal strain
HSC	high strength concrete
ISO	International Organization for Standardization
LITS	load-induced thermal strain
MATLAB	programming software by MathWorks, Inc.

NBCC	Nation Building Code of Canada
NIST	National Institute of Standards and Technology
NRC	National Research Council Canada
NSC	normal strength concrete
S1	vector of total strain values of all layers
S2	vector of equivalent linear thermal strain values of all layers
S3	vector of free thermal strain values of all layers
S4	vector of self-induced thermal strain values of all layers
S5	vector of linear loading strain values of all layers
S6	vector of mechanical strain values of all layers

Chapter 1 Introduction and Outline of the Thesis

1.1 Introduction

The National Building Code of Canada (NBCC, 2020) provides fire resistance requirements for various building groups and structural components. These requirements stipulate the minimum acceptable duration for a component to resist fire. For concrete sections, engineers can follow the acceptable prescribed solution, which involves satisfying minimum values for the section dimensions and the concrete cover. Those prescribed provisions were based on decades-long research and were proven to provide acceptable fire safety. With new material technology and construction methods, engineers have the opportunity to specify much higher concrete strength, allowing the use of smaller structural members. However, such higher-strength concrete cannot be used without either an updated prescribed fire safety solution or a calculation method to ensure fire safety.

For prestressed concrete girders of highway bridges, current bridge design codes do not account for fire exposure. However, fire damage contributes to about 3% of all bridge failures (MCEER, 2013). Bridge fire is normally severe because of the existence of fuel, which can lead to the closure of critical transportation pathways (Kodur, 2022). To ensure our safety, engineers need to estimate the structural behaviour of bridge girders during fire exposure. Such a task is not easily achievable based on the current knowledge and available tools.

The use of prestressed girders in bridges and critical floors of buildings is very common. The use of high-strength concrete (HSC: $f_c' > 55$ MPa) in such girders is extremely beneficial as it will result in reduced dimensions and increased durability. Currently, the only available method to analyze HSC prestressed girders during fire exposure is the finite element method. Only experts in structural fire engineering can utilize this method as fire causes significant changes in the material stiffness and substantial thermal strains, leading to non-convergence. Thus, reliable simplified methods to ensure the safety of HSC prestressed girders are highly needed.

1.2 Research objective

The objectives of this research are:

- 1) to develop a numerical model to predict the structural behaviour of prestressed HSC girders exposed to a specific duration of a standard fire.
- 2) to provide a methodology to extend the model's applicability to natural fire events.
- 3) to understand the effect of concrete strength and section shape on the structural behaviour of prestressed HSC girders during exposure to a standard fire.

1.3 Thesis Outline

1.3.1 Chapter 1: Introduction

This chapter presents the objectives and brief outline of the thesis.

1.3.2 Chapter 2: Literature Review

A literature review covering topics related to the thesis objectives is presented in this chapter. Topics covered include design codes, fire severity, heat transfer calculations, material constitutive models, thermal expansion, explosive spalling, and moment-curvature analysis of sections exposed to fire.

1.3.3 Chapter 3: Simplified Modeling of Prestressed Concrete Girders during Fire Exposure

To evaluate the behaviour of structures exposed to fire and estimate their structural fire resistance, engineers need design tools to overcome the complexities associated with structural analysis during fire exposure. These complexities include the uneven distribution of temperature within the structural elements and the deterioration in material properties. This chapter introduces a simplified numerical model to evaluate the flexural behaviour of bonded prestressed high-strength concrete sections exposed to fire. The model accounts for transient strains and explosive spalling phenomenon. It starts by predicting the temperature distribution within a structural element using 2-D finite difference analysis. It then uses one-dimensional sectional analysis to estimate the

section behaviour. An iterative calculation algorithm is developed to estimate the effect of fire exposure on the moment-curvature relationship of an HSC prestressed section. An example demonstrating the use of the model is also given.

1.3.4 Chapter 4: Equivalent standard Fire Duration for Prestressed Concrete Girders Exposed to Natural Fire

The numerical model in the previous chapter is based on the ASTM E119 standard fire, which has a specific time-temperature curve. This chapter extends the application of this model to apply to any natural fire. The chapter provides a methodology to estimate the equivalent duration of ASTM E119, which produces similar internal temperature distribution within an HSC prestressed section. The methodology is the first to cover different section shapes and account for explosive spalling in a simplified manner.

1.3.5 Chapter 5: Girder design parameters study

A parametric study is conducted in this chapter to evaluate the moment-curvature diagram of different prestressed sections. Considered variables are the concrete strength, section dimensions, and section shape. The structural performance of the considered cases was defined using their moment-curvature diagrams. Regression analysis was then performed to predict the moment-curvature diagram for the considered cases during fire exposure. Defining the moment-curvature diagrams allow engineers to estimate the structural behaviour of prestressed high-strength concrete girders during fire exposure.

1.3.6 Chapter 6: Summary, Conclusions, and future research

This chapter summarizes the major contributions of this thesis, lists the limitations of the developed software, and proposes future research to improve the accuracy of predicting the performance of HSC prestress girders exposed to fire.

1.4 Reference

ASTM. E119-20. *Standard Test Methods for Fire Tests of Building Construction and Materials*. American Society for Testing and Materials, West Conshohocken, PA, USA. 2020

CPCI. *CPCI design manual*. Canadian Precast Prestressed Concrete Institute. Ottawa Ontario, Canada, 2017.

Kodur and Gil, *Fire hazard in concrete bridge: review, assessment and mitigation strategies*, Structure and Infrastructure Engineering, <https://doi.org/10.1080/15732479.2022.2152465>, Dec. 2022

Lee and Mohan, *A Study of U.S. Bridge Failures (1980-2012)*, MCEER, University at Buffalo, Technical Report MCEER-13-0008, 2013

NRC Canada, *Nation Building Code of Canada, 2020 Volume 1*, Ottawa, Canada, 2020

Chapter 2 Literature Review

2.0 Introduction

This chapter presents a literature review on the structural performance of high-strength concrete (HSC) exposed to fire. The review covers the code provisions, fire properties, thermal and mechanical properties of concrete, steel, and strands, temperature distribution within a concrete section, and structural performance of HC members during fire exposure.

2.1 Code Provisions on Structural Fire Resistance

To assure structural integrity and protect occupants during a fire evacuation, building codes require the structural elements of a building to support their loads for a minimum duration of an assumed standard fire duration. Clauses 3.2.2.20 to 3.2.2.86 of NBCC (2020) specify the fire resistance rating (FRR), which ranges from 45 minutes to 2 hours depending on the occupancy category. To achieve the specified ratings, appendix D of NBCC (2020) provides a prescriptive approach, which relies on using adequate concrete cover and section dimensions. NBCC (2020) also provides an objective fire design approach, which is not widely used because it requires sophisticated analysis. Neither engineers nor officials approving the designs have the background or the tools for such analysis. In the USA, ASCE 7-16 (2018) introduced performance-based design in structural fire engineering. The load applied to the structure during a fire event is given as “ $(0.9 \text{ or } 1.2) D + A_k + 0.5 L + 0.2 S$ ”, where D is dead load, A_k is the load or load effect resulting from a fire event, L is live load, S is snow load. In Europe, EN 1991-1-2 (2002) has also introduced performance-based design to structural fire engineering. ASTM E119 (2020) provided defined the failure of a girder during fire exposure to correspond to applied service load exceeding the girder capacity or temperature in tension reinforcing steel exceeding 593°C . BS 476-20 (2014) gave a limit on the girder deflection during a fire of $L/20$ and on the rate of deflection increase of $\frac{L^2}{9000d}$ mm/minute, where L is the length of the girder (mm), and d is the depth of the beam (mm).

2.2 Fire Temperature

2.2.1 Standard Fire

The hot air temperature of the fire is controlled by many factors, which are not practical to use while defining the fire rating of different construction materials. Based on statistical data and engineering judgment, the “standard fire temperature scenario” was introduced to simplify and standardize the representation of a severe heating scenario. This scenario is known to be conservative and to result in safe designs. However, it does not even remotely represent the trends of a naturally occurring fire (Cooper and Steckler, 1996). The two widely used prescribed fire models are ASTM E-119 (2020), Eq. 2.1 (a) and ISO 834 (2014), Eq. 2.1 (b). T is the fire temperature in °C and t is the time in minutes. The initial temperature for both models is set as 20°C. Two other fire models are given in EN 1991-1-2 (2002), representing hydrocarbon fire, Eq. 2.1 (c), and external fire, Eq. 2.1 (d). Figure 2.1 shows the time-temperature curves for the four fires. The fire models by ASTM E119, Eq. 2.1 (a), and ISO 834, Eq. 2.1 (b) are almost identical. The hydrocarbon fire represents a more severe, and thus can present a threat to concrete bridges. The external fire, which can represent a wildfire, has a lower fire temperature than the given by the standard fire.

$$T = 20 + 750 [1 - e^{(-0.49\sqrt{t})}] + 22.0\sqrt{t} \quad \text{Eq.2.1 (a)}$$

$$T = 20 + 345 \log_{10}(1 + 8 t) \quad \text{Eq.2.1 (b)}$$

$$T = 20 + 1080 (1 - 0.325e^{(-0.167t)} - 0.675e^{(-2.5t)}) \quad \text{Eq.2.1 (c)}$$

$$T = 20 + 660 (1 - 0.687e^{(-0.32t)} - 0.313e^{(-3.8t)}) \quad \text{Eq.2.1 (d)}$$

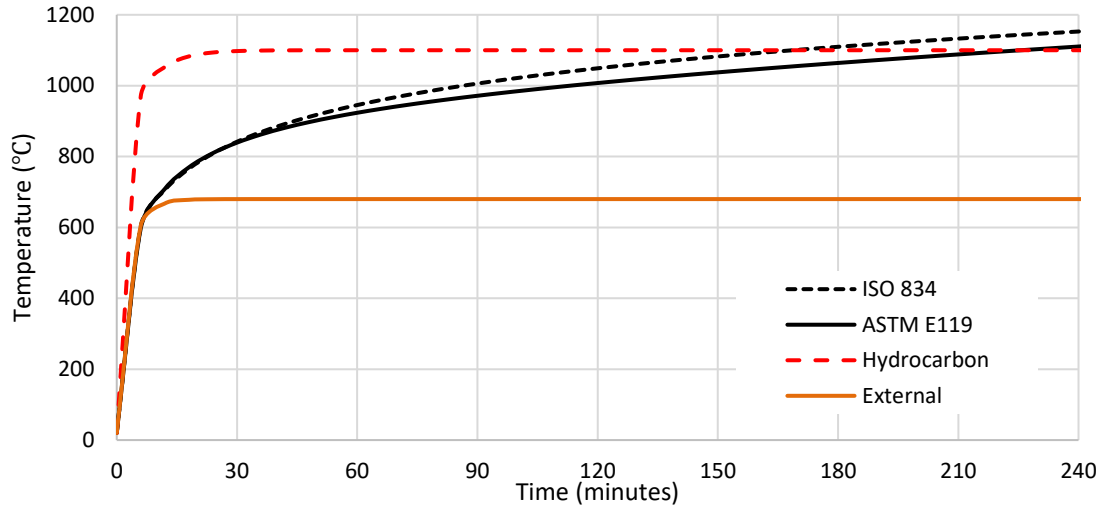


Figure 2.1 Comparison of standard fire time-temperature curves

2.2.2 Natural Fire and Equivalent Design Fire

To conduct performance-based design in structural fire engineering, engineers need to consider the potential natural fire. The stages of a natural fire are growth, fully developed fire, and decay. Figure 2.2 shows a comparison between the fire used in the full-scale experimental tests by Lennon (2004) and the standard fire. In this case, the fire temperature was higher than the standard fire temperature. The second difference is the decaying branch, which is common for all-natural fire curves.

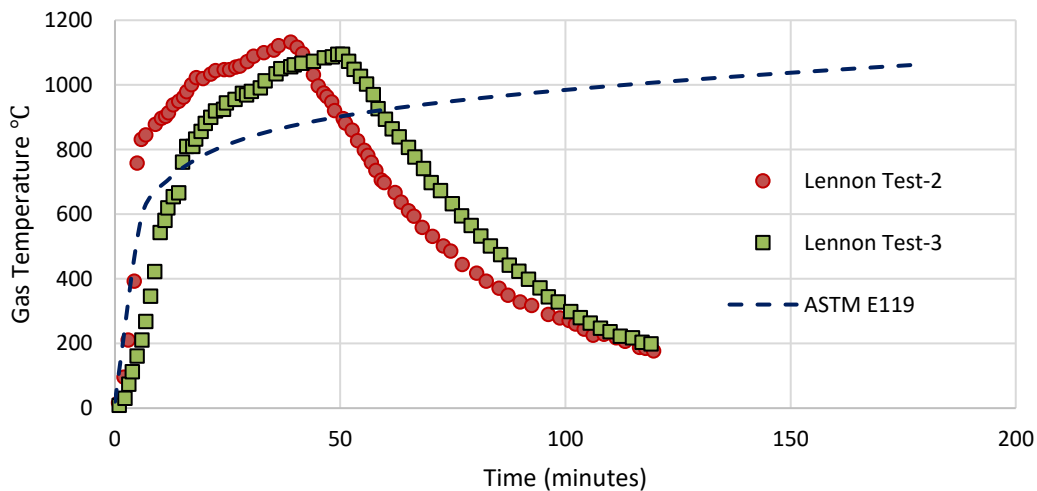


Figure 2.2 Comparison of natural fire and standard fire

Based on specific parameters of the fire compartment, Annex A and annex F of EN 1991-1-2 provide a simplified approach for estimating the potential natural fire curve. These parameters include the floor area, number of openings, and fuel load. Fig. 2.3 shows examples of the temperature curves developed using the EuroCode methodology. The examples represent small, moderate, and large fires. It also shows fires with rapid heating and cooling stages.

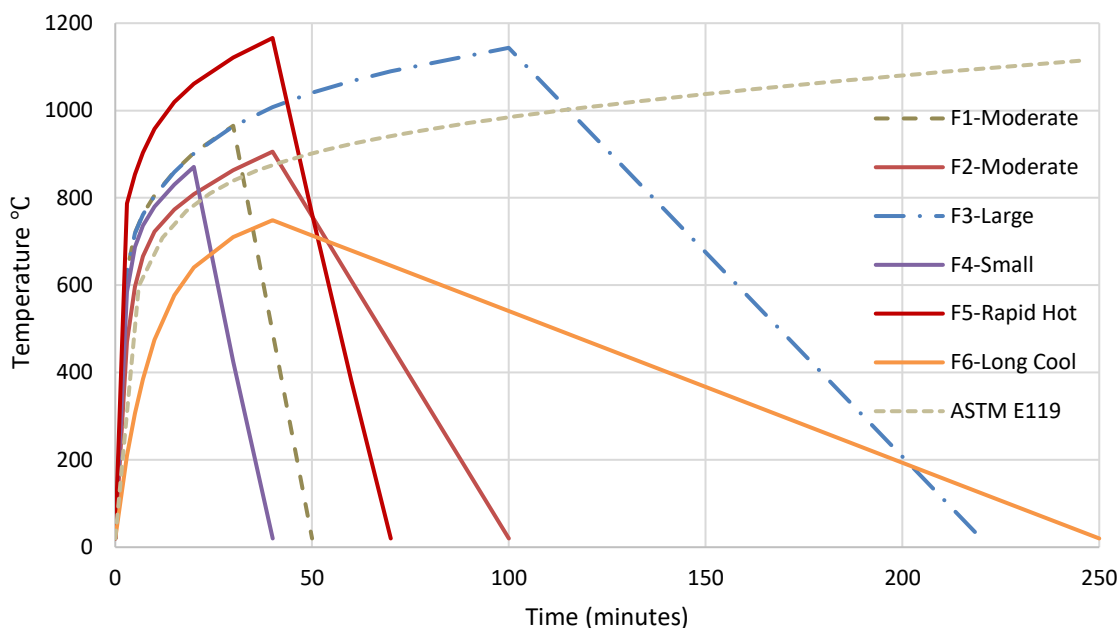


Figure 2.3 Design fire temperature profile examples

To use the wealth of knowledge available for standard fire curves, researchers have developed methods to estimate the equivalent duration of a standard fire that can represent the effect of a considered natural fire. Kuehnen (2019) presented a discussion of the time equivalency methods and concluded that (1) the ‘equal area method’ does not accurately account for the energy of the fire as it ignores the heating rate, maximum temperature, and cooling rate, (2) The ‘maximum temperature method’ can be accepted for sections that can be characterized by a single uniform temperature during fire exposure, which excludes concrete cross-sections given the significant temperature gradients within them, (3) The energy methods provide good accuracy as they are based on matching the accumulated thermal energy from both a natural fire and a standard fire with an equivalent duration (t_e), and (4) The ‘load capacity concept’ can only be used to estimate

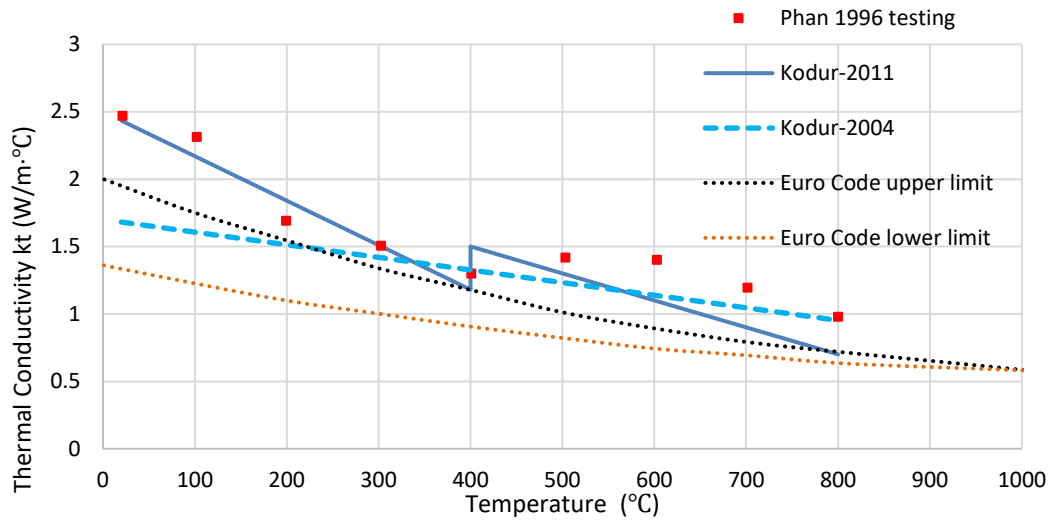
the capacity during fire exposure. Kuehnen (2019) developed an average internal temperature profile method (AITP) to measure the fire severity on concrete members. The t_e is defined as the duration of standard fire required to generate the same AITP in a concrete section as experienced by a selected natural fire.

2.2.3 Concrete Thermal Properties

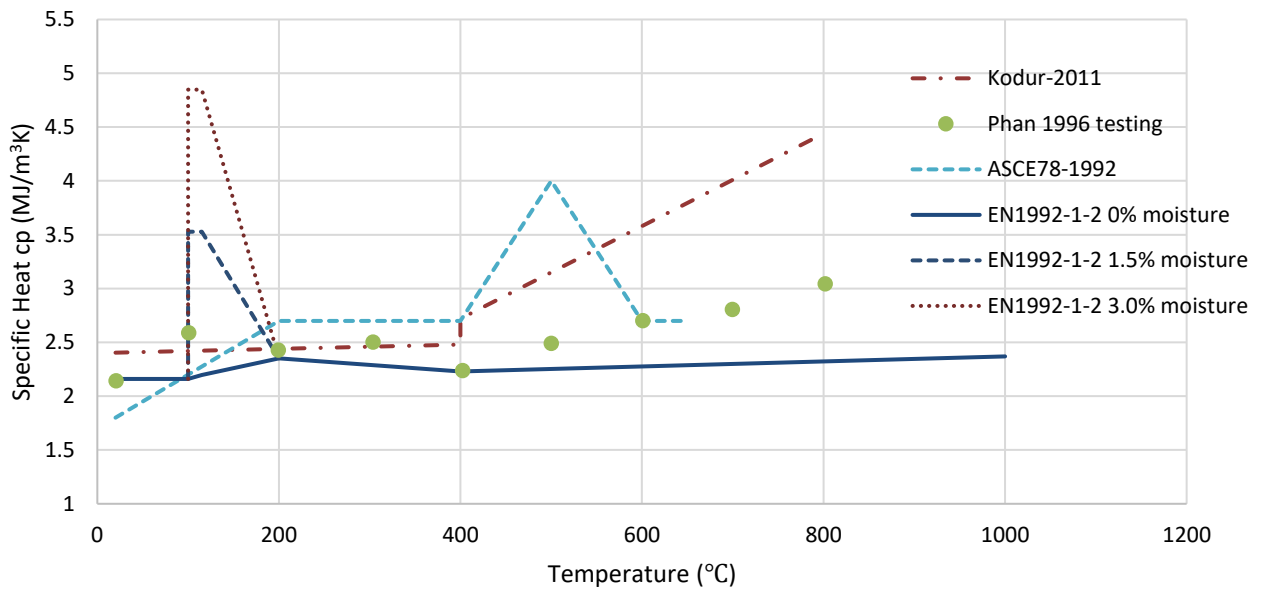
To simulate the temperature distribution through the concrete structure under fire, the thermal conductivity, specific heat, thermal diffusivity, and mass loss should be known. Due to the complex nature of concrete material, a range of data is needed to represent various types of concrete. Phan (1996) has concluded that the thermal properties vary with fire temperature and that there are notable differences between normal-strength concrete (NSC) and high-strength concrete (HSC).

Thermal Conductivity k_t ($\text{W}/\text{m}\cdot^\circ\text{C}$) is the ability of concrete to conduct heat, defined as the ratio of the rate of heat flow to the temperature gradient. HSC has a higher thermal conductivity compared with NSC since HSC is a much denser material and has fewer voids. Kodur et al. (2004, 2011) proposed a series of models for HSC thermal properties. The Euro Code EN1992-1-2 (2002) did not provide separate models for different types of concrete but provided the lower and upper limit values of concrete thermal conductivity. Figure 2.5 (a) shows a comparison of the models for thermal conductivity.

Volumetric thermal capacity c_p ($\text{J}/\text{m}^3\text{K}$) is the amount of heat energy to be supplied to an object to produce a unit change in its temperature, which is the product of specific heat and density. For concrete material, c_p is highly influenced by the aggregate type, moisture content, and concrete temperature (Phan, 1996). However, it is not affected by concrete strength. Commonly acceptable models can be found in ASCE Manuals #78 (1992), EN1992-1-2 (2002), and Kodur (2011). Figure 2.5 (b) shows a comparison of volumetric thermal capacity models.



(a) Thermal Conductivity of HSC



(b) Specific Heat Capacity of HSC

Figure 2.4 Concrete Thermal Conductivity and Specific Heat

The concrete density changes with the fire temperature due to the loss of moisture. Euro Code EN1992-1-2 provides the density at different values of elevated temperatures. However, the NIST Guidelines (Phan, 2010) recommend using a constant number for concrete density, since it does not vary significantly over the temperature range typically associated with common fires.

2.2.4 Concrete Surface Temperature

To accurately evaluate the structural performance of a concrete member under fire exposure, the concrete surface temperature, which represents a boundary condition for heat transfer analysis, needs to be evaluated. As concrete has a low thermal conductivity and a moderate thermal capacity, its surface temperature would be lower than the fire temperature. Wickström (1986) proposed a concept of Adiabatic Surface Temperature (AST; T_{AST}) for modelling structures in fire. AST combines the fire model outputs, which include gas temperature, radiation, and convection boundary conditions. Wickström (1986) assumed that the concrete structure is semi-infinite, and proposed Eq. 2.2 to evaluate the surface temperature (T_w) as a function of the fire temperature T_f , the compartment time factor Γ (=1.0 for a standard fire), the concrete thermal conductivity k in W/m·K, the thermal conductivity of normal weight concrete k_1 which is given in Figure 2.5, the concrete density ρ in kg/m³, the density of normal weight concrete ρ_1 (2400 kg/m³), the concrete specific heat c in J/kg·K, the specific heat of normal strength concrete c_1 (1000 J/kg·K)

$$T_w = \left[1 - 0.0616 \cdot \left[\left(\frac{\sqrt{\Gamma}}{\gamma_i} \right) t \right]^{-0.88} \right] T_f \quad \text{Eq.2.2}$$

$$\gamma_i = \frac{\sqrt{k\rho c}}{\sqrt{k_1\rho_1 c_1}}$$

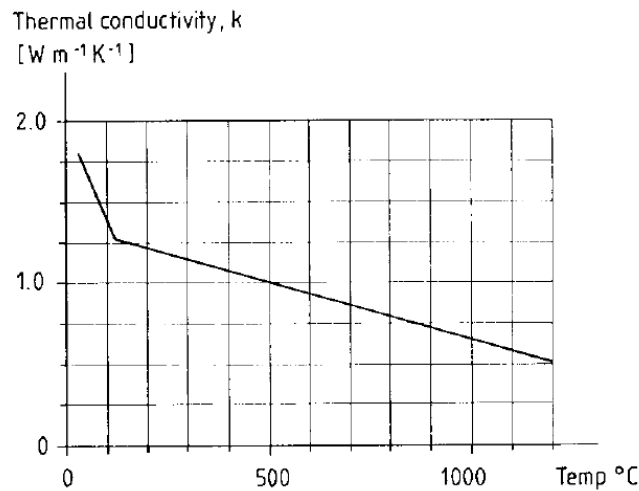


Figure 2.5 Value of k_1 for Equation 2.3 (Wickström, 1986)

2.2.5 Temperature distribution

Heat is transferred from fire by both radiation and convection to the boundary elements and by conduction to the inner elements. Thermal radiation occurs due to the conversion of thermal energy into electromagnetic energy resulting in the emission of photons and electromagnetic waves away from the fire. This radiated energy results in rising the temperature of the surrounding objects based on their thermal properties (Kodur, 2010). Convection is the transfer of thermal energy by the mass movement of gases or liquids. In this process, fire increases the surrounding air temperature causing it to flow upward towards the ceiling resulting in a heat transfer to the adjacent structural members in contact with this hot air. The heat transferred by convection represents not more than 10% of that transferred by radiation (Kodur, 2004). Conduction, on the other hand, is the transfer of internal energy by diffusion and collision of adjacent molecules, atoms, and electrons within an element. The heat flows from the hotter to the colder part of the body until thermal equilibrium is achieved.

Temperature distribution within a reinforced concrete section subjected to elevated temperatures can be predicted experimentally or numerically. The finite difference method can predict the temperature variation within a cross-section taking into account the temperature dependence of thermal material properties. It provides relatively accurate predictions for monolithic structural members exposed to fire from one or more sides. However, this process is not practical to be used in design offices as it requires an enormous amount of time to build and execute an iterative procedure for the analysis. Details for the finite difference calculations are given by ASCE-78 (Lie, 1992). The calculation procedure is carried out by dividing the concrete section into right-angled rhombus and triangle elements. The temperature is represented at the centers of each rhombus element and the hypotenuse mid-point of each triangular element. The steel bars are considered perfect conductors due to their significantly higher thermal conductivity relative to the surrounding concrete material. Thus, the temperature in each steel bar is considered equal to the temperature of the adjacent concrete elements. The heat analysis is carried out in time steps with the aid of a chosen standard fire relationship. At any given time, the temperature in each element is calculated by solving the corresponding heat equation with the knowledge of the temperature at the previous time increment. Under normal environmental conditions, concrete may hold about 3% moisture by volume. The influence of moisture is considered by assuming that at a temperature

of 100°C, all heat conducted to the element is used to evaporate the water rather than increasing its temperature.

Wickstrom (1986) provided a simplified method to predict the temperature distribution within a concrete cross-section during exposure to fire. Achenbach (2017) discussed a theoretical procedure based on solving the 1-D heat transfer differential equation as Eq.2.3 and conducted a sensitivity analysis to identify the governing parameters of the temperature calculation. Equation 2.3 can be extended to a system of equations for a 2-D mesh. Mathworks (2022) provided many functions within the software of MATLAB, specifically for solving heat transfer problems by idealizing the concrete as a homogeneous and isotropic material when transferring heat, which is true on the macro scale.

$$\frac{\partial T(x,t)}{\partial t} = \frac{\lambda}{\rho \cdot c_p} \cdot \frac{\partial^2 T(x,t)}{\partial x^2} \quad \text{Eq. 2.3}$$

where λ = thermal conductivity [W/m K], ρ = density [kg/m³] and c_p = specific heat [J/kg K].

2.3 High-Strength Concrete Mechanical Properties Under Elevated Temperatures

High-strength concrete is defined as concrete with ambient compressive strength (f_{c20}) greater than 55MPa (ACI 363R, 1992). It gained increasing interest in the structural design of buildings, bridges, and tunnels as it has a superior mechanical capacity as compared to NSC. Concrete is known to be superior to steel in fire resistance. However, it was shown that HSC behaves differently than NSC (Phan, NISTIR 5934,1996). This section focuses on the mechanical properties of HSC.

HSC compressive strength ($f'_{c,T}$) at elevated temperatures is of primary interest. EN 1992-1-2 (2002) provides Table 2.1, which specifies the ratio of strength loss for different classes of HSC (class 1: C55/67 to C60/75; class 2: C70/85 to C80/95; and class 3: C90/105). Phan (NIST, 1996) proposed a model for HSC compressive strength under elevated temperature, which is given by Eq. 2.4. Kodur (2004) proposed the model given by Eq. 2.5. Figure 2.6 provides the comparison between the different models, which shows that all models provide similar trend.

$$f'_{c,T} = f_{c,20} \quad T \leq 50 \text{ } ^\circ\text{C} \quad \text{Eq.2.4}$$

$$f'_{c,T} = f_{c,20} [1.28 - 0.056T] \quad 50 \text{ } ^\circ\text{C} < T \leq 100 \text{ } ^\circ\text{C}$$

$$f'_{c,T} = 0.72 f_{c,20} \quad 100 \text{ } ^\circ\text{C} < T \leq 350 \text{ } ^\circ\text{C}$$

$$f'_{c,T} = f_{c,20} [1.31 - 0.00168T] \quad 350 \text{ } ^\circ\text{C} < T \leq 778 \text{ } ^\circ\text{C}$$

$$f'_{c,T} = 0 \quad T > 778 \text{ } ^\circ\text{C}$$

$$f'_{c,T} = f'_c [1.0 - 0.003125(T-20)] \quad T < 100 \text{ } ^\circ\text{C} \quad \text{Eq.2.5}$$

$$f'_{c,T} = 0.75 f'_c \quad 100 \text{ } ^\circ\text{C} < T \leq 400 \text{ } ^\circ\text{C}$$

$$f'_{c,T} = f'_c [1.33 - 0.00145T] \quad 400 \text{ } ^\circ\text{C} < T$$

Table 2.1 Reduction of strength at elevated temperature (EN 1992-1-2, 2002)

T (°C)	f'_{cT}/f'_c		
	EN1992-1-2: class 1	EN1992-1-2: class 2	EN1992-1-2: class 3
20	1	1	1
50	1	1	1
100	0.9	0.75	0.75
200	0.9	0.75	0.7
250	0.9	0.75	0.675
300	0.85	0.75	0.65
400	0.75	0.75	0.45
500	0.6	0.6	0.3
600	0.45	0.45	0.25
700	0.3	0.3	0.2
800	0.15	0.15	0.15
900	0.08	0.1125	0.08
1000	0.04	0.075	0.04
1100	0.01	0.0375	0.01
1200	0	0	0

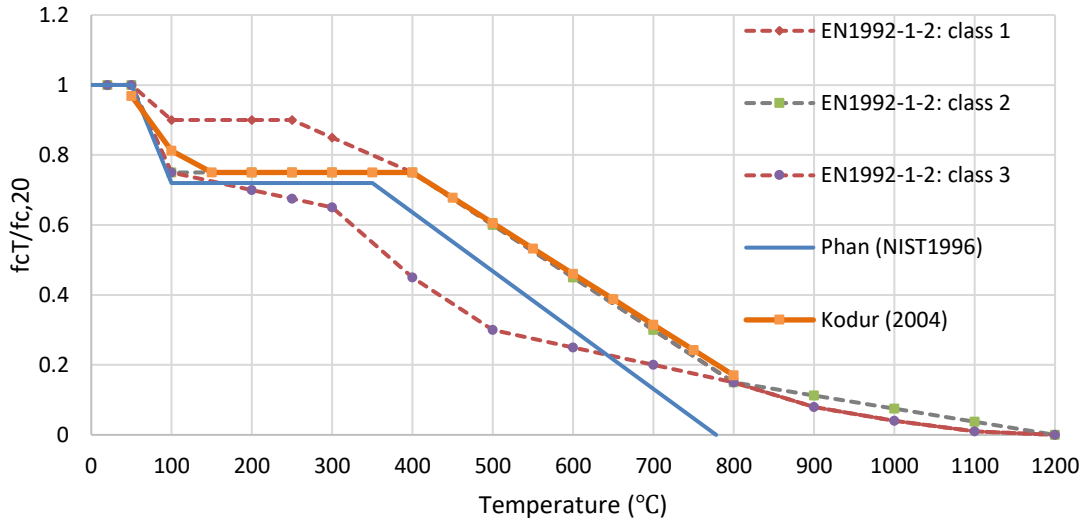


Figure 2.6 Comparison of HSC strength models at elevated temperatures

The tensile strength of concrete (f_{ct}) is much lower than its compressive strength, which is the reason behind ignoring it in the ultimate limit state design provisions. Existing research showed that the tensile strength of concrete is related to its compressive strength and that it decreases with fire temperature in a nearly linear manner, NSC and HSC have almost the same rate of tensile strength deterioration (Phan, 1994). Euro Code EN 1992-1-2 (2002) provides Eq. 2.6, which can be used to evaluate the concrete tensile strength at elevated temperatures.

$$\frac{f_{ct,T}}{f_{ct}} = \begin{cases} 1.0 & 20 < T \leq 100^{\circ}\text{C} \\ 1.2 - \frac{T}{500} & 100 < T \leq 600^{\circ}\text{C} \end{cases} \quad \text{Eq. 2.6}$$

The elastic modulus of concrete is largely related to its compressive strength at ambient temperature but declines rapidly with increasing temperature. The variation of HSC's modulus of elasticity at elevated temperatures in general follows the trend observed for NSC (Phan, 1996). Figure 2.7 compares the numerical model by Knennane and Baker (1992), Eq. 2.7, and the test results by Castillo (1990). Where E_{ci} and E_{ciT} are the initial modulus values at ambient and elevated temperatures, respectively.

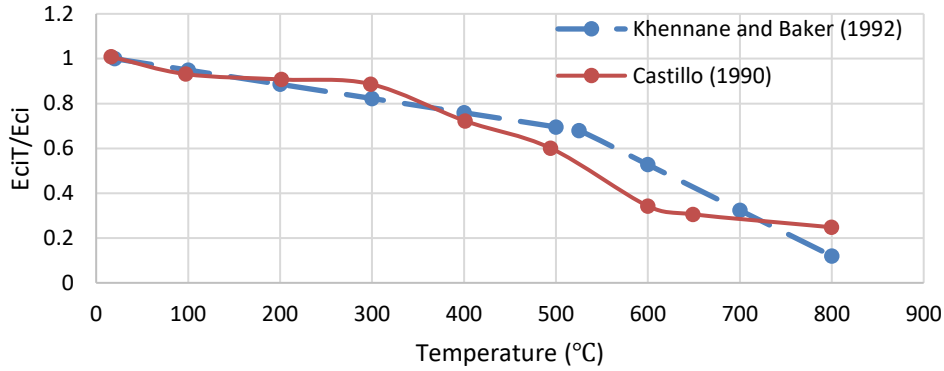


Figure 2.7 modulus of elasticity at elevated temperatures

$$E_{ciT} = (-0.000634T + 1.012673)E_{ci} \quad 20^{\circ}\text{C} \leq T \leq 525^{\circ}\text{C} \quad \text{Eq. 2.7}$$

$$E_{ciT} = (-0.002036T + 1.749091)E_{ci} \quad 525^{\circ}\text{C} \leq T \leq 800^{\circ}\text{C}$$

Stress-strain curves for NSC and HSC have significant differences at ambient and elevated temperatures. Furumura et al. (1995) tested cylinders to generate stress-strain curves for NSC and HSC during heating and after heating. HSC stress-strain curves showed a brittle response below 500°C. Above 500°C, the stress-strain curves showed a more ductile response. For both NSC and HSC, the strains at peak stress during heating and after heating increased rapidly with temperature. Kodur et al. (2014) proposed the stress-strain curve given by Eq. 2.8. Where ε is the mechanical strain corresponding to $f_{c,T}$. For an 80 MPa HSC, the stress-strain curves are illustrated in Figure 2.8 for different temperature values.

$$f_{c,T} = \begin{cases} f'_{c,T} \left[1 - \left(1 - \frac{\varepsilon}{\varepsilon_{o,T}} \right)^H \right], & \varepsilon \leq \varepsilon_{o,T} \\ f'_{c,T} \left[1 - \left(\frac{30}{130 - f'_c} \cdot \frac{\varepsilon - \varepsilon_{o,T}}{\varepsilon_{o,T}} \right)^2 \right], & \varepsilon > \varepsilon_{o,T} \end{cases} \quad \text{Eq.2.8}$$

where: $\varepsilon_{o,T} = 0.0018 + (6.7f'_c + 6.0T + 0.03T^2) \times 10^{-6}$ (strain at peak stress)

$$H = 2.28 - 0.012f'_c$$

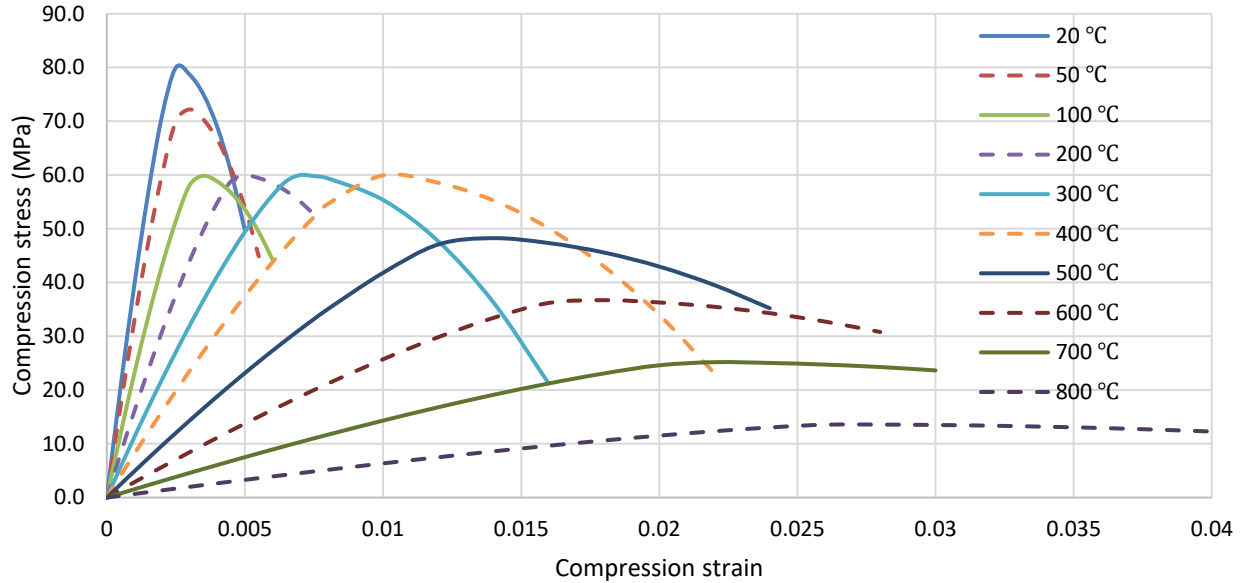


Figure 2.8 HSC stress-strain curves at elevated temperatures

2.3.4 Strain at elevated temperatures

The total strain can be split into 4 components (Terro, 1998; Khoury, 2002; Youssef, 2007; Gernay, 2012): $\epsilon_{total} = \epsilon_{th} + \epsilon_{f,T} + \epsilon_{tr} + \epsilon_{cr}$. Where ϵ_{th} is the free thermal strain, $\epsilon_{f,T}$ is the instantaneous stress-related strain, ϵ_{tr} is the transient creep strain and ϵ_{cr} is the time-depend creep strain. When we discuss the structure behaviour during fire exposure, the time duration is in the order of a few hours, so the time-depend creep strain can be assumed to be zero.

The aggregates in the concrete undergo expansion when subjected to a rising temperature. However, at elevated temperatures, thermal shrinkage can occur from the loss of water due to heating. Tests showed that for NSC, the overall expansion stops between temperatures of 600 and 1000°C. For HSC, the thermal expansion consistently increases with temperature. Eq. 2.9 given by Lie (1992) can be used to estimate the free thermal strain. Kodur (2004) confirmed that this equation applies to HSC. Figure 2.9 shows predictions of the equation against test results by Kodur et al. (2010).

$$\epsilon_{th} = [0.004(T^2 - 400) + 6(T - 20)] \times 10^{-6} \quad \text{Eq.2.9}$$

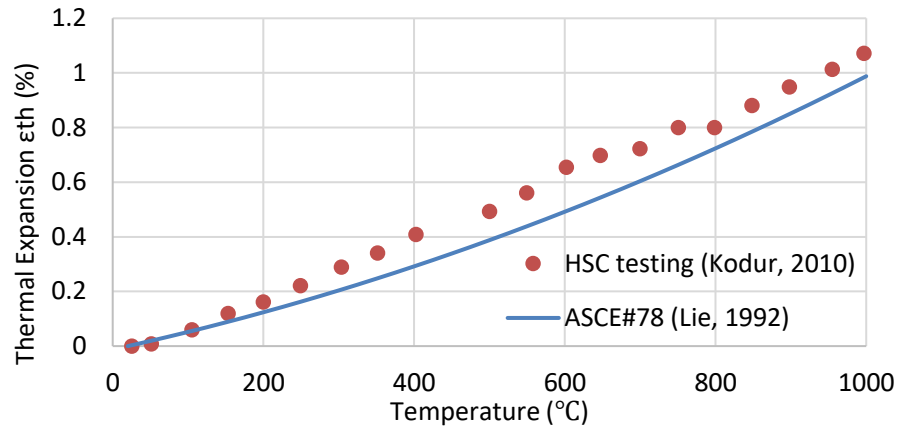


Figure 2.9 Free thermal expansion strain of HSC

The transient creep strain (ϵ_{tr}) happens when a loaded concrete is heated for the first time (Khoury, 2002). The transient strain is not recovered during unloading and/or cooling. In experiments, the transient creep is obtained as the difference in strain between a steady-state test and a transient test. Figure 2.10 shows the relative proportions of the concrete strain components. It shows that transient strains are the largest component.

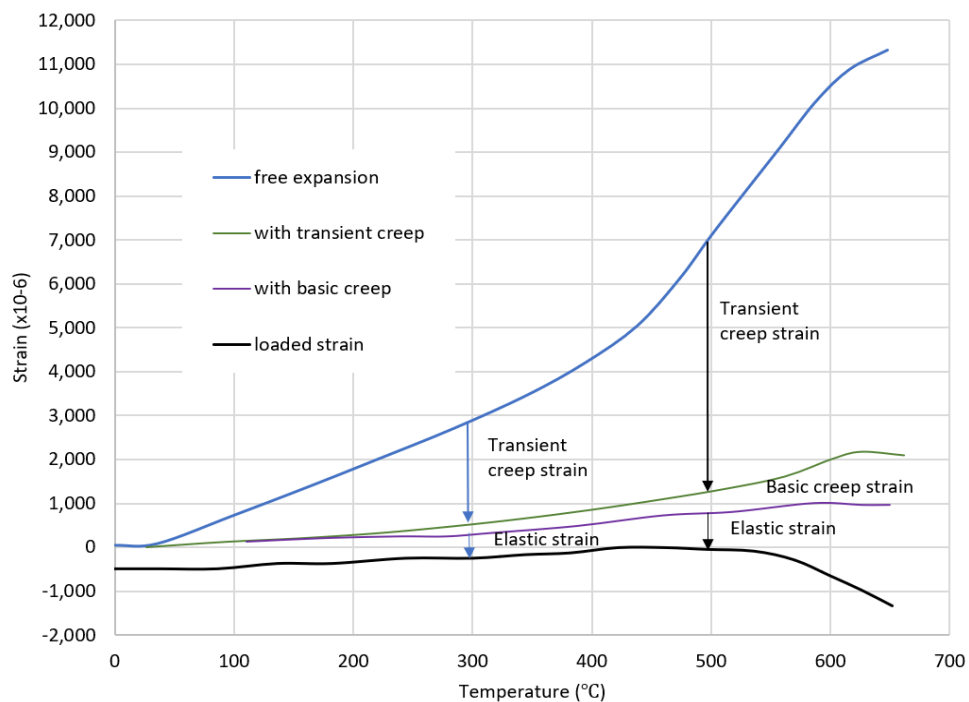


Figure 2.10 Concrete strain components

Terro (2002) proposed a numerical model for the load-induced thermal strain (LITS), which includes transient creep ε_{tr} , drying creep, basic creep, and changes in elastic strain with temperature. If the heating duration is short (and for the first time), the transient strain dominates the behaviour. To account for the transient creep of a loaded member with a first-time fire attack, the stress-strain curve can be linearly shifted, which is adopted by the current Euro Code EN1992-1-2 (2004) implicit method.

Based on the recent review of the literature regarding transient thermal strains of concrete, the explicit model for the transient thermal strain is not very successful, the reason is that the transient thermal strain must be the result of both thermal-induced physical-chemical effects and mechanical stress, (Khennane, 2009). The implicit model, which defines the mechanical strain curves at certain temperatures, already includes the transient thermal strain, which is reflecting the real-world situation of “loaded structure under fire exposure”, such as expressed in EC1992-1-2 (2004), Terro (1998), and Kodur (2004).

2.3.4 Compressive failure strain

The fact that the stirrups will be severely affected by the fire temperature makes the concrete behaves like un-confined concrete (ACI committee 363, 1992). The modified ultimate strain ε_{cu} for high-strength concrete can be predicted using Equation 2.10 (Neville and Terro, 1998).

$$\varepsilon_{cuT} = \frac{4.942}{10^3} - \frac{6.995}{10^5} f'_{cT} + \frac{3.993}{10^7} f'^2_{cT} \quad \text{Eq.2.10}$$

Where, f'_{cT} is HSC strength at elevated temperatures.

2.3.5 Spalling of High-Strength Concrete under Fire

The performance of HSC under fire conditions is considered worse than NSC, mainly because of explosive spalling. Spalling is defined as the breaking of layers or pieces of concrete surface when exposed to fire (Dwaikat, 2010). Spalling causes loss of concrete cover, and thus exposes the deeper layers of concrete and the steel bars to the hot gas of fire. This damage makes the reinforcement temperature raises rapidly, which leads to the loss of structural stability and integrity (Kodur, 2000). Table 2.2 presents the parameters that influence the fire performance of HSC and

quantifies the extent of their influence on spalling. Two major hypotheses happen during spalling, pore pressure build-up and restrained thermal dilatation.

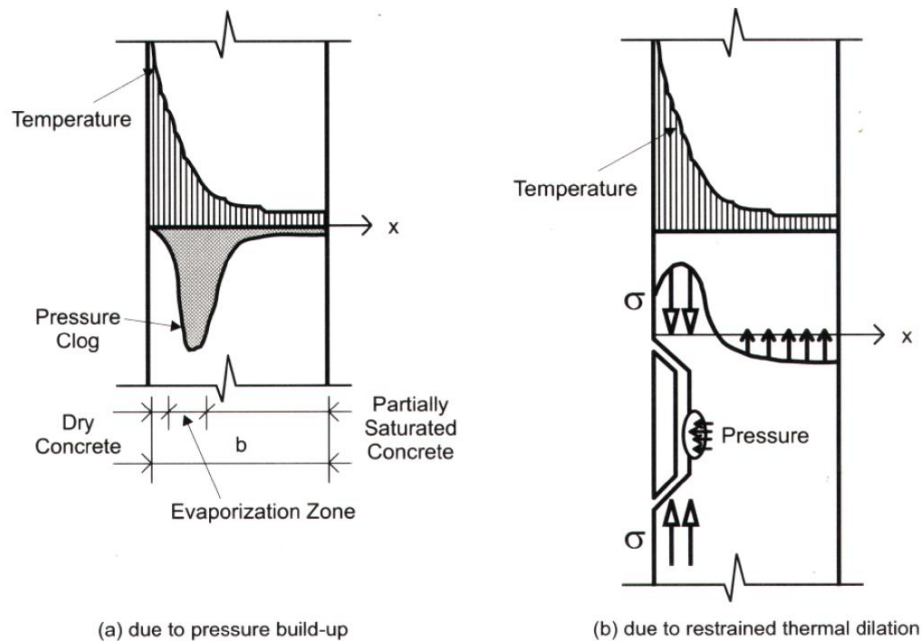


Figure 2.11 Illustration of the HSC spalling mechanism (Kodur, 2000)

Pore pressure build-up happens more severely in HSC because the material is denser and has low permeability as compared with NSC. Heat generates extremely high vapour pressure. For example, at 300°C, the pressure could reach 8 MPa, which is higher than the tensile capacity of most concrete. Figure 2.11(a) shows that the pressure built up is near the heated surface. Due to the brittle nature of concrete failure under tension, the spalling would happen suddenly and explosively. Spalling continues until reaching a temperature of about 600°C, which destroys the concrete microstructure faster than the vapor pressure buildup.

Restrained thermal dilatation is based on the nature of the temperature gradient near the heated surface of concrete, which will cause uneven thermal expansion inducing compressive stresses parallel to the heated surface. This stress, which is applied on a thin layer, is released through the brittle fracture of concrete as illustrated in Figure 2.11(b). Pore pressure plays a secondary role in this case by accelerating the spalling.

Table 2.2 Parameters affect the HSC spalling

Parameter	Influence	explanation
Concrete strength	High concrete strength is more susceptible to spalling	Higher strength could be attributed to lower permeability, more susceptible to spalling. 80~100MPa $10^{-15} \sim 10^{-19}$ m/s; and 30~40 MPa $10^{-12} \sim 10^{-13}$ m/s
Concrete density	Lightweight concrete is spalling more	Higher spalling in lightweight HSC, which has higher free moisture in the lightweight aggregate.
Load Intensity/type	More loading more spalling Eccentric and bending members have more spalling	The type and intensity of load have a significant influence on spalling. Loaded HSC member is susceptible to higher spalling. Eccentric loading induces additional compressive and tensile stress, which increases spalling.
Moisture content	Higher relative humidity, higher the spalling	Higher relative humidity leads to higher spalling.
Fire intensity	Faster heating rate, higher fire intensities, the higher the spalling	The extent of spalling is much higher when the HSC is exposed to a faster heating rate or higher fire intensities, such as hydrocarbon fire.
Aggregate type	Siliceous has higher spalling than carbonate aggregate concrete	Higher spalling in siliceous aggregate concrete than in carbonate aggregate concrete.
Specimen dimensions	The larger the size, the higher the risk of explosive spalling	The risk of explosive thermal spalling increases with the specimen size, larger structures would store more energy.

Kodur et al. (2004) did fire tests on HSC columns and concluded that spalling occurs when the temperature in the concrete reaches above 350°C. The tests showed that spalling occurs only outside the reinforcement cage. Shin et al. (2011) introduced a very simple approach based on experimental observations, Fig. 2.12. For a rectangular section of a simply supported beam, the top part is in compression and is susceptible to spalling and can be accounted for by removing parts of the section. Shin et al. assumed that after 20 minutes of fire exposure, the section area is reduced by 7.5%, which can be modelled by partially removing parts of the sides. After 50 minutes

of fire exposure, additional spalling happens and the section area reduces further to 82.5% of the original area. The additional reduction can be modelled by removing additional parts near the top of the section.

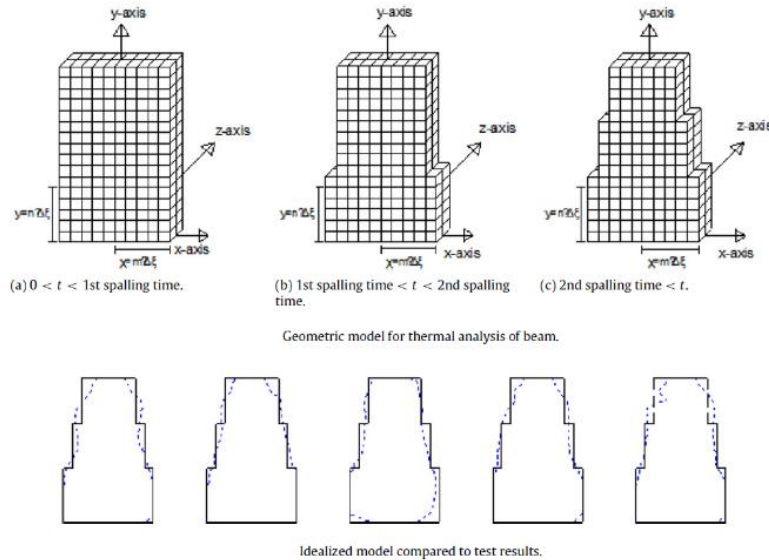


Figure 2.12 Simplified model to account for explosive spalling (Shin, 2011)

2.4 Reinforcing Steel Properties at Elevated Temperature

2.4.1 Strand Mechanical Properties

The commonly used prestressing strands in North America are the low-relaxation seven-wire strands, which have ambient temperature ultimate tensile stress of 1860 MPa. Prestressing strands exhibit a slight loss of strength for temperatures up to 200°C. Then, they start losing strength at a rapid pace. This strength loss is associated with a significant reduction in the failure strain (blue brittleness effect). Kodur (2016) noticed that strands stressed to 50% of their yielding stress rupture at around 450°C. Based on test data, Zhang (2007) proposed a mathematical approach to estimate the proportional strength, 0.2% yield strength, ultimate strength, and elastic modulus of seven-wire strands exposed to fire. Kodur (2016) also proposed a set of relationships to estimate the reduction in yield strength, ultimate strength, failure strain, and elastic modulus of prestressing strands at elevated temperatures. The Eurocode EN1992-1-2 (2004) provides a tri-linear model for the stress-strain relationships of the strands at different temperatures. A review of the literature

shows that this model ignores some of the important features of the response, such as the strain hardening phase and the decrease in the failure strain at higher temperatures. As a result, the Eurocode model is over-conservative for strength and unconservative for strains (Kodur, 2016). A comparison of the Eurocode model and test results (Kodur, 2016) is shown in Figure 2.13.

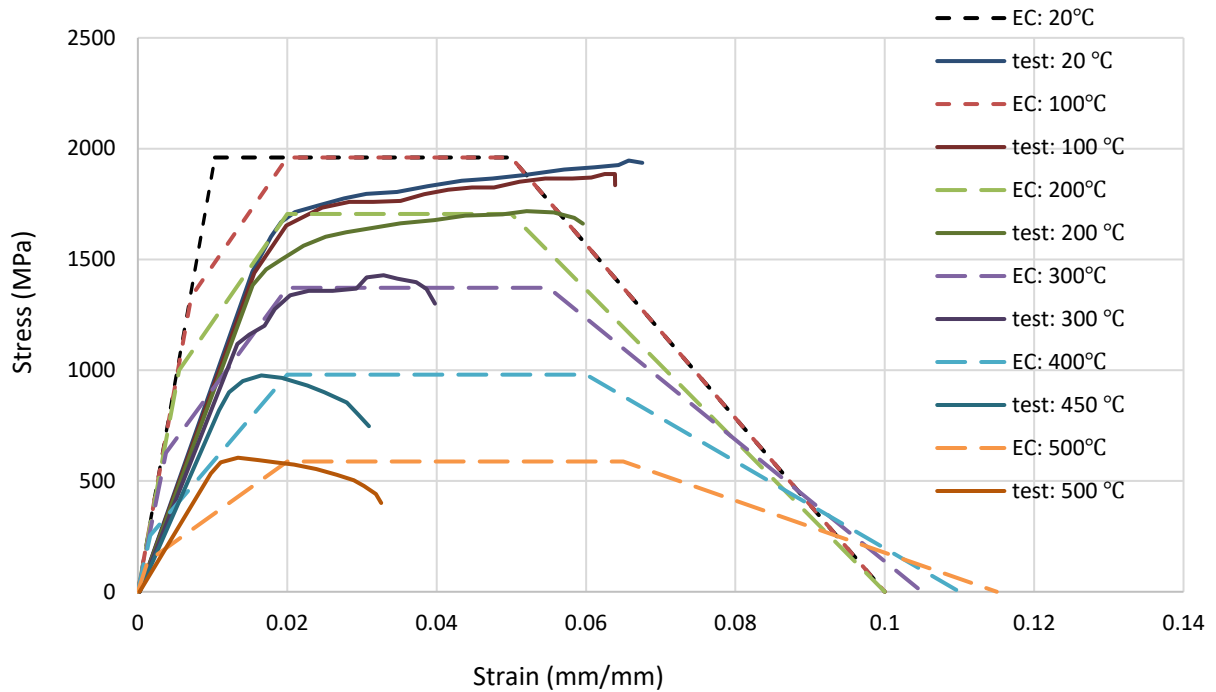


Figure 2.13 Comparison of Euro Code model and testing curves of strand stress-strain relationship

2.4.2 Properties of regular steel bars at elevated temperatures

The mechanical properties of reinforcing bars include yield strength, ultimate strength, elastic modulus, and related strains. Yield strength and modulus of elasticity of reinforcing steel bars decrease with temperature. At high temperatures, the total strain of the steel bars is a combination of thermal and load strains (Li and Purkiss, 2005). The Eurocode EN 1992-1-2 (2004) model for steel bars assumes an elastic-plastic behaviour at temperatures lower than 100°C with ambient values for the yield strength (f_{ys}) and the elastic modulus (E_s). At higher temperatures, f_{ys} and E_s are reduced by factors $k_{y,T}$ and $k_{E,T}$, respectively. The shape of the stress-strain curve also changes at higher temperatures to include a transition curve between the proportional stress and the

perfectly plastic stage. Eurocode defines the proportional stress (f_p) at the initiation of this nonlinear behaviour. f_p is initially assumed to be equal to f_{ys} at temperatures below 100°C, and then reduces with increasing temperature by a factor $k_{p,T}$. Following the nonlinear region, the yield plateau is reached at a yield strain ε_y and ends at ultimate strain ε_u . Fracture at strain ε_{fr} is then reached as a linear declining branch from the yield plateau. Eurocode sets constant values for ε_y , ε_u , and ε_{fr} as: 0.02, 0.10, and 0.15, respectively, for Class A (low ductility); and 0.02, 0.15, and 0.20, respectively, for Class B (high ductility).

Lie (1992) provided a stress-strain model for steel bars exposed to fire. The model defines a proportional strain ε_p , which is a function of the steel ambient temperature yielding stress ($\varepsilon_p = 4 \times 10^{-6} f_{y0}$). When the steel strain (ε_s) is less than ε_p , the steel stress is calculated by multiplying ε_s by the modulus of elasticity, which is only affected by the temperature (T). When $\varepsilon_s > \varepsilon_p$, the steel stress is ε_s multiplied by a factor, which is a function of T , ε_s , and ε_p . This model has a post-yield hardening tendency, which is distinctively different from the Eurocode post-yield plateau model.

2.5 Moment-curvature of prestressed Beam section

The principle of reinforced concrete structure design is to efficiently use the compressive resistance of concrete and tensile resistance of steel to achieve a perfect balance of the yielding and ultimate stress-strain of different materials. In a properly designed prestressing member, the stresses from the external loads are counteracted by the prestress loads so that cracks and deformations are much smaller than for regular reinforced concrete members. An ideal flexural behaviour of a prestressed concrete beam would have the moment-curvature relationship shown in Figure 2.15 (Youssef, 2020). Under dead load only, the beam would have a negative curvature (camber). Applying the live load to the beam, its behaviour will be between the decompression and cracking points.

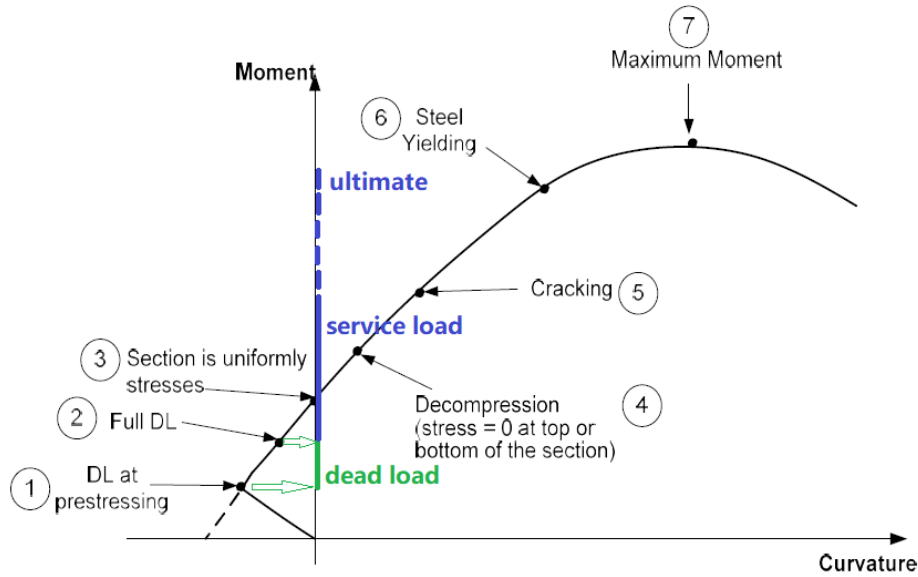


Figure 2.14 Ideal moment-curvature curve of a prestressed beam

In the service stage of a prestressed beam, the top and bottom concrete stresses follow the linear elastic theory, Equation 2-14.

$$\begin{aligned} f_{top} &= \frac{-P_e}{A} + \frac{e \cdot P_e}{S_t} - \frac{M}{S_t} \geq f_{ce} \\ f_{bottom} &= \frac{-P_e}{A} - \frac{e \cdot P_e}{S_b} + \frac{M}{S_b} \leq f_{te} \end{aligned} \quad \text{Eq. 2.14}$$

Where: P_e is the effective prestressing force, A is the cross-section of the beam, e is the eccentricity of strands, S_t and S_b are the first moment of area of the top and bottom zones of the section, M is the specified moment, f_{ce} and f_{te} are the concrete compressive and tensile strengths.

To account for the nonlinear variation of thermal strains, Eq. 2.15 presents the equilibrium for the axial force and the bending moment. Using this equation with the thermal condition allows for evaluating the structural behaviour of a beam section including the strain distribution and curvature.

$$\begin{aligned} N &= \oint_{A_c} f_c dA_c + \oint_{A_s} f_s dA_s + \oint_{A_p} f_p dA_p \\ M &= -\oint_{A_c} f_c y dA_c - \oint_{A_s} f_s y dA_s - \oint_{A_p} f_p y dA_p \end{aligned} \quad \text{Eq.2.15}$$

2.6 Conclusions

The following points were reached in this chapter.

1. The behaviour of a concrete structural member exposed to fire is dependent on the thermal, mechanical, and deformation properties of the concrete. The properties of HSC ($f_{c20}' > 55$ MPa) vary differently with temperature than those of normal strength concrete (NSC, $f_c' < 55$ MPa). The strength loss of HSC is greater than NSC, and spalling occurs at around 200 to 350°C due to the resistance to water vapour transport during heating. The thermal properties of HSC are slightly different from NSC because HSC has a denser microstructure resulting from a relatively higher amount of cement and fewer voids. This results in a lower rate for the temperature transfer speed, which increases the temperature gradient in the element.
2. Natural fires are significantly different from standard fires. To utilize the wealth of knowledge associated with standard fire exposure, the use of a standard fire with a specific duration to represent a natural fire is very appealing. Many methods are available for establishing such an equivalent standard fire including a method that tries to match the temperature distribution for the two fires.
3. The strength of prestressing strands decays faster than regular steel bars. The prestressing load causes the strands to have an early rupture.
4. Modelling the behaviour of HSC prestressed members is challenging and the literature is missing simplified approaches that can be utilized by engineers.

2.7 Reference

Achenbacha et al., *Identification of the thermal properties of concrete for the temperature calculation of concrete slabs and columns subjected to a standard fire—Methodology and proposal for simplified formulations*, Fire Safety Journal, 87 (2017) 80-86, 2017

ACI, *Report No. ACI 363R-92, State-of-the-art report on high-strength concrete*, American Concrete Institute Committee 363, Detroit, Michigan, US, 1992

American Society for Testing and Materials, *ASTM E119-20, Standard Test Methods for Fire Tests of Building Construction and Materials*, PA, USA, 2020

American Society of Civil Engineers, *ASCE 7-16 Minimum Design Loads and Associated Criteria for Buildings and Other Structures*, Reston, VA, 2018

BSI, *BS 476-20:1987, Fire tests on building materials and structures - Method for determination of the fire resistance of elements of construction (general principles)*, British Standards Institution, 2014

Cooper and Steckler, *NISTIR 5842: Methodology for developing and implementing alternative temperature-time curves for testing the fire resistance of barriers for nuclear power plant applications*, NIST, MD, USA, 1996

CSA Canada, *CSA A23.3: Design of concrete structures*, Ottawa, Canada, 2019

Dwaikat, *Fire Induced Spalling In High Strength Concrete Beams*, Fire Technology, 46, (2010) 251–274, 2010

European Committee for Standardization, *EN 1991-1-2: Actions on Structures Exposed to Fire*, Brussels, Belgium, 2002

European Committee for Standardization, *EN 1992-1-2:2004, Eurocode 2: Design of concrete structures - Part 1-2: General rules - Structural fire design*, Brussels, Belgium. 2004

Gernay et al., *A formulation of the Eurocode2 concrete model at elevated temperature that includes an explicit term for transient creep*, Fire Safety Journal, 51(2012) 1–9, 2012

- International Code Council, Inc, *International Building Code 2018*, Washington, DC, 2018
- International Organization for Standardization, *ISO 834-11:2014 Fire resistance tests - Elements of building construction*, Geneva, Switzerland, 2014
- Khennane and Baker, *Plasticity models for the biaxial behaviour of concrete at elevated temperatures*, Computer Methods in Applied Mechanics and Engineering, Volume 100, Issue 2, October 1992, Pages 207-223, 1992
- Khoury et al., *Modelling of heated concrete*, Magazine of Concrete Research, 54, No. 2, April, 77-101, 2002
- Kodur et al., *Effect of Temperature on the mechanical properties of low relaxation seven-wire prestressing strand*, Construction and Building Materials 124 (2016) 74–84, 2016
- Kodur et al., *Effect of Temperature on Thermal Properties of Different Types of High-Strength Concrete*, Journal of Materials in Civil Engineering, Vol. 23, No. 6: 793-801, 2011
- Kodur et al., *Energy based time equivalent approach for evaluating fire resistance of reinforced concrete beams*, Fire Safety Journal 45 (2010), page 211–220, 2010
- Kodur et al., *Predicting the fire resistance behaviour of high strength concrete columns*, Cement & Concrete Composites 26 (2004) 141–153, 2004
- Kodur, *Properties of concrete at elevated temperatures*, ISRN Civil Engineering, Volume 2014, Article ID 468510, 2014
- Kodur, *Spalling in High Strength Concrete Exposed to Fire – Concerns, Causes, Critical Parameters and Cure*, Advanced Technology in Structural Engineering, Institute for Research in Construction, National Research Council of Canada, 2000
- Kuehnen, *Equivalent standard fire duration to evaluate internal temperatures in natural fire exposed RC beams*, Fire Safety Journal vol.108 102831, 2019
- Lennon, *The natural fire safety concept—full-scale tests at Cardington*, Fire Safety Journal 38 (2003) 623–643, 2003
- Lie, *ASCE Manuals and Reports on Engineering Practice, No.78: Structural Fire Protection*, American Society of Civil Engineers, ISBN 0-87262-888-4, 1992

- NRC Canada, *Nation Building Code of Canada, 2020 Volume 1*, Ottawa, Canada, 2020
- Phan, *High-Strength Concrete at High Temperature – An Overview*, NIST, 2002
- Phan, *NISTIR 5934: Fire performance of high-strength concrete A report of the state-of-the art*, National Institute of Standards and Technology, 1996
- Shin, *The structural behaviour and simplified thermal analysis of normal-strength and high-strength concrete beams under fire*, *Engineering Structures* 33 (2011) 1123–1132, 2011
- Terro, *Numerical modeling of the behaviour of concrete structures in fire*, *ACI Structural Journal*, March 1998
- Wickstrom, *A very simple method for estimating temperature in fire exposed concrete structures*, Swedish National Testing Institute, Fire Technology Technical Report SP-RAPP, 1986
- Youssef, *General stress–strain relationship for concrete at elevated temperatures*, *Engineering Structures* 29 (2007) 2618–2634, 2007
- Youssef, *Lecture notes of “CEE9628, Prestressed Concrete”*, UWO, London, ON, Canada, 2020
- Yu, *Fire-Resistance Mechanism and Residual Bearing Capacity of Prestressed Concrete Beams after Fire Exposure*, *Journal of Structural Engineering*, ASCE, ISSN 0733-9445, 2021
- Zhang, *Mechanical property of steel strand at high temperature*, *Journal of Harbin Institute of Technology*, Vol.39, No.6, 2007

Chapter 3 Simplified Modeling of Prestressed Concrete Girders during Fire Exposure

Abstract

To evaluate the behaviour of structures exposed to fire and estimate their structural fire resistance, engineers need design tools to overcome the complexities associated with structural analysis during fire exposure. These complexities include the uneven distribution of temperature within the structural elements and the deterioration in material properties. This chapter introduces a simplified numerical model to evaluate the flexural behaviour of bonded prestressed high-strength concrete sections exposed to fire. The model starts by predicting the temperature distribution within a structural element using 2-D finite difference analysis. It then uses one-dimensional sectional analysis to estimate the section behaviour. An example demonstrating the use of the model is also given.

3.0 Introduction

The “Best Practice Guidelines for Structural Fire Resistance Design of Concrete and Steel Buildings” (NISTIR 7563, 2009) stipulates that structural design for fire safety can be achieved either by controlling the fire spread or preventing structural collapse. This chapter focuses on the development of a simplified model to predict the structural behaviour of prestressed concrete girders during fire exposure, and thus addresses the latter approach.

To analyze and design a concrete structure exposed to fire, NISTIR 7563 (2009) highlights the need to address technical issues, which are considerably different from regular concrete structural design. These issues include the assumption of the applied loads during a fire incident; estimation of the internal forces associated with thermal strains; accounting for degradation in material properties; accounting for explosive spalling; examining the effect of the potential large deflections on the strength and global stability; and understanding the potential failure mechanisms. The model developed in this chapter addresses these issues.

The use of finite element analysis to predict the structural behaviour of concrete girders during fire exposure has many challenges and requires significant expertise. Challenges include accounting

for variations in the material properties within the cross-section based on the temperature contours. Another challenge is resolving analysis issues associated with negative tangential modulus, which is expected during fire exposure. Such problems can be addressed at the research level, e.g., Kumar and Kodur (2021) addressed the FEM convergence issues associated with the significant changes in stiffness arising from temperature-induced softening in the material properties.

To overcome the complexities associated with conducting finite element analysis of normal-strength concrete girders exposed to standard fire, El-Fitiany and Youssef (2009) developed a simplified sectional analysis method. This method was then utilized by El-Fitiany and Youssef (2014) to propose equivalent stress block parameters suitable for estimating the flexural capacity of RC beams exposed to fire. The simplified sectional analysis method starts by evaluating the temperature distribution within a cross-section using transient thermal analysis. El-Fitiany and Youssef (2009) utilized the finite difference method (FDM) to complete this step. Then, they developed rules to convert the obtained two-dimensional temperature contours to one-dimensional variation, which allows applying principles of equilibrium of forces and compatibility of strain distribution to estimate the moment-curvature relationship. This method was later utilized by other researchers, such as Kuehnen (2019), who extended the method to be valid for natural fire exposure, and Sabsabi (2021), who extended the method to be used for the structural analysis of glass panels.

Numerous tests were conducted to evaluate the mechanical properties of HSC at elevated temperatures as compared to normal-strength concrete (Castillo, 1990; Phan, 1996; Kodur, 2004). HSC was found to be different in the strength loss pattern as it loses its strength much faster in the intermediate temperature range (100~400 °C) and is more prone to explosive spalling at the intermediate temperature range (NISTIR 6726, 2001). Spalling of HSC reduces or eliminates the cover protecting the steel bars from the high fire temperature and reduces the section dimensions. Experimental tests by Phan (1996), Kodur (2000), Dwaikat (2010) have shown that explosive spalling is affected by the fire temperature, concrete moisture content, concrete pores, stress distribution, and concrete tensile resistance.

This chapter provides a simplified tool to predict the duration an HSC prestressed beam can withstand a fire incident, as well as estimate its deformation throughout the fire duration. The proposed tool will not only save time and computing efforts but will also allow the users to develop

a deep understanding, and thus develop their engineering sense in the area of structural fire engineering.

3.1 Modeling Approach

The developed tool applies a modified version of the methodology developed by El-Fitiany and Youssef (2009). The modifications include accounting for the material properties of high-strength concrete and prestressing strands, making the tool valid for any section shape, and modelling of explosive spalling. Also, a user-friendly interface was developed for the tool, which utilizes MATLAB and EXCEL software. A flowchart of the overall procedure is shown in Figure 3.1. Transient thermal analysis is conducted first. Then, the modified sectional analysis is utilized to predict the section behaviour. The following general assumptions were made.

- 1) The concrete member is assumed homogenous and isotropic, i.e., ignoring the concrete microstructure.
- 2) Thermal analysis is conducted assuming the member is uncracked, i.e., ignoring the effect of the mechanical damage on the temperature distribution within the element.
- 3) Euler–Bernoulli hypothesis is valid at elevated temperatures, i.e., plane sections remain plane.
- 4) A perfect bond exists between concrete and the reinforcing bars and strands.
- 5) The member's behaviour is governed by flexural deformations.
- 6) Loads are applied statically.

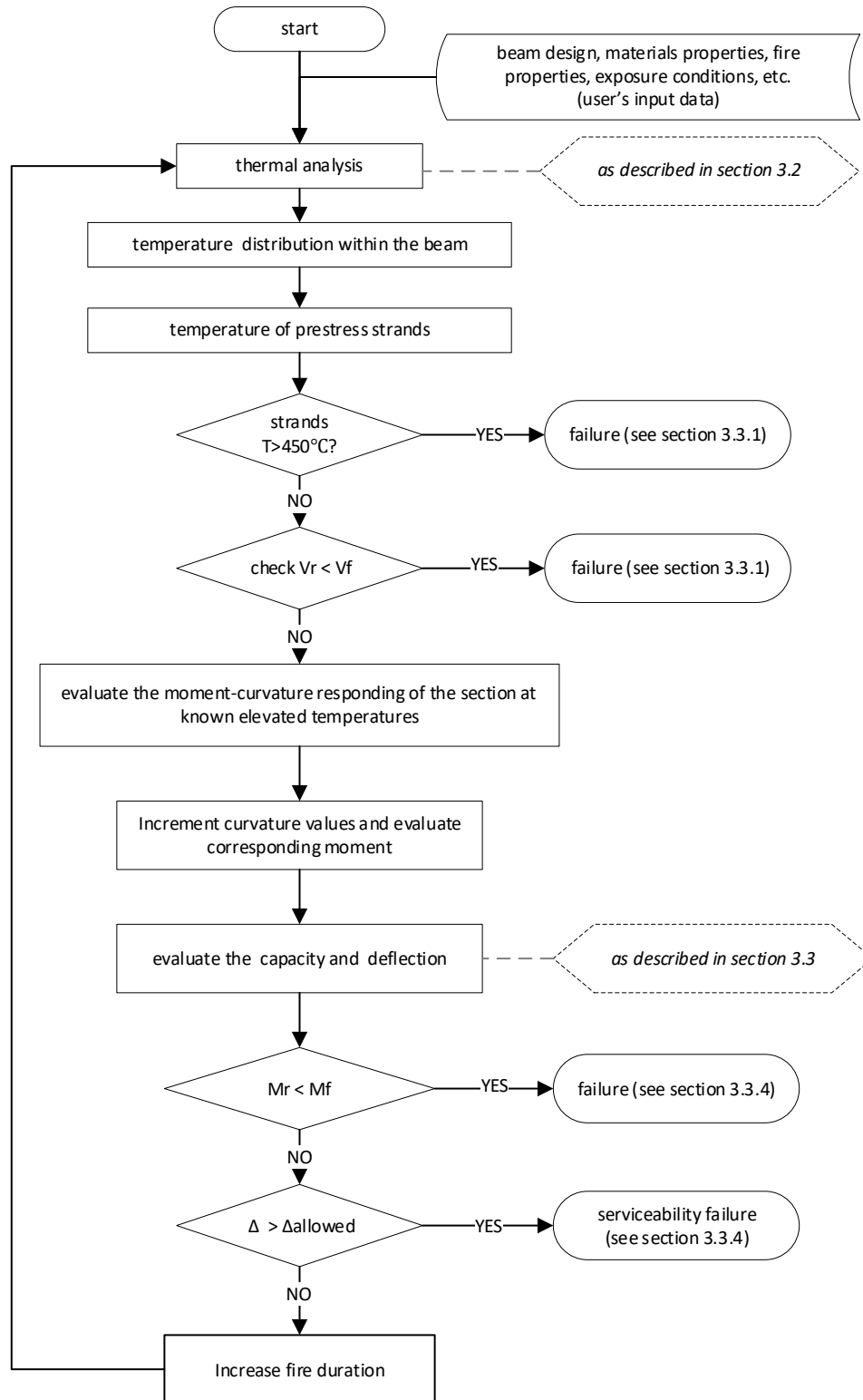


Figure 3.1 Overall procedure to evaluate a prestress girder's fire performance

3.2 Transient Thermal Analysis

The effect of the strands and rebars on the distribution of the temperature within the concrete section is ignored due to their relatively small size. Also, heat transfer along the longitudinal axis of the beam is ignored, simplifying the transient-thermal analysis to a two-dimensional problem.

3.2.1 Thermal properties of HSC

The thermal capacity (c_p), and conductivity (k_t) of high-strength concrete are modelled following EuroCode (EN1992-1-2, 2004) and Kodur et al. (2011). c_p is calculated as the product of the density (ρ in kg/m^3) and the specific heat (c in $\text{J/kg } ^\circ\text{C}$). Eq. 3.1 estimates the value of c at different temperatures (T in $^\circ\text{C}$) as per the EuroCode (EN1992-1-2, 2004). k_t is modelled following Kodur et al. (2011), Eq. 3.2.

$$c = \begin{cases} 900 & 20^\circ\text{C} \leq T \leq 100^\circ\text{C} \\ 900 + (T - 100) & 100^\circ\text{C} < T \leq 200^\circ\text{C} \\ 1000 + (T - 200)/2 & 200^\circ\text{C} < T \leq 400^\circ\text{C} \\ 1100 & 400^\circ\text{C} < T \leq 1000^\circ\text{C} \end{cases} \quad \text{Eq. 3.1}$$

$$k_t = \begin{cases} 2.5 - 0.0033 \times T & 20^\circ\text{C} \leq T \leq 400^\circ\text{C} \\ 2.3 - 0.0020 \times T & 400^\circ\text{C} \leq T \leq 800^\circ\text{C} \end{cases} \quad \text{Eq. 3.2}$$

3.2.2 Concrete surface temperature

At a specific standard fire duration, the surface temperature of the concrete is calculated using Equation 3.3, which was recommended by Wickstrom (1986).

$$T_w = \eta_w T_f = 1 - 0.0616 \cdot t_w^{-0.88} \quad \text{Eq. 3.3}$$

where T_w is the concrete surface temperature ($^\circ\text{C}$), T_f is the fire temperature ($^\circ\text{C}$), t_w is the equivalent exposure time (hours), $t_w = (\sqrt{F}/\gamma_i)t$, and \sqrt{F}/γ_i is the factor to adjust the difference between the compartment fire and concrete properties.

3.2.3 Spalling of HSC in this numerical model

The literature is still missing a universal spalling model. Thus, a simple model was adopted in this research. The model is based on experimental observations by other researchers. Spalling is

simulated by reducing the section dimensions, i.e., by removing layers of the concrete cover. Spalling was assumed to only affect the concrete cover as prestressed concrete beams are expected to have an adequate number of stirrups preventing spalling of the concrete core as observed by Kodour (2004). The concrete surface temperature was assumed to be the sole factor for spalling and was included in the model as an input parameter, which is expected to vary between 350°C and 500°C as observed by Kodour (1998) and Phan (1996). In the model, once the temperature for any of the elements within the cover reaches the spalling temperature, heat transfer calculations are repeated after removing the affected elements. Figure 3.2 shows an example of spalling occurring during heat transfer calculations. Spalling is assumed to only affect HSC, so the NSC concrete slab did not experience any spalling.

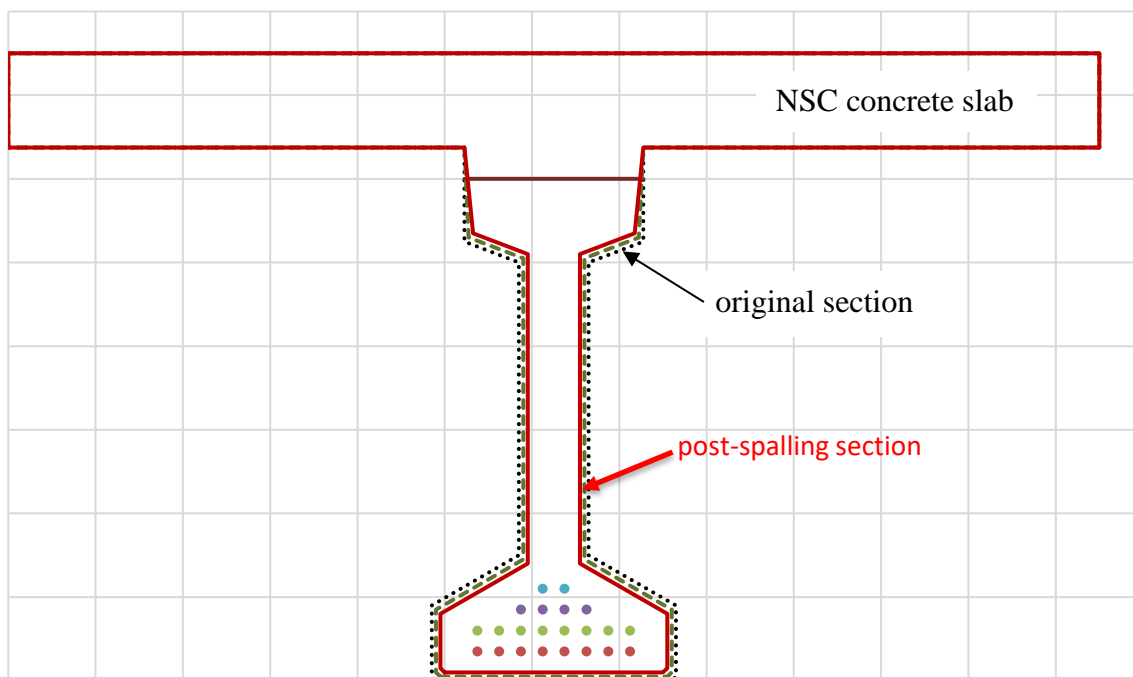


Figure 3.2 Section before and after spalling

3.2.4 Heat transfer calculations

The analysis starts by dividing the beam section into a finite number of meshed elements, as shown in Figure 3.3 for a CPCI-1200 girder with a topping slab. The time-dependent concrete surface temperature, estimated in the previous section, is then applied as a boundary condition for the

concrete section. Heat, within the section, is assumed to be only transferred by conduction. Thus, the temperature of the elements can be calculated by discretization of both the spatial and time domains of the heat transfer differential equation, Equation 3.4.

$$\rho c \frac{\partial T}{\partial t} - k_t \nabla^2 T = 0 \quad \text{Eq. 3.4}$$

Where ρ : density (kg/m³), c : specific heat (J/kg°C), k_t : thermal conductivity (W/m°C). Eq. 3.4 is solved numerically using MATLAB. The solution typically requires iterations because of the dependence of the thermal properties on the temperature and the reduction of the section dimensions because of spalling. The utilized MATLAB's built-in functions are:

1. *thermalProperties*, which is used to define the material thermal properties based on the element's temperature.
2. *thermalBC*, which defines the boundary conditions as the given concrete surface temperatures.
3. *thermalIC*, which defines the initial conditions including the initial temperature and the mesh to be used for the next iteration.

As spalling changes the section dimensions, the original thermal mesh becomes invalid and a revised thermal mesh is developed. The pre-spalling temperature distribution is used to define the initial condition and the surface temperature. In this case, the built-in functions cease to be feasible because of MATLAB limitations. Thus, the partial differential equation, Equation 3.4, was solved in a classical way using MATLAB's function "*parabolic*". This function solves the general case presented by Eq. 3.5 (where m , u , c , a , f are the parameters of the mathematical expression). To solve Eq. 3.4, m , a , and f are set equal to zero. Also, u , d , and c are replaced with T , ρc , and k_t . The resulting temperature contours for the example CPCI-1200 girder after 60 minutes of ASTM standard fire exposure is shown in Fig. 3.3 (c).

$$m \frac{\partial^2 u}{\partial t^2} + d \frac{\partial u}{\partial t} - \nabla(c * \nabla u) + au = f \quad \text{Eq. 3.5}$$

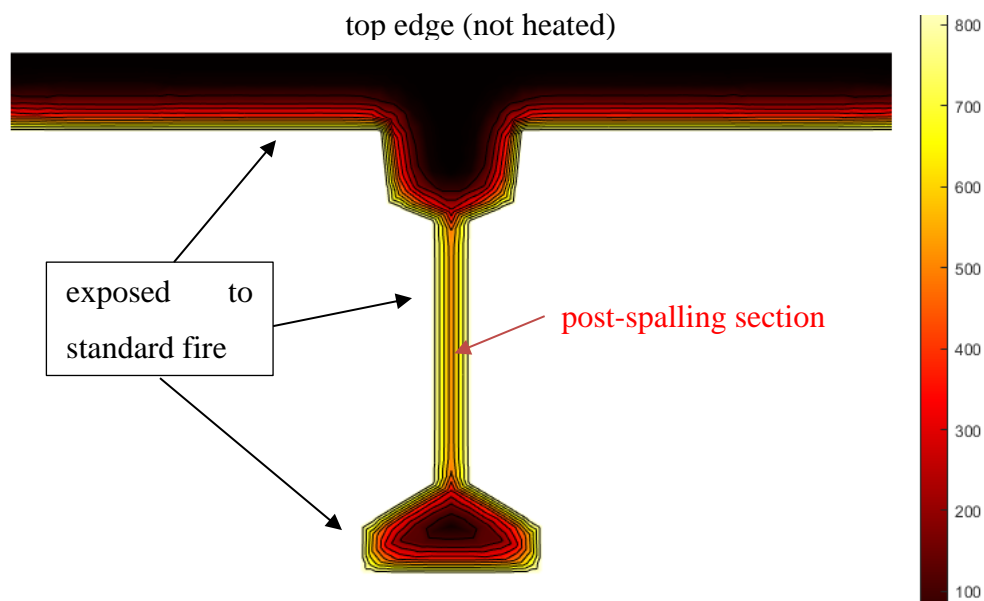
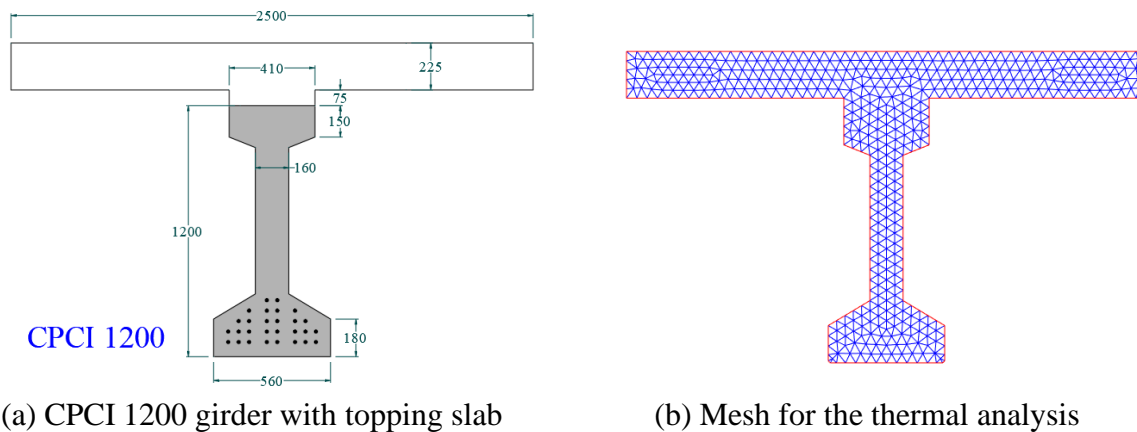


Figure 3.3 Heat transfer analysis for CPCI-1200 girder with a topping slab

3.3 Mechanical Analysis

This section details the proposed assumptions and steps to predict the structural behaviour of a prestressed concrete girder during exposure to fire based on the thermal transient analysis results.

3.3.1 Material constitutive models

Eq. 3.6 (a), proposed by ASCE-78 (1992) and NIST Technical Note 1681 (2010), is used to define the thermal expansion coefficient of concrete ($\varepsilon_{th,c}$) at elevated temperatures. The thermal expansion coefficient of steel bars and strands ($\varepsilon_{th,s}$) is calculated using Eq 3.6 (b), which is also recommended by ASCE-78 (1992) and NIST (2010).

$$\varepsilon_{th,c} = (0.008T + 6) \times 10^{-6} \quad \text{Eq. 3.6 (a)}$$

$$\varepsilon_{th,s} = (0.004T + 12) \times 10^{-6} \quad T < 1000^\circ\text{C} \quad \text{Eq. 3.6 (b)}$$

The stress-strain curve for high-strength concrete (HSC) is assumed to follow the model proposed by Kodur (2014), Eq. 3.7. Where $\varepsilon_{o,T}$ is the strain at peak strain, ε is the mechanical concrete strain corresponding to concrete stress $f_{c,T}$.

$$f_{c,T} = \begin{cases} f'_{c,T} \left[1 - \left(1 - \frac{\varepsilon}{\varepsilon_{o,T}} \right)^{2.28 - 0.012f'_c} \right], & \varepsilon \leq \varepsilon_{o,T} \\ f'_{c,T} \left[1 - \left(\frac{30}{130 - f'_c} \cdot \frac{\varepsilon - \varepsilon_{o,T}}{\varepsilon_{o,T}} \right)^2 \right], & \varepsilon > \varepsilon_{o,T} \end{cases} \quad \text{Eq. 3.7 (a)}$$

$$\varepsilon_{o,T} = 0.0018 + (6.7f'_c + 6.0T + 0.03T^2) \times 10^{-6} \quad \text{Eq. 3.7 (b)}$$

$$f'_{c,T} = \begin{cases} f'_{c,20} [1.0625 - 0.003125(T - 20)] & T < 100^\circ\text{C} \\ 0.75f'_{c,20} & 100^\circ\text{C} \leq T \leq 400^\circ\text{C} \\ f'_{c,20} [1.33 - 0.00145T] & T > 400^\circ\text{C} \end{cases} \quad \text{Eq. 3.7 (c)}$$

The model implicitly accounts for transient strains developed during the initial heating stage. Thus, the strain value ($\varepsilon_{o,T}$), which corresponds to the maximum concrete stress, includes the transient strain component (ε_{tr}).

The ultimate strain (ε_{uT}) is estimated by increasing the ultimate strain at ambient temperature (ε_{u20}) by the ratio of the ε_{oT} at the elevated temperature and its value at T of 20 °C. The value of ε_{u20} is estimated based on Eq. 3.9 by Ozbakkaloglu et al. (2004). Where f_{c20} ' is the concrete compressive strength at ambient temperature. The tensile strength of concrete was ignored. Figure 3.4 shows an example of the increase in strains at elevated temperatures.

$$\varepsilon_{u20} = 0.0036 - (f_{c20}' - 30) \times 10^{-5} \quad \text{where: } 30 \text{ MPa} \leq f_{c20}' \leq 120 \text{ Mpa} \quad \text{Eq. 3.9}$$

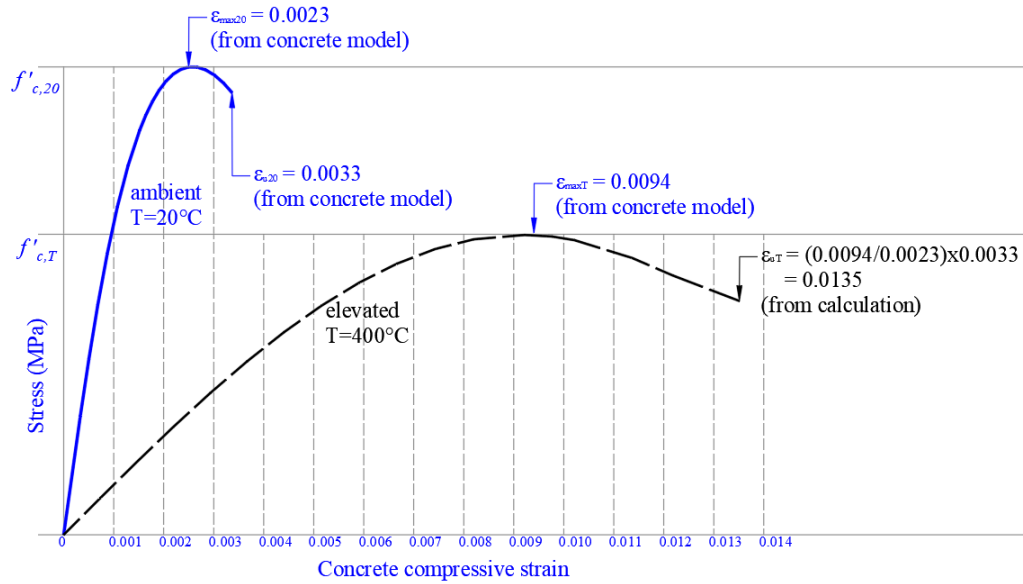


Figure 3.4 Concrete ultimate strain at elevated temperatures

The stress-strain model for the prestressing strands is assumed to follow the testing data of Shakya et al. (2016), shown in Figure 3.5. These data are based on experiments on strands pre-tensioned to 50% of their ultimate capacity (f_{pu}) before exposure to elevated temperatures. Failure of these strands was observed at a temperature of 450°C (Kodur, 2016).

Based on Figure 3.5, the constitutive model for the strands can be assumed bilinear. Using regression analysis, Eq. 3.10 was developed to define the main points for the model, which are the yield strength (f_{pyT}), the ultimate strength (f_{puT}), the failure strain (ε_{pkT}), and the elastic modulus (E_{pT}). f_{py} , f_{pu} , ε_{pk} , and E_p define the values of these variables at ambient temperature.

$$\begin{aligned} f_{pyT} &= \left(\frac{6 \times T^4}{10^{12}} - \frac{6 \times T^3}{10^9} - \frac{9 \times T^2}{10^8} - \frac{6 \times T}{10^4} + 1.0196 \right) \cdot f_{py} \\ f_{puT} &= \left(\frac{T^4}{10^{12}} + \frac{3 \times T^3}{10^9} - \frac{6 \times T^2}{10^6} + \frac{6 \times T}{10^4} + 0.9895 \right) \cdot f_{pu} \\ \varepsilon_{pkT} &= \left(\frac{-7 \times T^4}{10^{11}} + \frac{T^3}{10^7} - \frac{6 \times T^2}{10^5} + \frac{8.2 \times T}{10^4} + 0.8276 \right) \cdot \varepsilon_{pk} \\ E_{pT} &= \left(\frac{7 \times T^4}{10^{12}} - \frac{9 \times T^3}{10^9} + \frac{2 \times T^2}{10^6} - \frac{2 \times T}{10^4} + 1.0099 \right) \cdot E_p \end{aligned} \quad \text{Eq. 3.10}$$

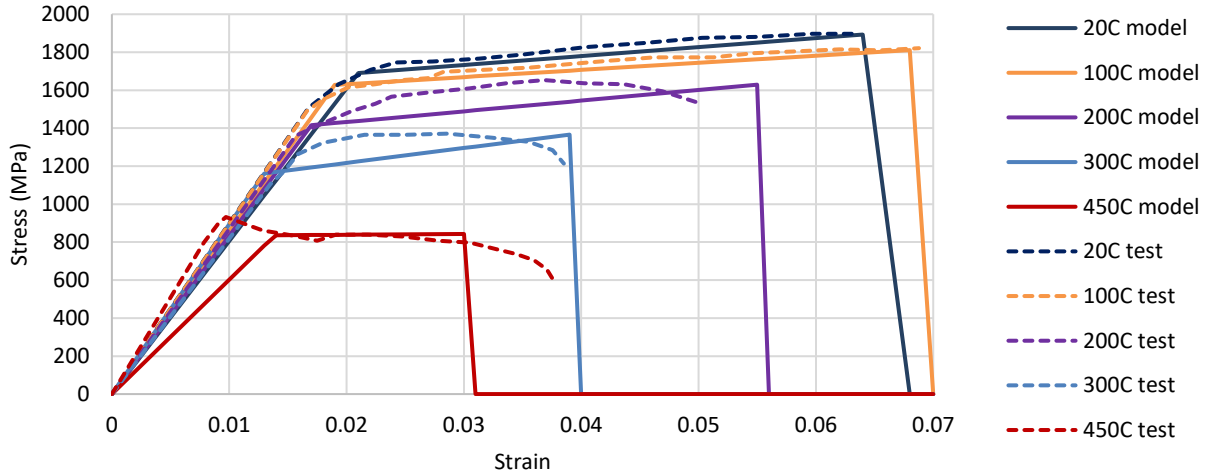


Figure 3.5 Stress-strain model for 7-wire-strand at elevated temperatures

For regular reinforcing steel, the constitutive model, Eq. 3.11, given by ASCE-78 (1992), is used after modifying it to follow the post-yielding behaviour recommended by the Euro code (EN 1992-1-2:2004). Strain hardening was assumed to be equal to zero, i.e., stress remains constant after yielding.

$$f_{sT} = \frac{F(T,0.001)}{0.001} \varepsilon_s \quad \varepsilon_s \leq \varepsilon_{sp} \quad \text{Eq. 3.11 (a)}$$

$$f_{sT} = \frac{F(T,0.001)}{0.001} \varepsilon_{sp} + F(T, (\varepsilon_s - \varepsilon_{sp} + 0.001)) - F(T, 0.001) \quad \varepsilon_s > \varepsilon_{sp}$$

$$\varepsilon_{sp} = 4 \times 10^{-6} f_{syo} \quad \text{Eq. 3.11 (b)}$$

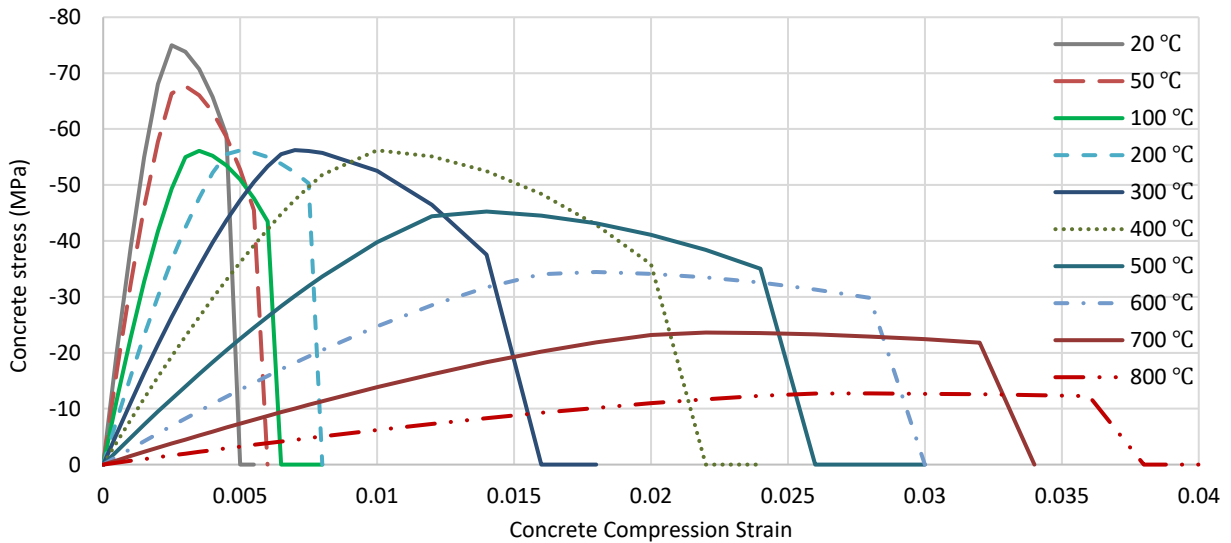
$$F(T, 0.001) = (50 - 0.04T) \left[1 - e^{(-30+0.03T)\sqrt{0.001}} \right] \times 6.9 \quad \text{Eq. 3.11 (c)}$$

$$F(T, (\varepsilon_s - \varepsilon_{sp} + 0.001)) = (50 - 0.04T) \left[1 - e^{(-30+0.03T)\sqrt{\varepsilon_s - \varepsilon_{sp} + 0.001}} \right] \times 6.9 \quad \text{Eq. 3.11 (d)}$$

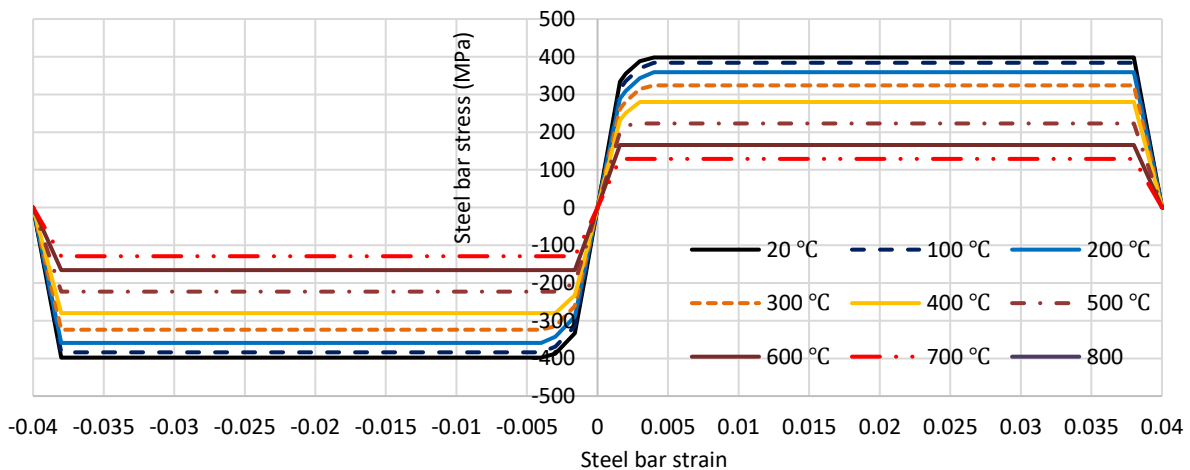
$$f_{syT} = \left[1.0 + \frac{T}{900 \ln\left(\frac{T}{1750}\right)} \right] f_{syo} \quad (0 < T \leq 600^\circ\text{C}) \quad \text{Eq. 3.11 (e)}$$

Where: T is the steel reinforcement temperature in $^\circ\text{C}$, ε_s is the steel strain, ε_{sp} is the proportional steel strain, f_{sT} is the steel stress at T , f_{syT} is the steel yield stress at T , and f_{syo} is the steel yield stress at ambient temperature.

The constitutive relationships for concrete, strands, and steel were added to MATLAB as spreadsheets that contain the stresses and corresponding strains at different temperatures. For given values of strain and temperature, MATLAB conducts a two-way linear interpolation to define the corresponding stress value. Figure 3.6 and Tables 3.1 and 3.2 show examples of the material data charts and tables for 75 MPa HSC and Grade 400 MPa steel bars.



(a) Constitutive model of HSC at elevated temperatures ($f'_{c20}=75\text{MPa}$)



(b) Constitutive model of a reinforced steel bar at elevated temperatures ($f_{syo} = 400\text{MPa}$)

Figure 3.6 Examples of HSC and reinforcing steel constitutive model charts

Table 3.1 Stress-strain data for HSC considering $f'_{c20}=75\text{MPa}$

f'_c (MPa)	75																
H	1.38																
T (°C)	$\epsilon_{0,T}$	f'_{cT} (Mpa)	f_{cT} (MPa)														
0	0.0023025	75	0.0	5.3	0.0	-21.5	-40.8	-70.4	-73.0	-62.9	0	0	0	0	0	0	0
50	0.0026775	67.96875	0.0	4.2	0.0	-16.9	-32.3	-57.8	-67.7	-63.0	-52.8	0	0	0	0	0	0
100	0.0032025	56.25	0.0	2.9	0.0	-11.7	-22.7	-41.7	-55.0	-55.2	-51.0	-43.5	0	0	0	0	0
150	0.0038775	56.25	0.0	2.4	0.0	-9.8	-19.0	-35.6	-49.0	-56.2	-54.8	-51.2	-45.4	0	0	0	0
200	0.0047025	56.25	0.0	2.0	0.0	-8.1	-15.8	-30.1	-42.4	-52.2	-56.2	-55.0	-52.3	0	0	0	0
250	0.0056775	56.25	0.0	1.6	0.0	-6.7	-13.2	-25.4	-36.3	-45.8	-53.3	-56.2	-55.3	-53.4	0	0	0
300	0.0068025	56.25	0.0	1.4	0.0	-5.6	-11.1	-21.5	-31.0	-39.7	-47.3	-53.3	-56.2	-55.7	-52.6	0	0
350	0.0080775	56.25	0.0	1.1	0.0	-4.7	-9.4	-18.3	-26.6	-34.4	-41.4	-47.6	-52.8	-56.2	-55.3	0	0
400	0.0095025	56.25	0.0	1.0	0.0	-4.0	-8.0	-15.7	-22.9	-29.8	-36.2	-42.1	-47.3	-51.8	-56.2	-35.8	0
450	0.0110775	50.8	0.0	0.8	0.0	-3.1	-6.2	-12.2	-18.0	-23.4	-28.6	-33.5	-38.0	-42.1	-48.8	-41.0	0
500	0.0128025	45.4	0.0	0.6	0.0	-2.4	-4.8	-9.5	-14.0	-18.3	-22.5	-26.4	-30.2	-33.6	-39.8	-41.1	0
550	0.0146775	39.9	0.0	0.4	0.0	-1.9	-3.7	-7.3	-10.8	-14.2	-17.5	-20.6	-23.6	-26.5	-31.7	-38.4	0
600	0.0167025	34.5	0.0	0.3	0.0	-1.4	-2.8	-5.6	-8.2	-10.9	-13.4	-15.8	-18.2	-20.5	-24.7	-34.1	0
650	0.0188775	29.1	0.0	0.3	0.0	-1.1	-2.1	-4.2	-6.2	-8.1	-10.1	-11.9	-13.7	-15.5	-18.8	-29.0	-26.1
700	0.0212025	23.6	0.0	0.0	0.0	-0.8	-1.5	-3.0	-4.5	-5.9	-7.3	-8.7	-10.0	-11.3	-13.8	-23.2	-22.4
750	0.0236775	18.2	0.0	0.0	0.0	-0.5	-1.1	-2.1	-3.1	-4.1	-5.1	-6.0	-7.0	-7.9	-9.7	-16.8	-17.8
800	0.0263025	12.8	0.0	0.0	0.0	-0.3	-0.7	-1.3	-2.0	-2.6	-3.2	-3.8	-4.4	-5.0	-6.2	-11.0	-12.7
1200		0	0.0	0.0	0.0	0.0	0.0	0.0	0.0	0.0	0.0	0.0	0.0	0.0	0.0	0.0	0.0
+ve is compression		ϵ	-0.001	-0.00012	0	0.0005	0.001	0.002	0.003	0.004	0.005	0.006	0.007	0.008	0.01	0.02	0.03

3.3.2 Shear capacity

I- and T-shaped girders usually have thin webs, which make them prone to shear failure. Diab (2014) introduced a simplified method to estimate the shear capacity of a reinforced concrete section during a fire. The method evaluates the average concrete strength ($f'_{cT \text{ average}}$) and the average yield strength of the stirrups ($f_{ysT \text{ average}}$) at a specific fire duration. Then, utilizes the CSA A23.3 (2019) shear capacity formula, Eq. 3.12, to estimate the shear capacity. Diab (2014) used the values recommended by CSA A23.3 (2019) for β_v (0.18), θ_v (35°), and λ (1.0). The same methodology was utilized to estimate the shear capacity of prestressed girders. The program terminates if the shear capacity is reached.

$$\begin{aligned}
 V_{rT} &= V_{cT} + V_{sT} + V_{pT} \\
 V_{cT} &= \lambda \cdot \beta_v \cdot \sqrt{f'_{cT \text{ average}}} \cdot b_w \cdot d_v \\
 V_{sT} &= A_v \cdot f_{ysT \text{ average}} \cdot d_v \cdot \cot\theta_v / s
 \end{aligned}
 \tag{Eq. 3.12}$$

3.3.3 Flexural behaviour

This section details the methodology used to estimate the flexural behaviour of prestress HC beams.

3.3.3.1 Average Temperatures

As beams are only resisting uniaxial moments, a one-dimensional temperature distribution is adequate for the analysis. A modified version of the method proposed by El-Fitiany and Youssef (2009) was utilized to transform the two-dimensional temperature distribution into a one-dimensional distribution. In this method, the section is divided into horizontal layers that have the same height as the thermal analysis elements, as shown in Figure 3.6 (a). Then, three average temperatures are calculated for each layer. The free thermal expansion calculations utilize the first average temperature (avg_temp1), which is the weighted average of the temperature of the elements within the layer. Calculations of stresses within the section utilize the second average temperature (avg_temp2). To calculate this temperature, the concrete strength (f'_{cT}) for each thermal element is first calculated based on its temperature. Then, avg_temp2 is calculated to result in the average concrete strength (f'_{cT}) for the layer. A third average temperature (avg_temp3) is

proposed in this research to accurately estimate the member behaviour. This average temperature is calculated at different curvature values to result in the average secant modulus (E_{cT}^{sc}) corresponding to the layer strain.

3.3.3.2 Strain Components

The average temperatures (avg_temp1) calculated in section 3.3.3.1 form a nonlinear distribution with higher temperatures at the exposed surfaces than the core as shown in Figure 3.7. Such a nonlinear distribution results in a nonlinear free thermal strain distribution ϵ_{th} (S3), which violates the plane section assumption.

Figure 3.8 shows the strain components. For rectangular sections, El-fitiyany and Youssef (2009) proposed that thermal-self-induced strains ϵ_{st} (S4) are developed to maintain the plane section assumption. They result in equivalent-linear thermal strains $\bar{\epsilon}_{Lth}$ (S2), which is the sum of S3 and S4. The same assumption is followed in this research. However, a modification was applied to the analysis method, as El-Fitiyany and Youssef (2009) calculated these strains before conducting the stress analysis. In this research, the calculation of these strains is combined with the stress analysis. The total strain ϵ_{tot} (S1) represents the section's physical deformation.

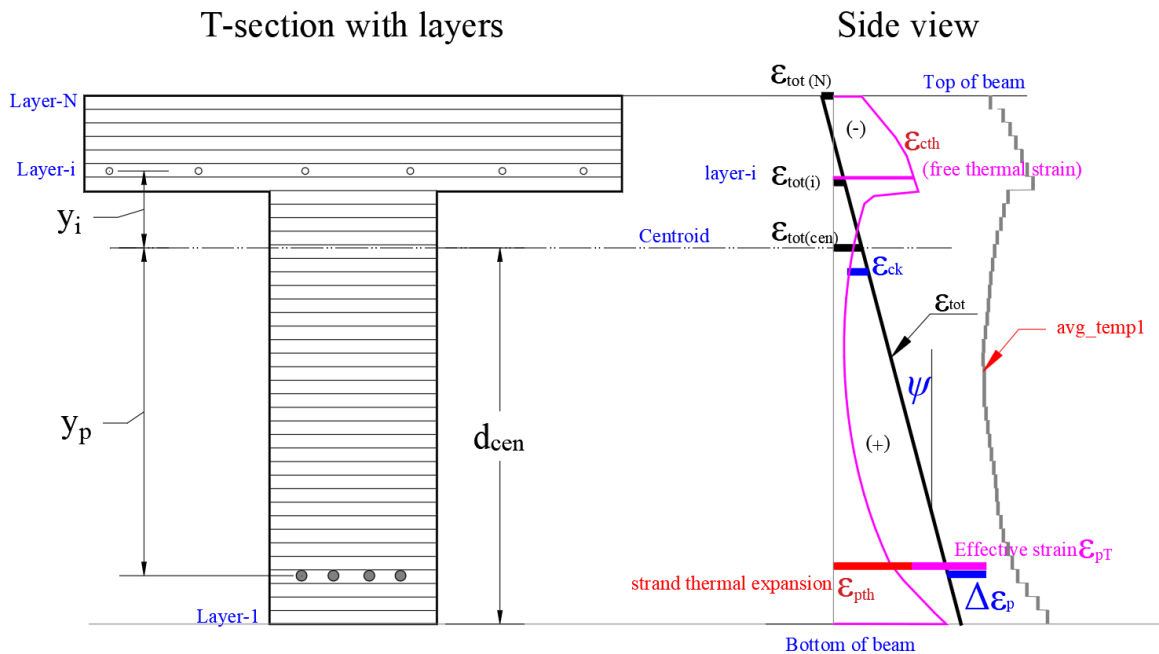


Figure 3.7 The simplified 1-D model and associated strains

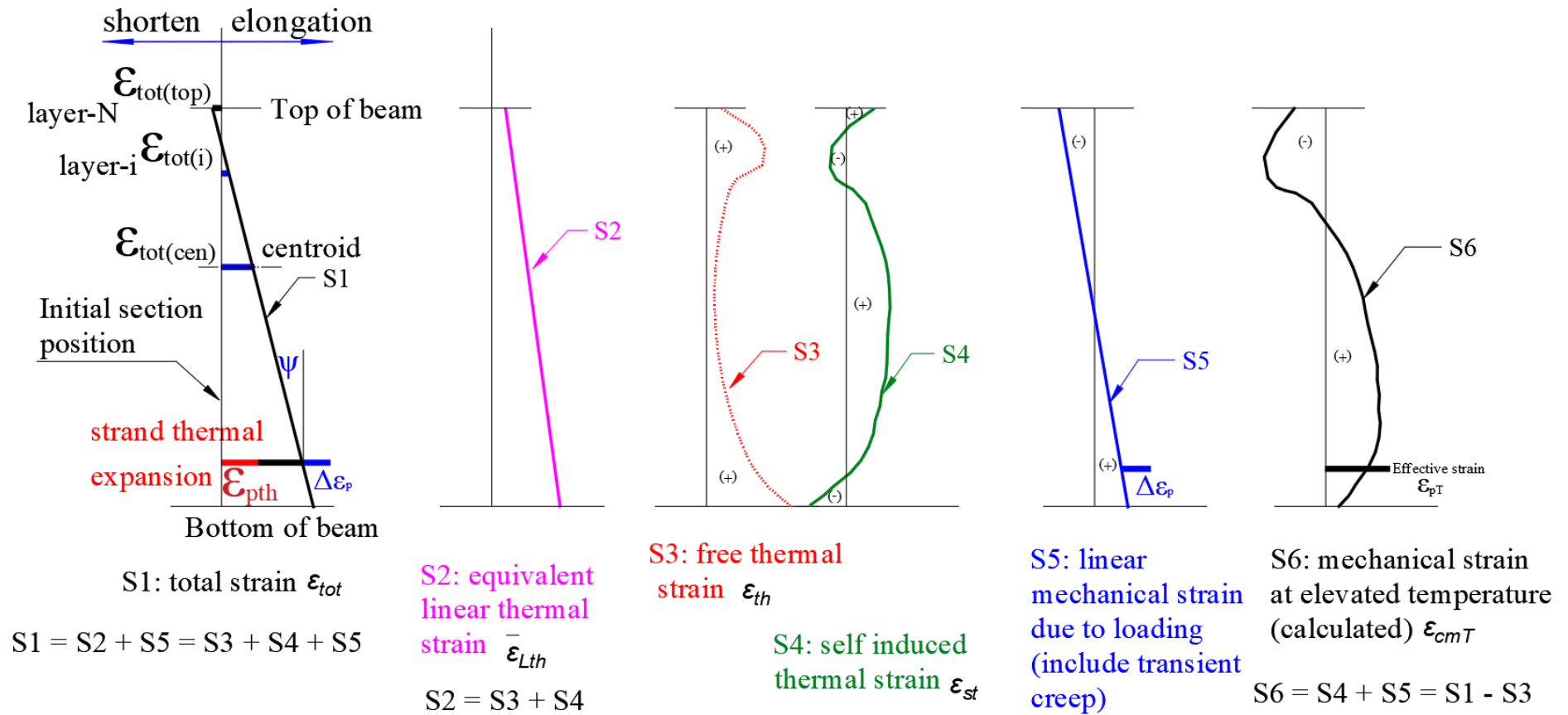


Figure 3.8 Strain components in the 1D model at elevated temperatures

The total strain ε_{tot} (S1) follows the principle of “plane section remains plane”, i.e. the variation of the total strain along the section height is linear and can be defined by the centroidal strain (ε_{cen}) and the curvature (Ψ). S1 is equal to the sum of S3, S4, and the load-induced strains ε_{cT} (S5).

The total strain at the top of the section is $\varepsilon_{tot(top)}$ and at any layer i $\varepsilon_{tot(i)}$. The effective mechanical strains ε_{cmT} (S6), which will correspond to the stresses in the section, are the sum of S4 and S5 or the difference between S1 and S3. The prestress strand strains have similar components. The final effective prestress strain ε_{pT} can be calculated by adding the prestressing strain ($\Delta\varepsilon_p$) and the total concrete strain at the location of the strands (S1) then subtracting the free thermal expansion of the strands (ε_{pth}), i.e., $\varepsilon_{pT} = \Delta\varepsilon_p - \varepsilon_{pth} + S1$. In the MATLAB program, **S1 to S6** values are stored in $1 \times N$ vectors, where N is the number of element layers.

3.3.4 Stresses and Forces

The values for effective strains (S6) in each of the concrete section layers, strands, and steel bars are known from the previous steps. Multiplying these strains with the secant modulus (E_{cT}^{SC} for concrete, E_{pT}^{SC} for strands, and E_{sT}^{SC} for steel bars) results in the average layer stress (f_{cT} for concrete, f_{pT} for strands, and f_{sT} for steel bars), Eq. 3.13. The internal forces for each concrete layer, steel bar, and strand can then be evaluated as the product of the stress and corresponding areas for concrete $\cdot A_c$, strands $\cdot A_p$, and steel bars A_s , Eq. 3.14.

$$\begin{cases} f_{cT} = E_{cT}^{SC} \cdot (\varepsilon_{tot} - \varepsilon_{cth}) \\ f_{pT} = E_{pT}^{SC} (\varepsilon_{tot} + \Delta\varepsilon_p - \varepsilon_{pth}) \\ f_{sT} = E_{sT}^{SC} (\varepsilon_{tot} - \varepsilon_{sth}) \end{cases} \quad \text{Eq. 3.13}$$

The internal forces on each layer are products of stress and the material's area, as Eq.3.14:

$$\begin{cases} N_c = f_{cT} \cdot A_c = E_{cT}^{SC} \cdot (\varepsilon_{tot} - \varepsilon_{cth}) \cdot A_c \\ N_p = \sum f_{pT} \cdot A_p = \sum [E_{pT}^{SC} (\varepsilon_{tot} + \Delta\varepsilon_p - \varepsilon_{pth}) \cdot A_p] \\ N_s = f_{sT} \cdot A_s = E_{sT}^{SC} (\varepsilon_{tot} - \varepsilon_{sth}) \cdot A_s \end{cases} \quad \text{Eq. 3.14}$$

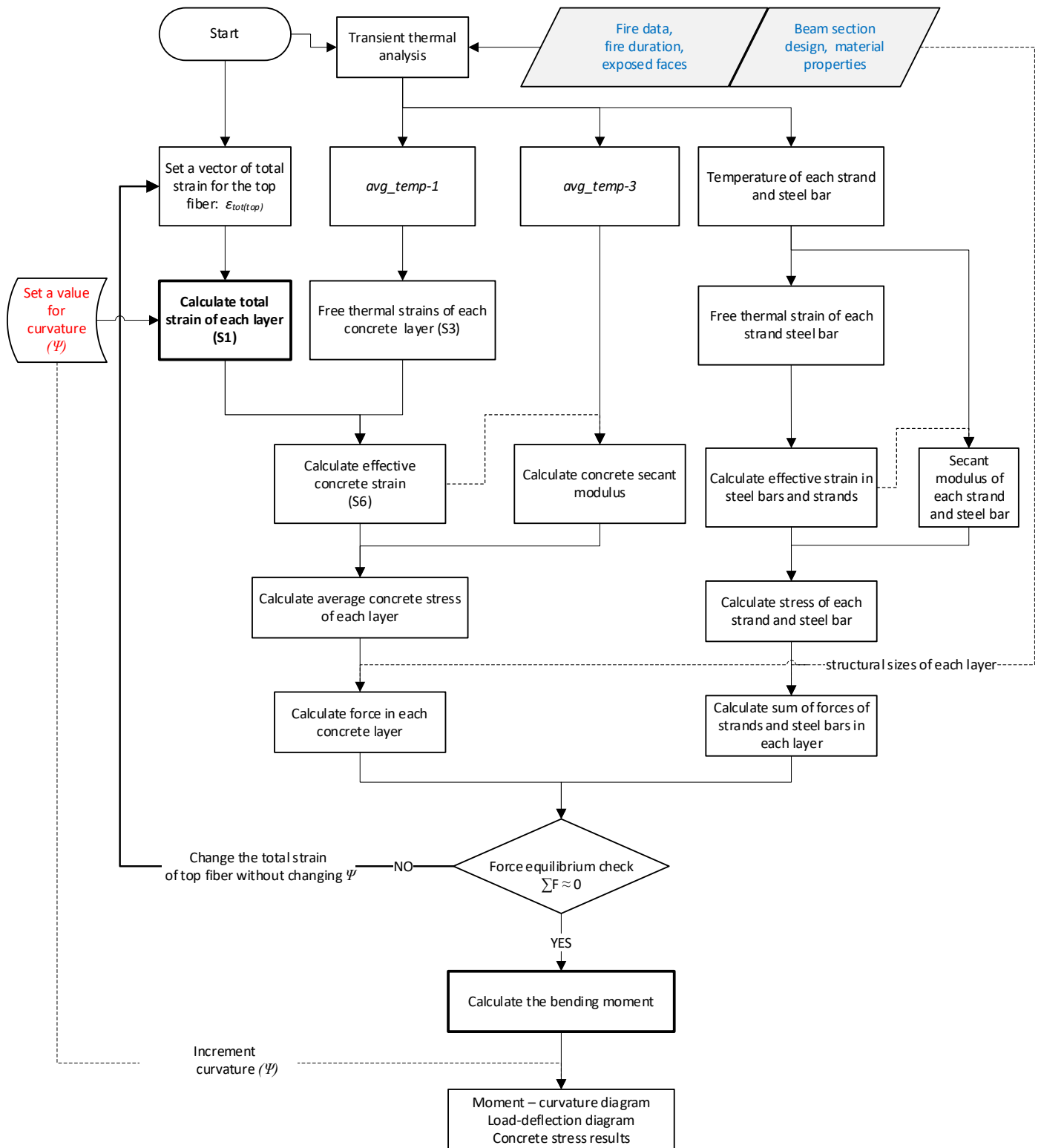


Figure 3.9 Constructing the moment-curvature diagram of a section

3.3.5 Moment-curvature Relationship

The solution strategy is summarized in Fig. 3.9 It starts by conducting the transient thermal analysis and calculating the three average temperatures. Then a total strain is assumed by setting values for the curvature and the total strain of the top fibre ($\varepsilon_{tot(top)}$). Force equilibrium is checked using Eq. 3.15. If the net force N on the section is not zero, then iterations are made by changing $\varepsilon_{tot(top)}$ while keeping the curvature constant until equilibrium is satisfied. The corresponding bending moment M is then calculated using eq. 3.16.

$$N = N_c + N_s + N_p$$

$$= \sum E_{cT}^{sc}(\varepsilon_{tot} - \varepsilon_{cth})A_c + \sum E_S^{sc}(\varepsilon_{tot} - \varepsilon_{sth})A_S + \sum\{E_P^{sc}(\varepsilon_{tot} + \Delta\varepsilon_p - \varepsilon_{pth})A_P\} \quad \text{Eq. 3.15}$$

$$M = \sum \sigma_{cT}A_c y + \sum f_{sT}A_S y + \sum f_{pT}A_P y$$

$$= \sum E_{cT}^{sc}(\varepsilon_{tot} - \varepsilon_{cth})A_c y + \sum E_{sT}^{sc}(\varepsilon_{tot} - \varepsilon_{sth})A_S y + \sum\{E_{pT}^{sc}(\varepsilon_{tot} + \Delta\varepsilon_p - \varepsilon_{pth})A_P\}y \quad \text{Eq. 3.16}$$

Repeating this process for different curvature values allows for establishing the moment-curvature ($M-\Psi$) relationship for a specific fire duration. The whole process is programmed using MATLAB. Input data is provided through Excel spreadsheets. The developed code can be used for any section shape.

3.3.6 Beam deformations

This study only focuses on simply supported girders. For indeterminate structures, such as continuous beams or beams with end restrains, calculations must account for the redistribution of internal stresses as explained by El-Fitiany (2014). The sectional moment-curvature diagram is used to estimate the beam deformations. Figure 3.10 (a) shows the curvature distribution along the length of a simply-supported girder and the corresponding deflection profile. The maximum curvature at midspan, at a distance X_n from the left support, is Ψ_n . Because of symmetry, only half of the beam is divided into $(n-1)$ segments having length L_i , starting at distance X_{i-1} and ending at distance X_i measured from the left support. Figure 3.10 (b) shows the assumptions for the derivation of the deflection equation, Eq. 3.17. α_{i-1} is the slope to the curvature diagram at node $(i-1)$ and β is the angle between the tangent line at node $(i-1)$ and the cord joining nodes $(i-1)$ and (i) . By applying the boundary conditions of $\Delta_I = 0$ and $\alpha_n = 0$ (slope at symmetry point is zero), the deflection of all nodes can be calculated.

3.4 Validation

The proposed numerical model is validated in this section using the experimental results for a pre-tensioned concrete beam tested under elevated temperatures by Kumar and Kodur (2021). The beam setup is shown in Figure 3.11. The simply-supported beam H1 had a length of 3962 mm, span of 3662 mm, width of 305 mm, and height of 406 mm. The concrete compressive strength was 78.4 MPa. The beam was pre-tensioned by five 13 mm seven-wire strands, having a constant eccentricity along the beam length of 139 mm. The initial prestressing stress was 1302 MPa. The stirrups and the top longitudinal bars had a yield strength of 415 MPa. A photo of the test setup is shown in Figure 3.12. Two hydraulic jacks located 1398 mm from the left and right supports applied two concentrated loads. The resulting maximum moment was 154.4 kN·m, which corresponds to 55% of the beam's flexural capacity at ambient temperature. All the sides of the middle 2440 mm length of the beam were exposed to ASTM E119 standard fire. The measured fire temperature in the heating chamber is shown in Figure 3.13, which is within 10% of the ASTM standard fire. The beam failed after 62 minutes of fire exposure.

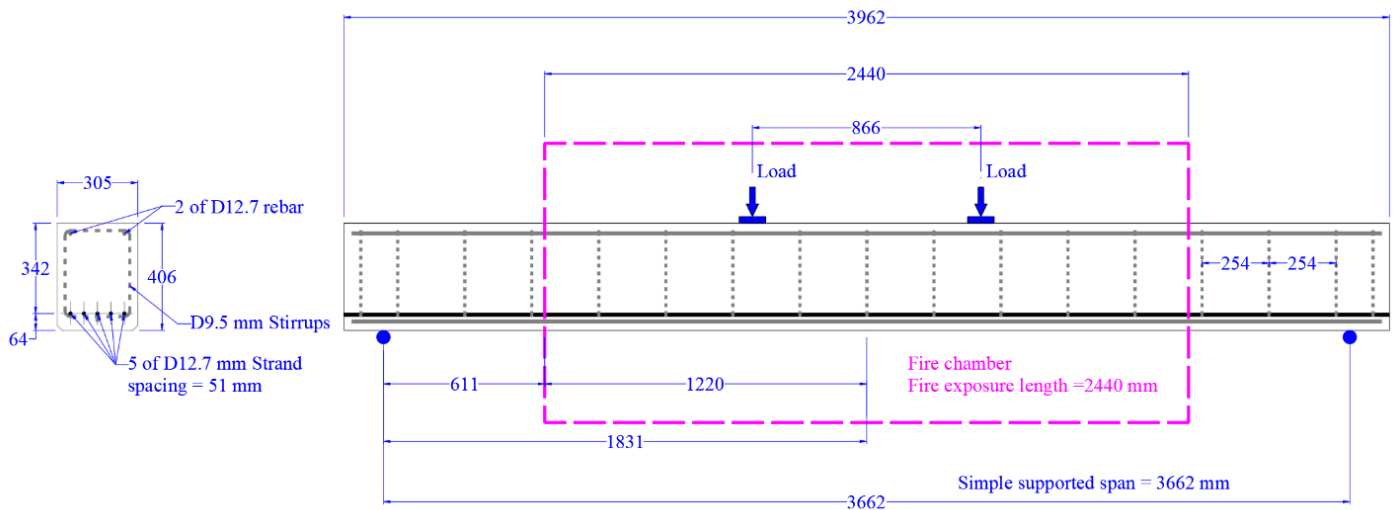


Figure 3.11 Structural details and loading of beam H1

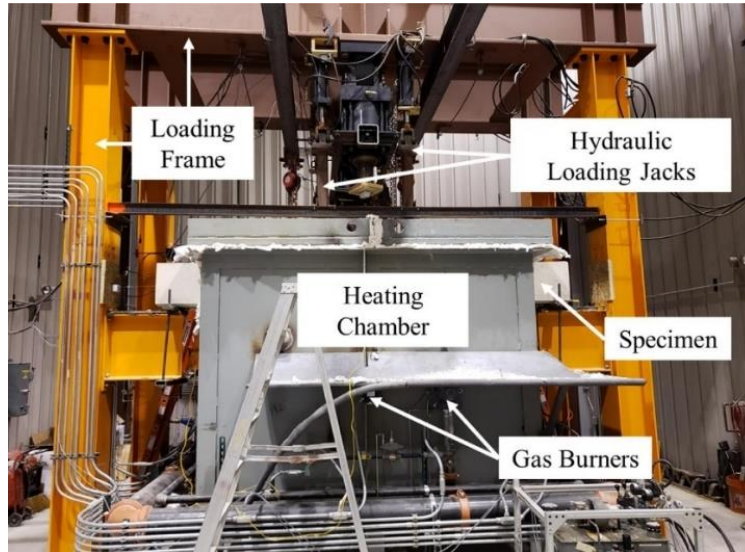


Figure 3.12 Test setup (Kumar 2021)

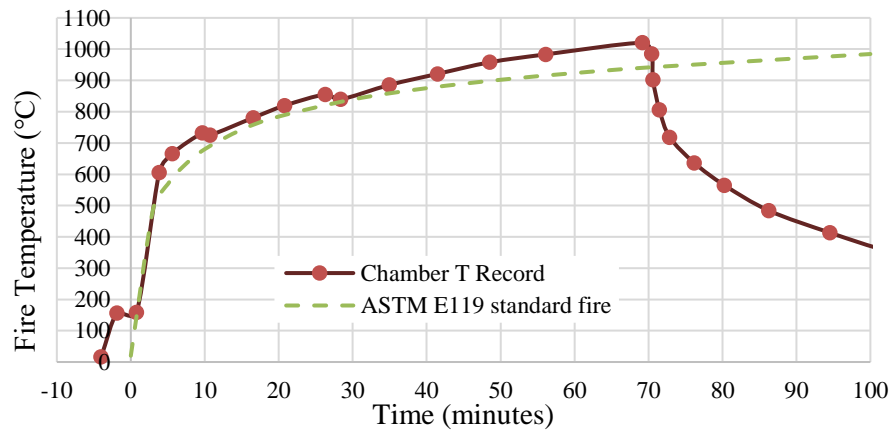


Figure 3.13 Fire temperature record inside the heating chamber

Figure 3.14 shows a comparison of the predicted temperatures and the measured ones at the locations of the middle strand and two points located above it at $\frac{1}{4}$ and $\frac{1}{2}$ the beam's height. In general, the accuracy of the model predictions is acceptable. The highest error was observed when comparing the temperatures at $\frac{1}{2}$ the beam's height. However, in the test, these temperatures increased to be equal to the temperatures at $\frac{1}{4}$ the beam's height after about 35 minutes of fire exposure. The reason for such an irrational increase is unknown.

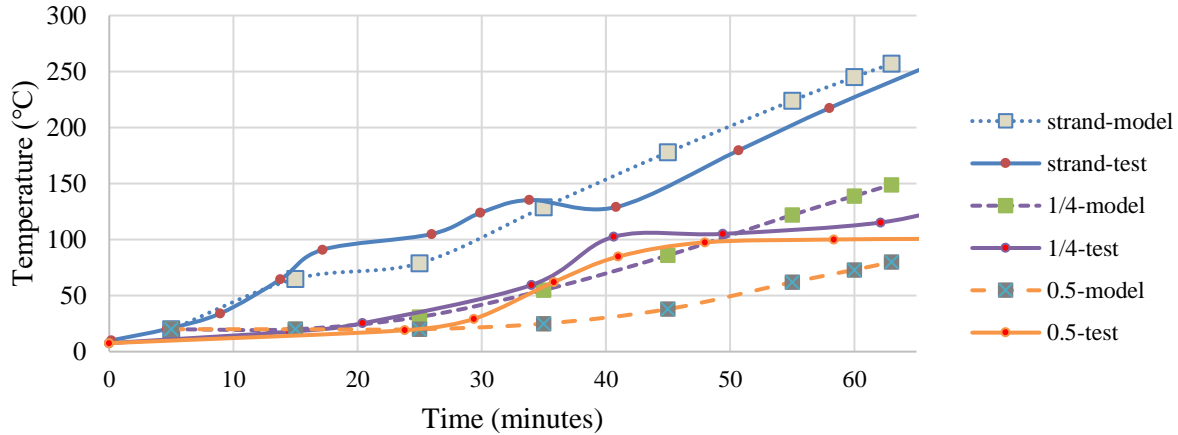


Figure 3.14 Experiment record and model predicted temperature comparison

The generated Moment-Curvature ($M-\Psi$) diagrams, predicted by the numerical model for the beam section, are shown in Figure 3.15 for fire durations from 5 minutes to 70 minutes. The constant moment applied to the middle portion of the beam (154.4 kN·m) is shown as a horizontal dashed line in Figure 3.15. This line lies between the predicted capacities for 60- and 65-minute durations, which perfectly matches the failure duration observed in the test (62 minutes).

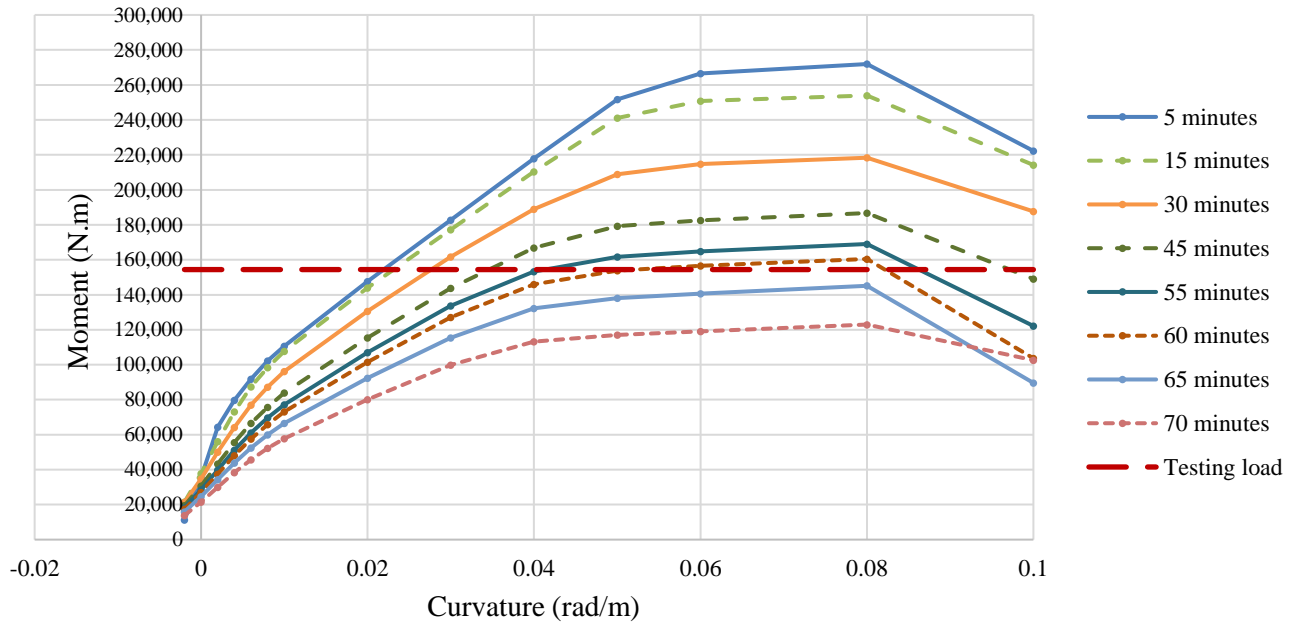
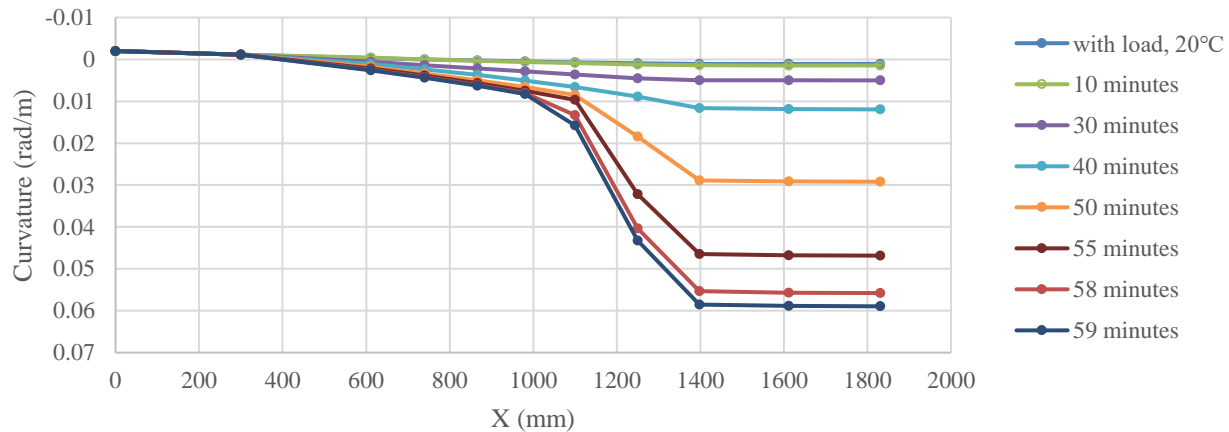
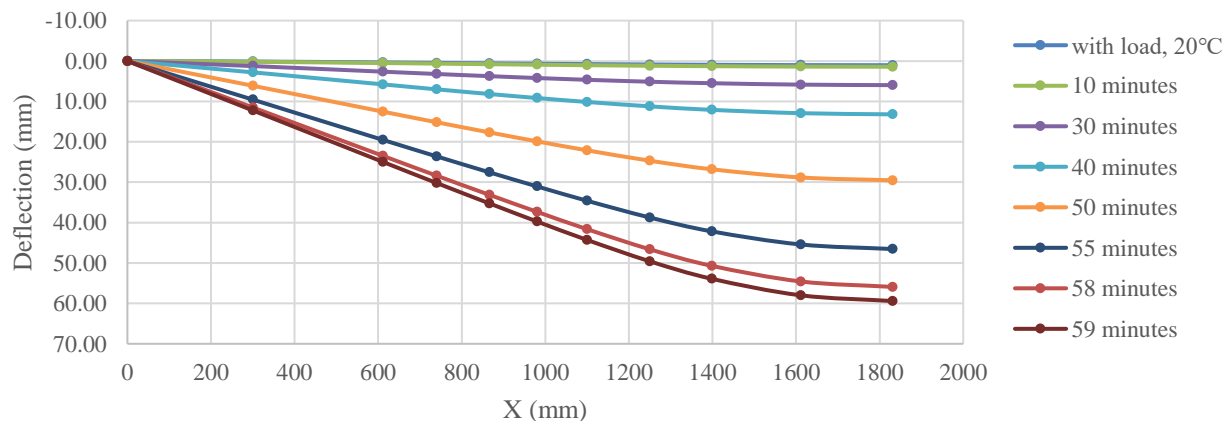


Figure 3.15 Moment-Curvature diagrams of the section of beam H1 at different fire durations

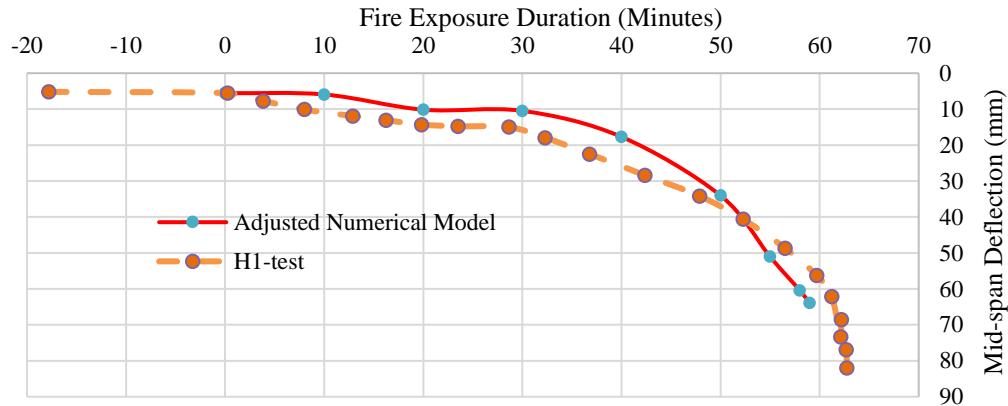
The curvature distribution along the beam length was sketched for different fire durations as shown in Figure 3.16 (a). Then, half the length of the beam was divided into 10 segments with lengths of 300 mm, 311 mm, 129 mm, 126 mm, 114 mm, 120 mm, 150 mm, 148 mm, 213 mm, and 220 mm. The choice of the length of the segments was based on the observed variation in the curvature distribution. For each fire duration, the deflections at different points were then calculated using Eq. 3.17 (a) and the overall deflection profile is sketched, in Figure 3.16 (b). The comparison of the experimental and numerical values for the mid-span deflection is shown in Figure 3.16 (c). The deflections from the numerical model are within 5 mm of the test values (difference less than 20%).



(a) Section curvature during fire exposure (half span)



(b) Section deflection profile during fire exposure (half span)



(c) Mid-span deflection comparison during fire exposure

Figure 3.16 Curvature and deflection of beam H1

3.5 Summary and Conclusions

The goal of this chapter is to develop a numerical model that can accurately estimate the fire duration at failure for prestressed high-strength concrete (HSC) beams. A simplified analysis approach is proposed in this chapter. The model uses a simplified 2D transient thermal analysis utilizing MATLAB functions while accounting for HSC explosive spalling in a simplified manner. The analysis estimates the temperature distribution within the section during the fire exposure, which is utilized to estimate both the shear capacity and flexural behaviour of the beam. The shear capacity is based on the average temperature of the concrete and the stirrups.

The section is then divided into horizontal layers and three average temperatures are calculated for each layer. These average temperatures allow for predicting the free thermal expansion, the concrete strength, and the secant modulus of each concrete layer. A solution procedure is developed to allow sketching of the moment-curvature diagrams at different fire durations. The procedure assumes that the linearity of the total strain is achieved by thermal-induced strains. A methodology based on the moment-area method in structural analysis is utilized to estimate the deflection of the prestressed beam at different fire durations.

Finally, the model was validated using experimental results of a prestressed HSC beam exposed to fire. The model presented in this chapter presents the first simplified analysis method to examine the structural behaviour of a prestressed HSC beam exposed to fire.

3.6 Reference

ASCE, (editor) Lie, *ASCE Manuals and Reports on Engineering Practice No. 78 Structural fire protection*, American Society of Civil Engineers, ISBN 0-87262-888-4, 1992

El-Fitiany and Youssef, *Assessing the flexural and axial behaviour of reinforced concrete members at elevated temperatures using sectional analysis*, *Fire Safety Journal*, 44 (2009) 691-703, 2009

El-Fitiany and Youssef, *Simplified Method to Analyze Continuous Reinforced Concrete Beams during Fire Exposure*, *ACI Structural Journal*, January-February 2014, Title No. 111-S14, 2014

EN 1991-1-2. *Eurocode 1: Actions on Structures - Part 1-2: Actions on Structures Exposed to Fire*. European Committee for Standardization. Brussels, Belgium. 2004

Kodur et. al., *A simplified approach for predicting temperature in reinforced concrete members exposed to standard fire*, *Fire Safety Journal*, 56 (2013) 39-51, 2013

Kodur et. al., *Effect of Temperature on Thermal Properties of Different Types of High-Strength Concrete*, *Journal of Materials in Civil Engineering*, Vol. 23, No. 6, June 1, 2011

Kodur et. al., *Predicting the fire resistance behaviour of high strength concrete columns*, *Cement & Concrete Composites*, 26 (2004) 141–153 doi:10.1016/S0958-9465(03)00089-1, 2004

Kuehnen, *Equivalent standard fire duration to evaluate internal temperatures in natural fire exposed RC beams*, *Fire Safety Journal*, 108 (2019) 102831, 2019

Kumar and Kodur, *Response of prestressed concrete beams under combined effects of fire and structural loading*, *Engineering Structures*, 246 (2021) 113025, 2021

Li Zhang et al., *Mechanical properties of prestressing steel in and after fire*, *Magazine of Concrete Research*, Paper 1500267, <http://dx.doi.org/10.1680/jmacr.15.00267>, 2015

Mathworks, *Partial Differential Equation Toolbox Documentation'User's Guide*, The MathWorks, Inc. 2022

NISTIR, (editor) Phan et al., *Best Practice Guidelines for Structural Fire Resistance Design*, National Institute of Standards and Technology, NISTIR 7563, 2009

NISTIR, (editor) Phan et al., *Best Practice Guidelines for Structural Fire Resistance Design of Concrete and Steel Buildings*, National Institute of Standards and Technology, NIST Technical Note #1681, 2010

NISTIR, Phan et al., *Mechanical properties of high-strength concrete at elevated temperatures*, National Institute of Standards and Technology, NISTIR 6726, 2001

Ozbakkaloglu, *Rectangular Stress Block for High-Strength Concrete*, ACI Structural Journal, V. 101, No. 4, July-August 2004

Sabsabi, *Simplified structural analysis of framed ordinary non-tempered glass panels during fire exposure*, Fire Safety Journal, 122 (2021) 103357

Shakya et. al., *Effect of temperature on the mechanical properties of low relaxation seven-wire prestressing strand*, Construction and Building Materials, 124 74–84, <http://dx.doi.org/10.1016/j.conbuildmat.2016.07.080>, 2016

Wickstrom, *A very simple method for estimating temperature in fire exposed concrete structures*, Swedish National Testing Institute, Fire Technology Technical Report SP-RAPP, 1986

Chapter 4: Equivalent standard Fire Duration for Prestressed Concrete Girders Exposed to Natural Fire

4.0 Abstract

To utilize the wealth of knowledge associated with standard fire curves, simplified equations are developed to estimate the equivalent duration of a standard fire for a given natural fire considering high-strength concrete (HSC) prestressed sections. The equations account for the natural fire characteristics, including maximum fire temperature (T_{max}), time at maximum temperature (t_{max}), and final fire duration (t_{final}); the equations also account for the section size. They were developed based on the internal temperature profiles (AITP) resulting from both the natural fire and the equivalent standard fire. The heat transfer calculations accounted for spalling of HSC in a simplified manner. Equations to estimate the equivalent duration of a standard fire (t_e) for CPCI standard girders were proposed.

Keywords: fire resistance ratio, prestressed concrete girder, design fire, natural fire, AITP method

4.1 Introduction

The numerical model introduced in chapter 3 is based on the thermal analysis results of a prestressed concrete section exposed to a standard fire temperature curve, ASTM E119 or ISO 834. To allow researchers and engineers to use the wealth of knowledge readily available for standard fire exposure and make the program developed in the previous chapter applicable to both standard and natural fires, the concept of equivalent standard fire duration is advantageous.

A natural fire curve provides the relationship between the actual compartment temperature and time during a fire incident. It can be divided into the ignition (smouldering), heating, and cooling stages. A standard fire curve, ASTM E119 or ISO 834, has a prescribed temperature history and is known to represent a conservative fire incident for building elements. EN 1991-1-2 can be used to predict the natural fire curve based on the compartment's physical properties. Figure 4.1 shows an example of standard and natural fire curves.

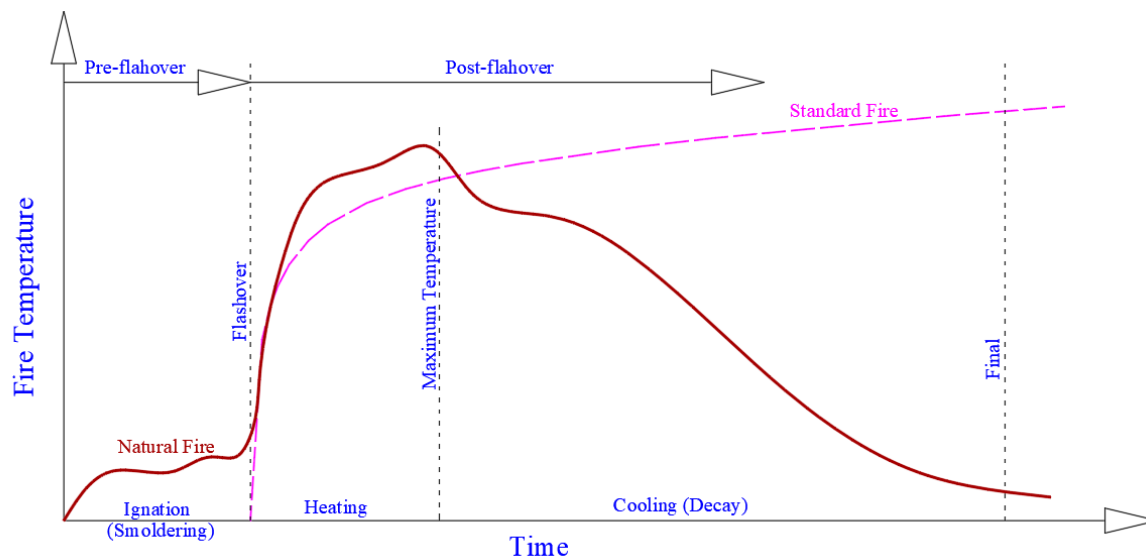


Figure 4.1 Standard and natural fire curves

Researchers tried different methods to estimate the standard fire duration (t_e) equivalent to a natural fire. Ingberg (1928) proposed the “equal area method”, which estimates t_e such that the area under the standard fire curve measured up to t_e is equal to the area under the natural fire curve. This method can result in deceiving answers as it does not account for the maximum temperature or the heating rate. Law (1971), Pettersson (1975), and Schneider et al. (1990) proposed the “maximum temperature method”, which defines t_e to correspond to the maximum temperature experienced during a natural fire. The maximum temperature approach is only valid for sections that experience a uniform temperature increase during fire exposure such as steel (Purkiss, 2007). For concrete sections, the fire performance is governed by the maximum temperature of the steel bars, concrete geometrical dimensions, load level, and concrete cover (Gao, 2013). Methods based on achieving the same load capacity (Buchanan, 2001) or the same deflection (Kodur and Dwaikat, 2010) require detailed thermal and structural analysis and are only valid either to estimate the load capacity or the deflection. Energy-based methods were proposed by Harmathy and Mehaffey (1982), Harada et al. (2000), Nyman (2002), and Kodur et al. (2010). In these methods, t_e is the time when the accumulated thermal energy from the standard fire matches that from the natural fire. These methods require a good amount of calculations and out of them, the method of Kodur et al. (2010) is the only one suitable for concrete elements. The average internal temperature profile

(AITP) method (Kuehnen, 2019) is based on finding t_e that produces a similar temperature gradient within the concrete section to the one produced by a natural fire.

This chapter utilizes the AITP concept to estimate the duration of a standard fire that is equivalent to a natural fire exposure considering HSC prestressed beams. To the best of the author's knowledge, the method developed in this chapter is the first to account for concrete spalling and section shape. The following sections provide details about the conducted parametric studies, the proposed AITP t_e , and a recommended size adjustment factor.

4.2 Natural Fire Curves

Kuehnen (2019) found that the natural fire curves defined in EN 1991-1-2 do not represent the whole spectrum of potential temperatures, heating rates, and cooling rates. This research uses a similar approach to that used by Kuehnen (2019). Fire curves are assumed to start at a temperature of 20°C and time zero and then follows the compartment fire curve given by Eq. 4.1 (Wickstrom, 1986) until reaching a time t_{max} , which corresponds to the maximum temperature T_{max} . The cooling stage is then represented as a line that joins T_{max} and the ambient temperature (20°C) point, which corresponds to a time t_{final} . The assumed ranges for the three parameters (t_{max} , T_{max} , and t_{final}) were determined based on natural fire data, summarized by Lennon (2004). These ranges are: $450\text{ °C} \leq T_{max} \leq 1250\text{ °C}$, $15\text{ min} \leq t_{max} \leq 120\text{ min}$, and $20\text{ min} \leq t_{final} \leq 240\text{ min}$. The same intervals chosen by Kuehnen (2019) were used as they result in reasonably spaced natural fires. The intervals for t_{max} were 5 min until a fire duration t of 30 min, then 15 min until t of 120 min. The intervals for t_{final} were 20 min. For T_{max} , the intervals were 100°C for temperatures from 450°C to 650°C, then 50°C. The cases, which had $t_{max} \geq t_{final}$, were excluded. A total of 1410 natural fire curves were used in this research, Table 4.1 and Figure 4.2.

$$T_f = 345 \log_{10}(480t^* + 1) \quad \text{Eq. 4.1}$$

where: t^* is the modified fire duration in hours ($t^* = \Gamma \cdot t$), t is the fire duration, Γ is the compartment time factor, and T_f is the compartment temperature (°C).

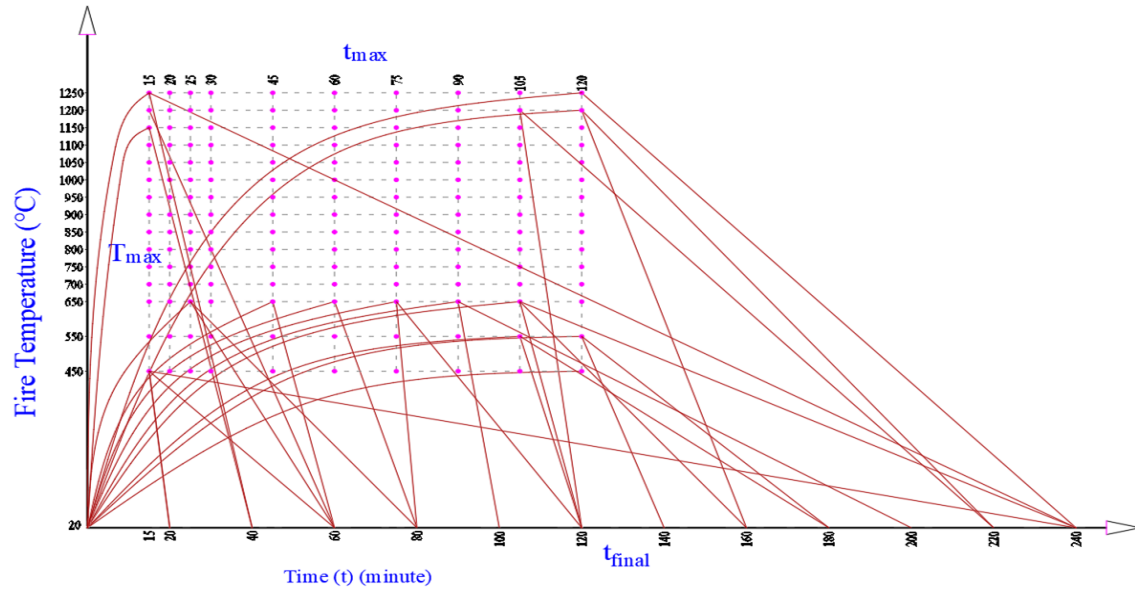


Figure 4.2 Natural fire curves

Table 4.1 Natural fire parameters for the considered cases

Design fire case index #	T_{max} (°C)	Design fire case index #	t_{max} (minutes)	t_{final} (minutes)
1~94	450	1~11	15	20~240
		89~94	120	140~240
95~188	550	95~105	15	40~240
		183~188	120	140~240
189~282	650	189~199	15	40~240
		277~282	120	140~240
283~376	700	283~293	15	40~240
		371~376	120	140~240
377~470	750	377~387	15	40~240
		465~470	120	140~240
471~564	800	471~481	15	40~240
		559~564	120	140~240
565~658	850	565~575	15	40~240
		653~658	120	140~240
659~752	900	659~669	15	40~240
		747~752	120	140~240
753~846	950	753~763	15	40~240
		841~846	120	140~240
847~940	1000	847~857	15	40~240
		935~940	120	140~240
941~1034	1050	941~951	15	40~240
		1029~1034	120	140~240
1035~1128	1100	1035~1045	15	40~240
		1123~1128	120	140~240
1129~1222	1150	1129~1139	15	40~240
		1217~1222	120	140~240
1223~1316	1200	1223~1233	15	40~240
		1311~1316	120	140~240
1317~1410	1250	1317~1327	15	40~240
		1405~1410	120	140~240

4.3 Thermal Gradient in a Concrete Section

Concrete has a low thermal conductivity and high thermal capacity compared to metals, which makes it a relatively good insulation material. However, during fire exposure, a steep two-dimensional thermal gradient develops within the concrete section. El-Fitiany and Youssef (2009) introduced a methodology to simplify this two-dimensional thermal gradient to a one-dimensional average internal temperature profile (AITP) across the section height, which was modified and utilized in the previous chapter.

The thermal gradients due to the natural fire and 1-minute-increment durations of the standard fire are first estimated. This step requires calculating the surface temperature of the concrete for the different durations of the standard fire, Eq. 3.3. For the case of natural fire, the compartment time factor Γ is first estimated and the surface temperature is then calculated. For the cooling stage, it was assumed that the concrete surface temperature is equal to the fire temperature.

The concrete surface temperature is used as a boundary condition for the thermal analysis, which was conducted using the method explained in Chapter 3. AITP-D for the natural fire is recorded based on the maximum temperature experienced by each layer during fire exposure. For the standard fire, the AITP-S for each fire duration is evaluated.

4.4 Equivalent exposure time

Figure 4.3 shows a flowchart of the methodology adopted to estimate the equivalent exposure time t_e . AITP-D is compared against the evaluated AITP-S for every minute of the standard fire. In each comparison, the difference between the two profiles is calculated, which allows for calculating the overall mean error. The t_e value is chosen to correspond to the AITP-S resulting in the minimum mean error.

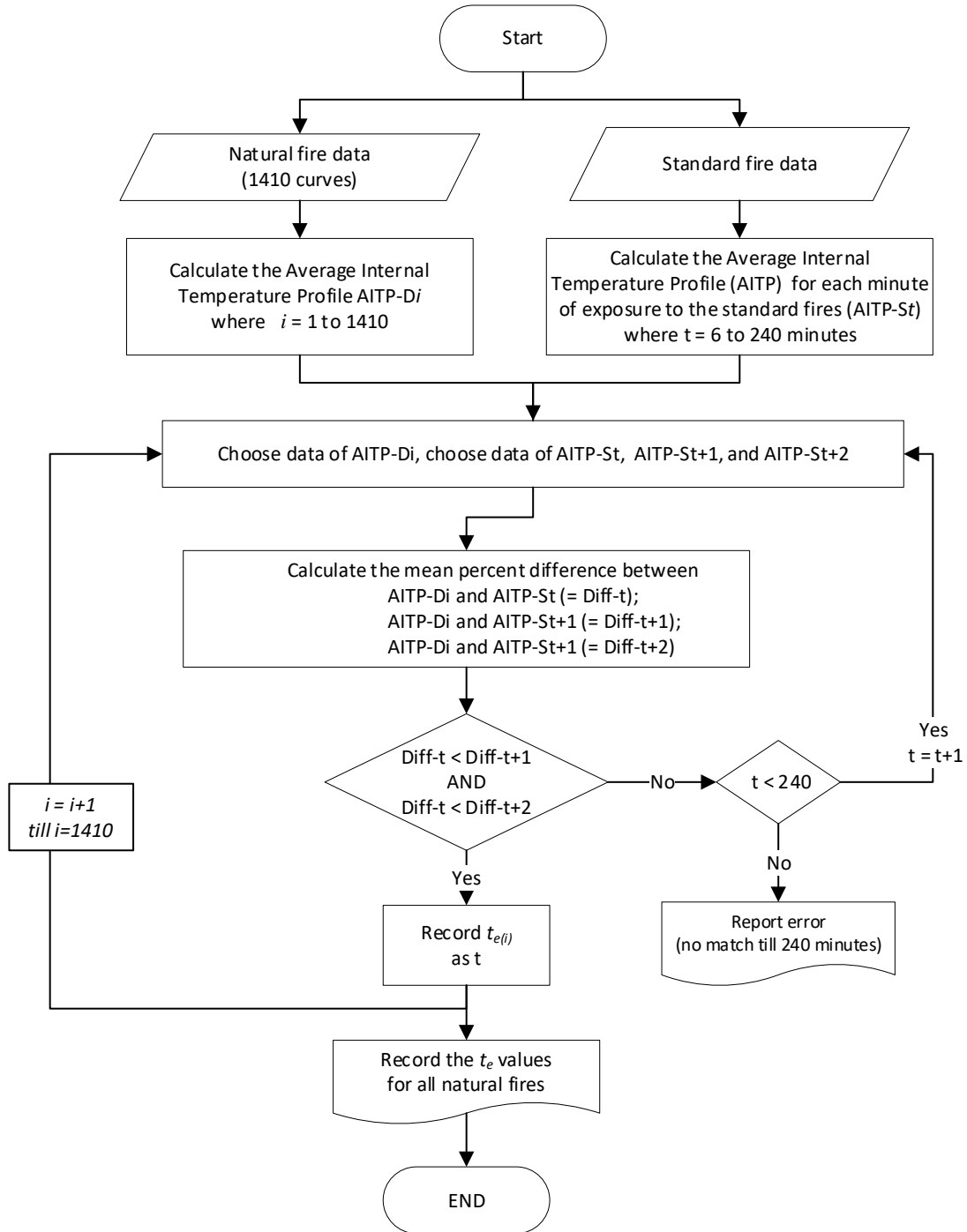
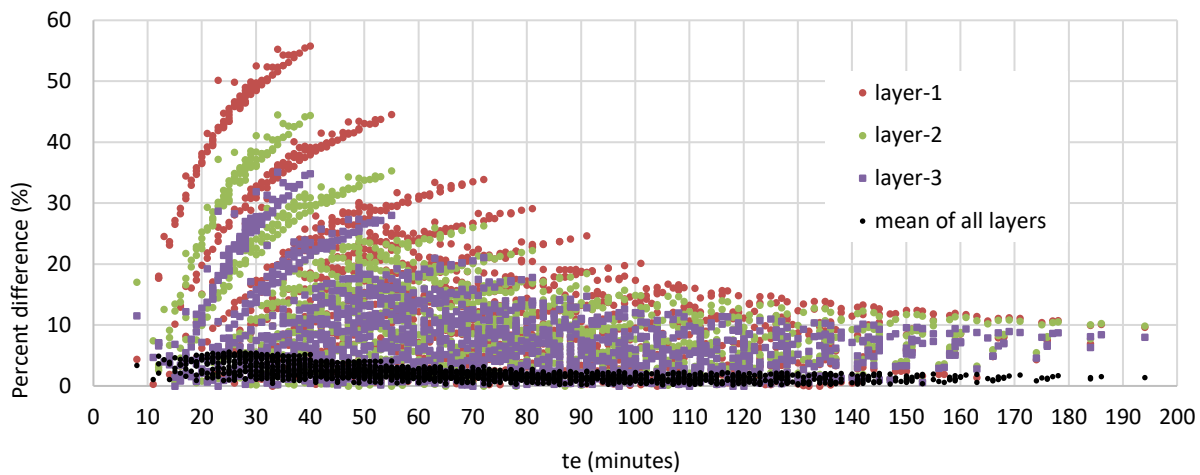
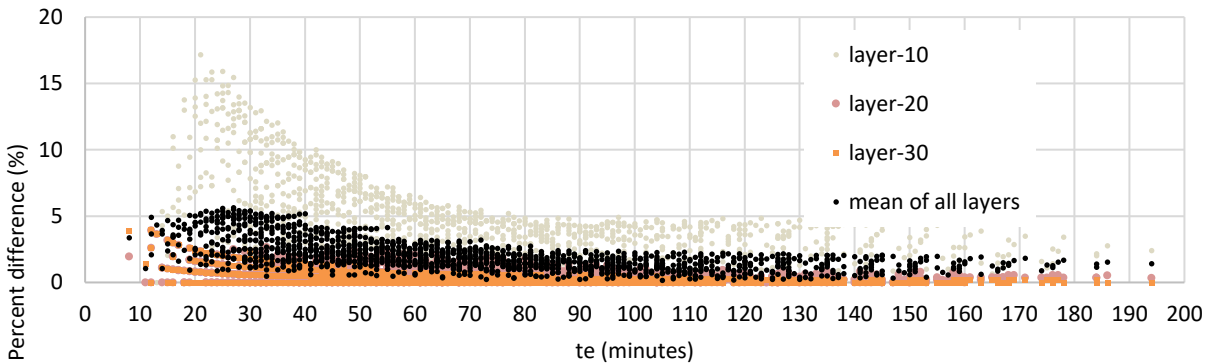


Figure 4.3 Flow chart to calculate AITP time equivalence (t_e)

A MATLAB code is used to conduct the analysis and derive the values of (t_e) for each of the 1410 natural fire curves. Results for a section of dimension 250 mm by 500 mm exposed to fire from three sides (sides and bottom) are discussed. After evaluating the t_e values, the mean and maximum errors, between the chosen AITP-S and the AITP-D, are compared in Figure 4.4. The overall mean error was less than 6%. However, the maximum difference for individual layers reached 60%. This error was higher for the layers directly exposed to the fire and reduced quickly within the section. It was also only observed at relatively low fire temperatures.



(a) Errors for layers 1, 2, and 3



(b) Errors for layers 10, 20, and 30

Figure 4.4 Errors in estimating temperatures using a standard fire with a duration of t_e

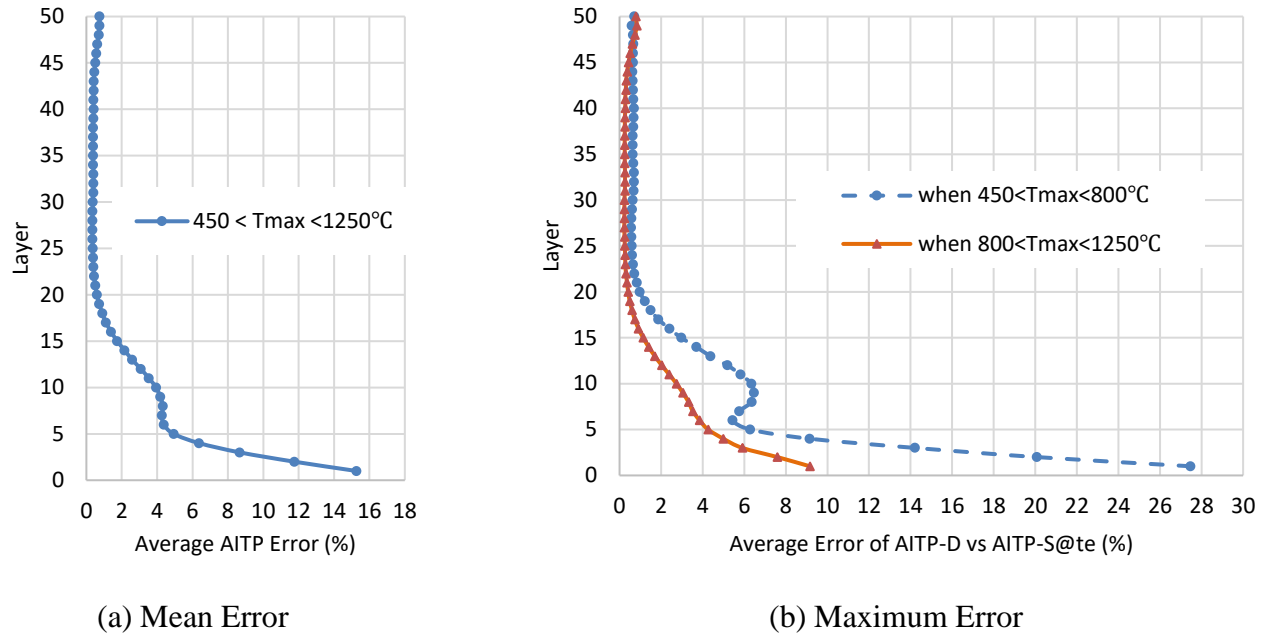


Figure 4.5 Error in predicting AITP profile using a standard fire.

Figure 4.5 shows the error in estimating the AITP profile along the section height. The mean error is shown in Figure 4.5 (a). The mean error at the bottom of the section is about 15% and decreases to about 4% at layer 5. The maximum error is sensitive to the maximum temperature of the design fire. Figure 4.5(b) shows that for T_{max} less than 800°C, the maximum error reaches 27% and decreases to 6% at layer 10. However, for higher T_{max} , the maximum error is only 9% and decreases to 3% at layer 10. The observed maximum error does not affect the moment capacity prediction of concrete beams as it is mainly affecting the concrete cover which is in tension.

4.5 Simplified equation for the time equivalence estimation

In this section, a formula is developed to estimate the equivalent fire duration based on the conducted parametric study for an HSC section with a width of 250 mm and a height of 500 mm. For natural fire i , the three control parameters are the maximum fire temperature (T_{max-i}), time to the maximum temperature (t_{max-i}), and the overall duration of the fire ($t_{final-i}$), Figure 4.1. Eq. 4.2 shows the general formula combining the dependent variable ($y_i = t_{e-i}$) and the explanatory variables (x_{pi}), which are given by Eq. 4.3. The final form for the equation is given by Equation 4.4.

$$y_i = \beta_0 + \beta_1 x_{1i} + \beta_2 x_{2i} + \beta_3 x_{3i} + \dots + \beta_p x_{pi} \quad \text{Eq. 4.2}$$

Where β_0 is a constant term and β_1 to β_9 are constants representing the slopes for each explanatory variable.

$$\begin{aligned} x_{1i} &= T_{max-i}; & x_{2i} &= t_{max-i}; & x_{3i} &= t_{final-i}; & x_{4i} &= T_{max-i}^2 \\ x_{5i} &= t_{max-i}^2; & x_{6i} &= t_{final-i}^2; & x_{7i} &= T_{max-i} \cdot t_{max-i} \\ x_{8i} &= t_{max-i} \cdot t_{final-i}; & x_{9i} &= t_{final-i} \cdot T_{max-i} \end{aligned} \quad \text{Eq. 4.3}$$

$$\begin{aligned} t_e &= \mathbf{A} + \mathbf{B} \cdot T_{max} + \mathbf{C} \cdot t_{max} + \mathbf{D} \cdot t_{final} + \mathbf{E} \cdot T_{max}^2 + \mathbf{F} \cdot t_{max}^2 + \mathbf{G} \cdot t_{final}^2 + \mathbf{H} \cdot T_{max} \cdot t_{max} + \\ &\mathbf{I} \cdot t_{max} \cdot t_{final} + \mathbf{J} \cdot t_{final} \cdot T_{max} \end{aligned} \quad \text{Eq. 4.4}$$

A Multiple Linear Regression was used to determine the coefficients A~J. Their values were found to be A=16; B= 2.8172×10^{-2} ; C=0.21871; D=- 0.29196; E= 2.4415×10^{-5} ; F= 2.0143×10^{-3} ; G= 3.7442×10^{-4} ; H= 2.6567×10^{-4} ; I=- $.5662 \times 10^{-3}$; and J= 5.9297×10^{-4} . Figure 4.6 compares the predictions of Eq. 4.4 and the t_e values evaluated in the parametric study. The equation provided good estimates with a correlation coefficient (R^2) of 99.06%. Figure 4.7 compares the error produced by the equation at different t_e . The error value is less than 10%. Higher more discrete errors can be observed at t_e values less than 40 minutes.

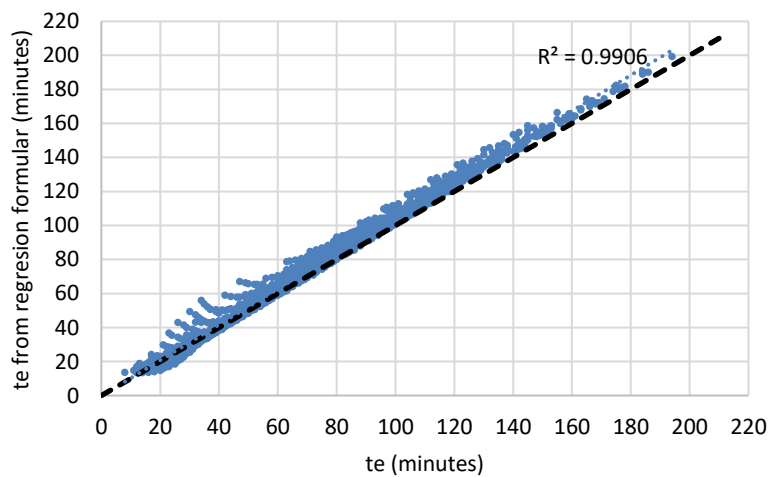


Figure 4.6 Accuracy of t_e prediction using Equation 4.4

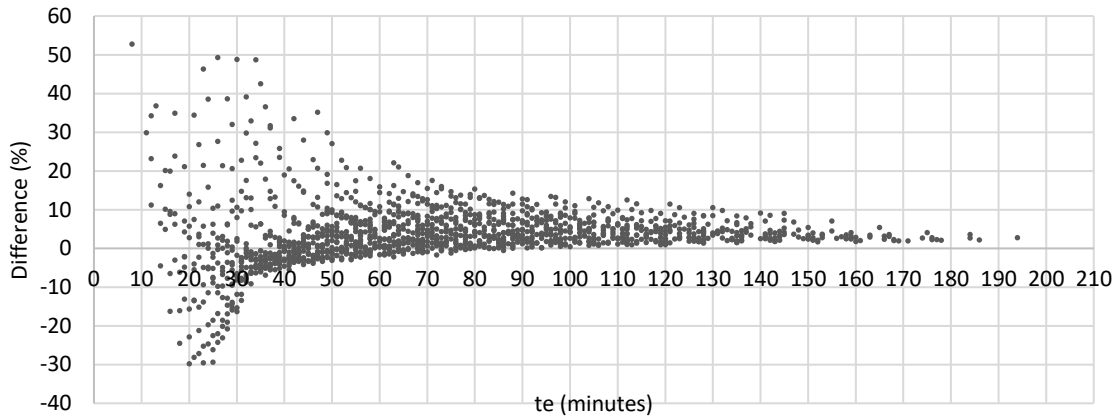


Figure 4.7 Error from using equation 4.4 at different t_e values

4.6 Influence of section size

The parametric study conducted in the previous section was for a 250 mm by 500 mm rectangular prestressed HSC section. To generalize the developed method, this section examines the beam size effect. The profile of errors, Fig. 4.5, shows higher values in a limited number of surface layers. Increasing the section height will increase the number of layers having constant temperature, which will result in a lower t_e error and decrease the mean error value. Thus, the section height was not considered to be an influencing factor.

A sensitivity study was conducted to examine the effect of the width (b) on t_e . Fewer natural fires were used for this study as the effect of short fires and low temperatures on wide sections is expected to be minor. The examined natural fires are shown in Table 4.2 and Figure 4.8. T_{max} was varied from 650°C to 1250°C with 100°C increments. t_{max} was varied from 30 minutes to 120 minutes with 15-minute increments. t_{final} was varied from 40 minutes to 240 minutes with 20 minutes increments. Cases with $t_{max} > t_{final}$ were excluded. A total of 420 natural fires were considered. The considered section width values are 250, 300, 400, 500, 600, 700, and 800 mm, which resulted in a total of 2940 analysis cases.

Figure 4.9 shows the effect of the section width on t_e . The design fire index is shown in Table 4.2. For lower values of T_{max} (650~850°C), the width can result in an error of up to 20% in the t_e value. For higher values of T_{max} (950~1250°C), the error reduces to 5%.

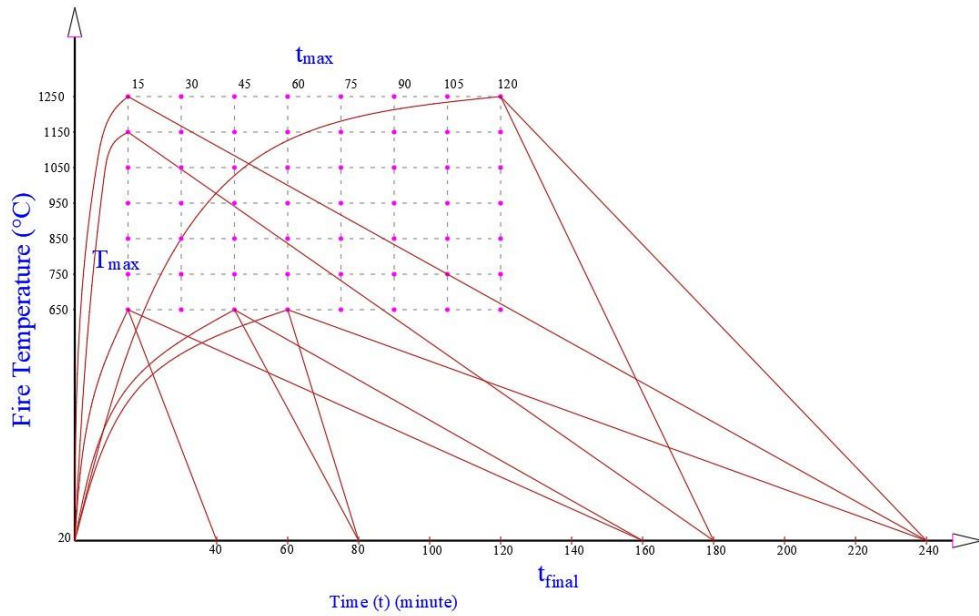


Figure 4.8 Natural fire curves to examine the effect of beam width

Table 4.2 Natural fire parameters for beam width evaluation

Design fire index #	T_{max} (°C)	index #	t_{max} (minutes)	t_{final} (minutes)
1~60	650	1~11	15	40~240
	
		55~60	120	140~240
61~120	750	61~71	15	40~240
	
		115~120	120	140~240
121~180	850	121~131	15	40~240
	
		175~180	120	140~240
181~240	950	181~191	15	40~240
	
		235~240	120	140~240
241~300	1050	241~251	15	40~240
	
		295~300	120	140~240
301~360	1150	301~311	15	40~240
	
		355~360	120	140~240
361~420	1250	361~371	15	40~240
	
		415~420	120	140~240

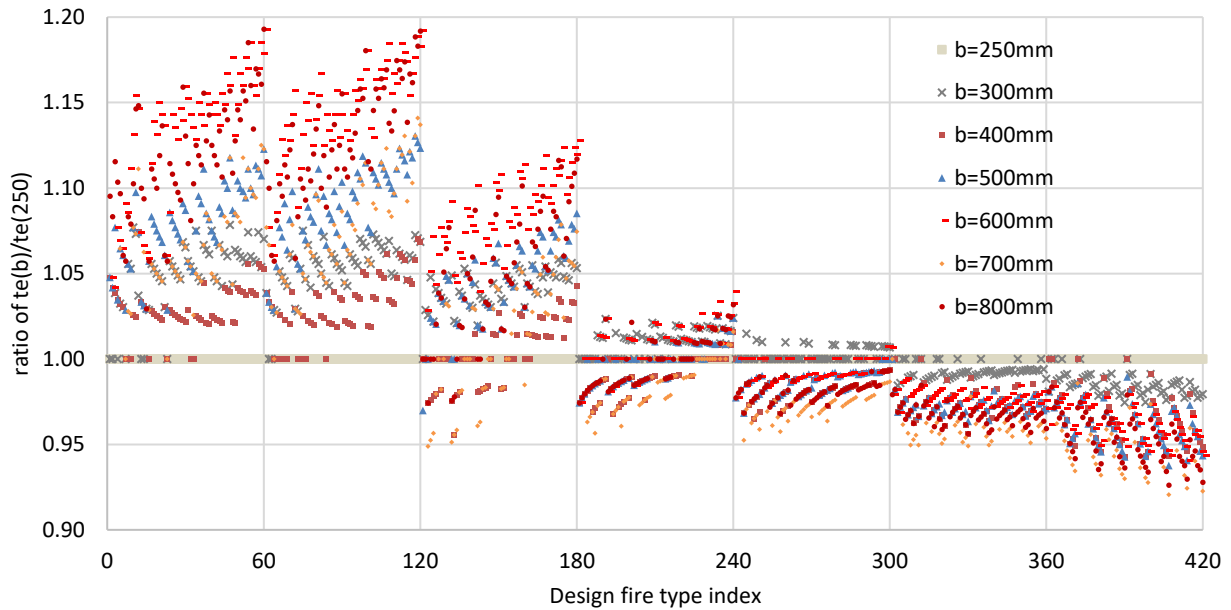


Figure 4.9 Effect of the section width on t_e

Examining the data presented in this section led to the development of Eq. 4.5, which calculates a width adjustment factor (φ_b). This factor should be multiplied by t_e given by Eq. 4.4 for a section width of 250 mm.

$$\varphi_b = \left[1.03 + \left(0.425 - \frac{T_{max}}{2000} \right) \left(\frac{t_{max}}{300} \right) - \frac{t_{final}}{10000} \right] \cdot \left[1 - \frac{b - 300}{25000} \left(\frac{T_{max}^2}{25000} - 0.056T_{max} + 13.9 \right) \right]$$

for $T_{max} = 650$ to 850°C and $b = 300$ to 800 mm

$$\varphi_b = 1.0 \quad \text{for } T_{max} \text{ 850~ 1250}^\circ\text{C} \text{ and } b = 300 \text{ to } 800 \text{ mm}$$

Eq. 4.5

4.7 Application of time equivalent method for non-rectangular sections

Previous research in this field has only addressed rectangular sections. In this section, the concept of t_e is examined for six CPCI standard prestressed girders, Figure 4.10. The topping slab is assumed to have a width of 2500 mm and a thickness of 225 mm. The concrete compressive strength for the girder and topping slab is assumed to be 80 MPa and 35 MPa, respectively. Concrete spalling was only considered for the prestressed girders.

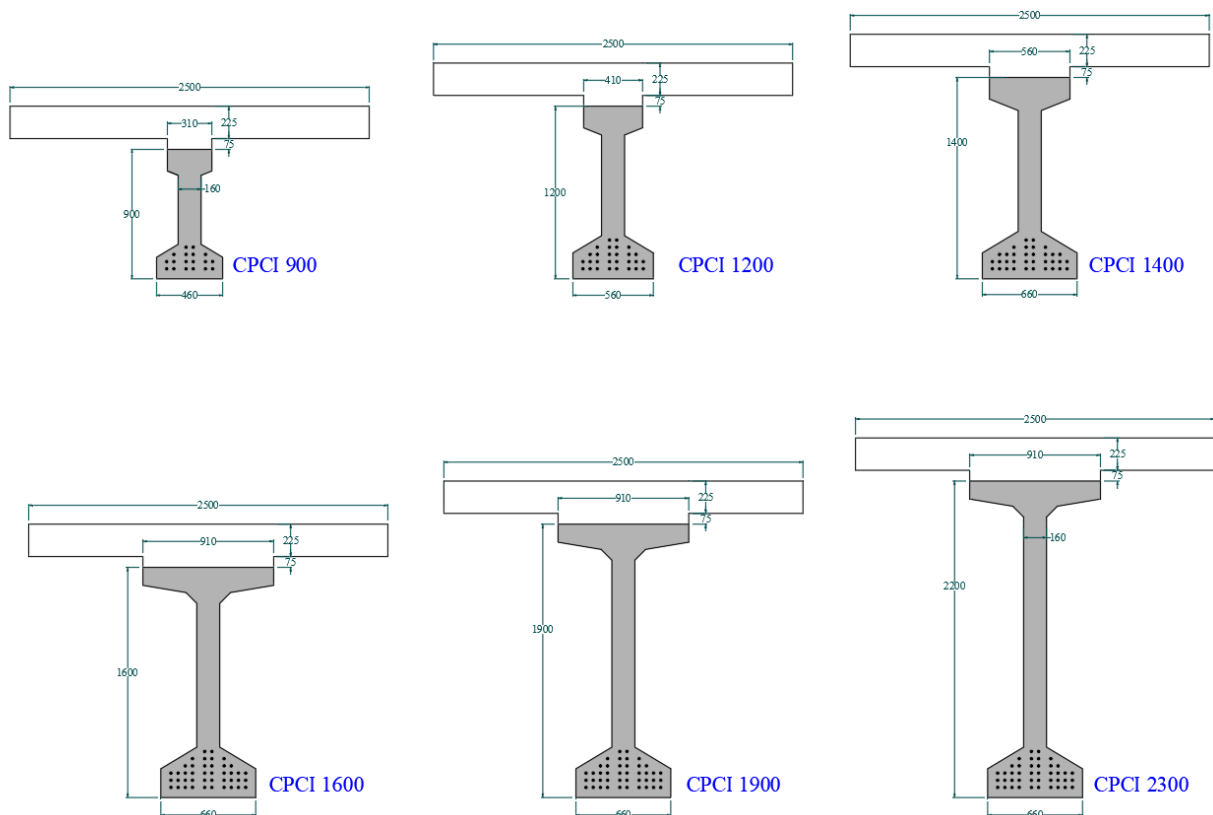


Figure 4.10 Sections of the considered CPCI girders

The equivalent standard fire exposure time (t_e) for the six CPCI girders was calculated for the 1410 natural fire cases. As the web width for the CPCI girders is only 160 mm, cases with t_e values higher than 88 minutes were excluded. At this duration, the average temperature for the web reaches 800 °C, which causes the girder to fail in shear.

Figure 4.11 shows the comparison of the t_e values. The six CPCI girders had almost the same t_e values for CPCI 1400 girder were a little different. The average errors resulting from using a standard fire with duration t_e are shown in Fig. 4.11. For the cooler and shorter natural fires, $t_e < 40$ minutes, the average error is 5 to 20%. For the hotter and longer design fire, $t_e > 40$ minutes, the average error is 1% to 6%.

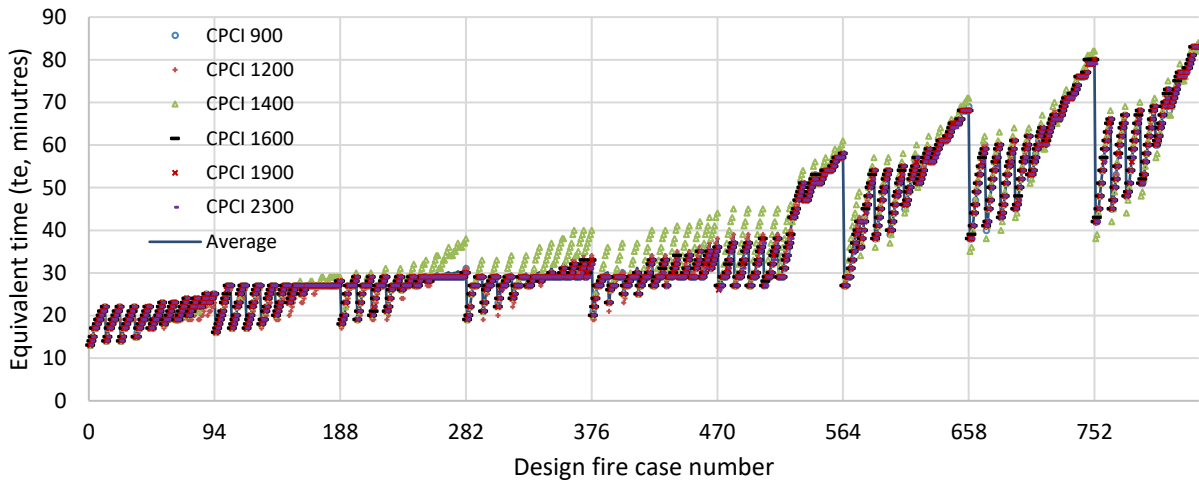


Figure 4.11 Equivalent standard fire exposure time (t_e) of CPCI girders

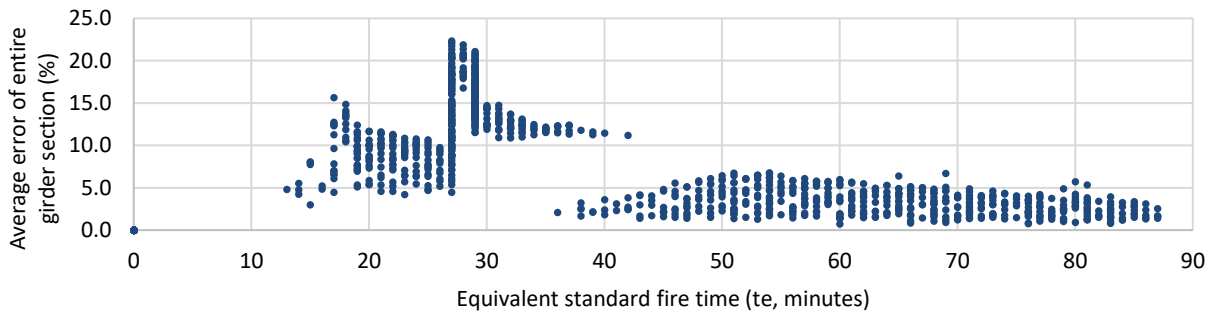


Figure 4.12 (a) CPCI 900 girder

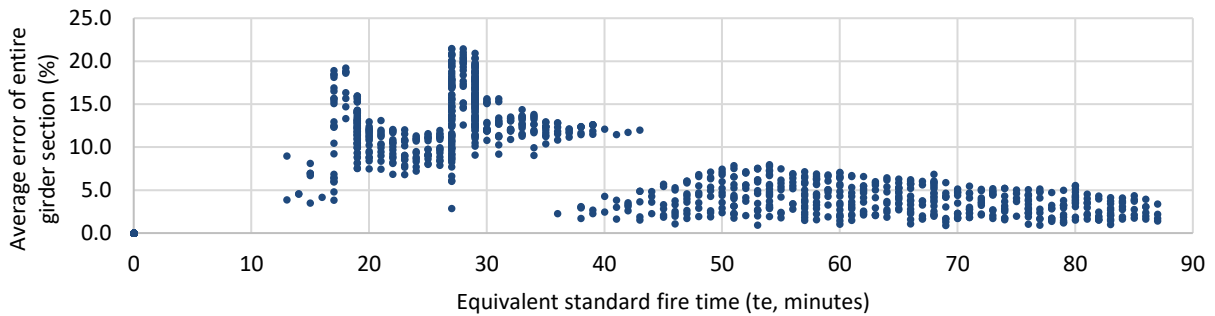


Figure 4.12 (b) CPCI 1200 girder

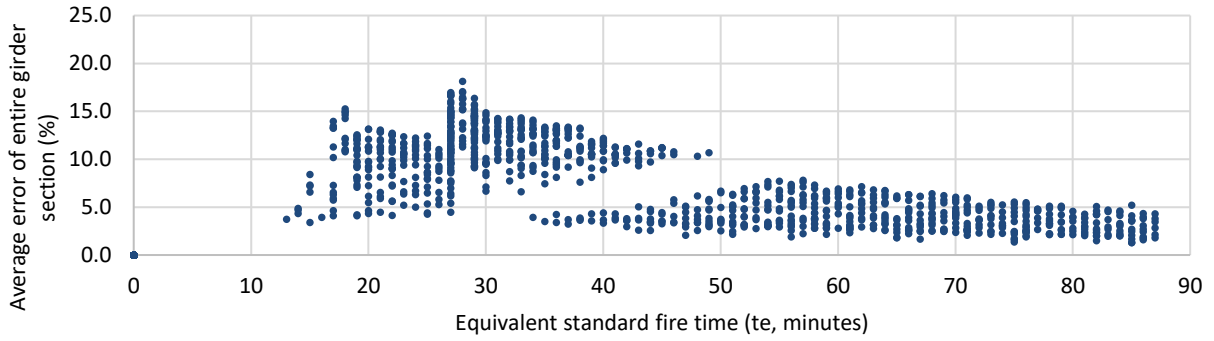


Figure 4.12 (c) CPCI 1400 girder

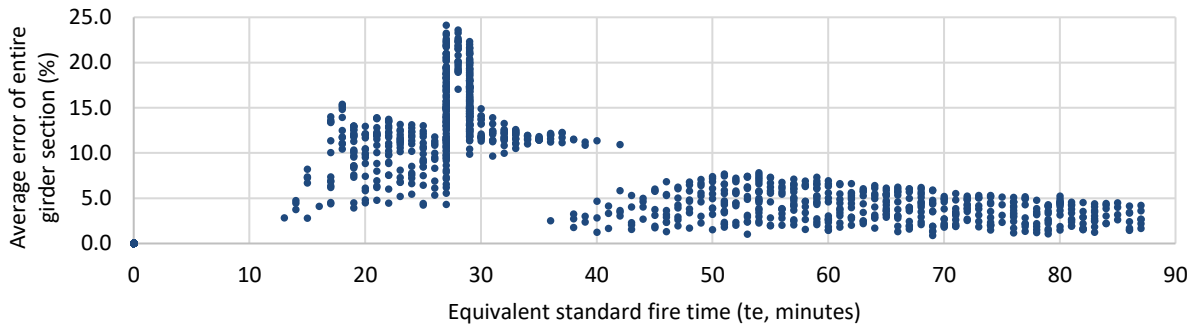


Figure 4.12 (d) CPCI 1600 girder

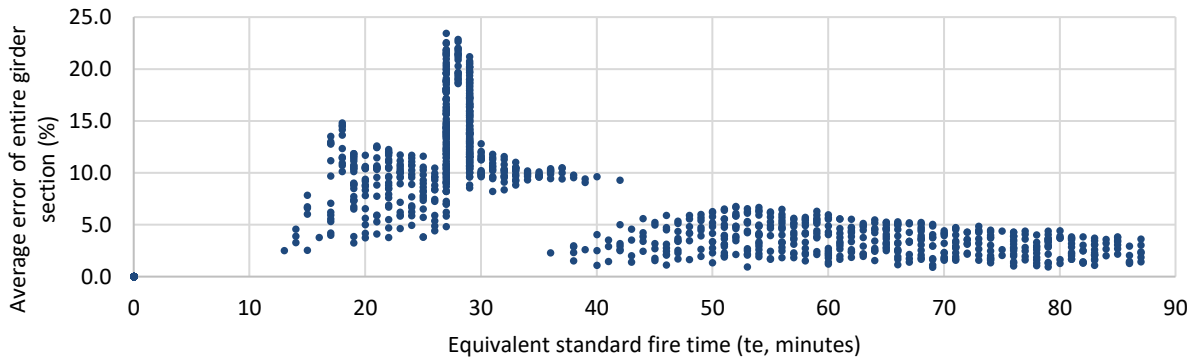


Figure 4.12 (e) CPCI 1900 girder

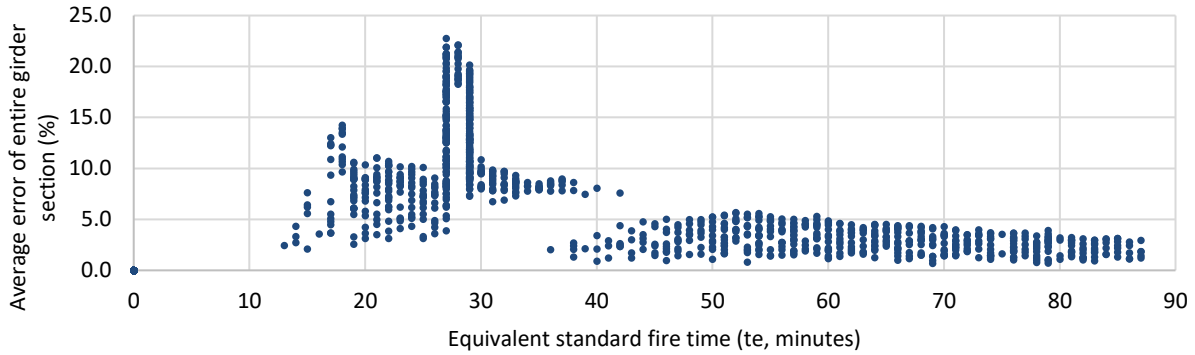


Figure 4.12 (f) CPCI 2300 girder

Figure 4.12 Mean error resulting from using t_e for CPCI girders

The analysis results were examined using regression analysis and Eq. 4.6 was developed. The equations provide an estimate for the equivalent duration for the examined CPCI girders. Figure 4.13 shows that the equation provides acceptable accuracy to predict t_e .

$$\left\{ \begin{array}{l} t_e = 25 \text{ minutes, when } T_{max} = 450^\circ\text{C} \\ t_e = 28 \text{ minutes, when } T_{max} = 550^\circ\text{C} \\ t_e = 30 \text{ minutes, when } T_{max} = 650^\circ\text{C} \\ t_e = 35 \text{ minutes, when } T_{max} = 700^\circ\text{C} \\ t_e = 38 \text{ minutes, when } T_{max} = 750^\circ\text{C} \end{array} \right. \quad \text{Eq. 4.6 (a)}$$

$$t_e = \mathbf{A} + \mathbf{B} \cdot T_{max} + \mathbf{C} \cdot t_{max} + \mathbf{D} \cdot t_{final} + \mathbf{E} \cdot T_{max}^2 + \mathbf{F} \cdot t_{max}^2 + \mathbf{G} \cdot t_{final}^2 \\ + \mathbf{H} \cdot T_{max} \cdot t_{max} + \mathbf{I} \cdot t_{max} \cdot t_{final} + \mathbf{J} \cdot t_{final} \cdot T_{max} \quad (\text{minutes})$$

$$\text{when } 800 \leq T_{max} \leq 1250^\circ\text{C} \quad \text{Eq. 4.6 (b)}$$

where: $\mathbf{A} = 24$; $\mathbf{B} = -0.058$; $\mathbf{C} = -0.87$; $\mathbf{D} = -0.15$; $\mathbf{E} = 6.704 \times 10^{-5}$;

$\mathbf{F} = 1.277 \times 10^{-3}$; $\mathbf{G} = -3.568 \times 10^{-4}$; $\mathbf{H} = 1.146 \times 10^{-3}$; $\mathbf{I} = -2.945 \times 10^{-4}$; $\mathbf{J} = 4.133 \times 10^{-4}$

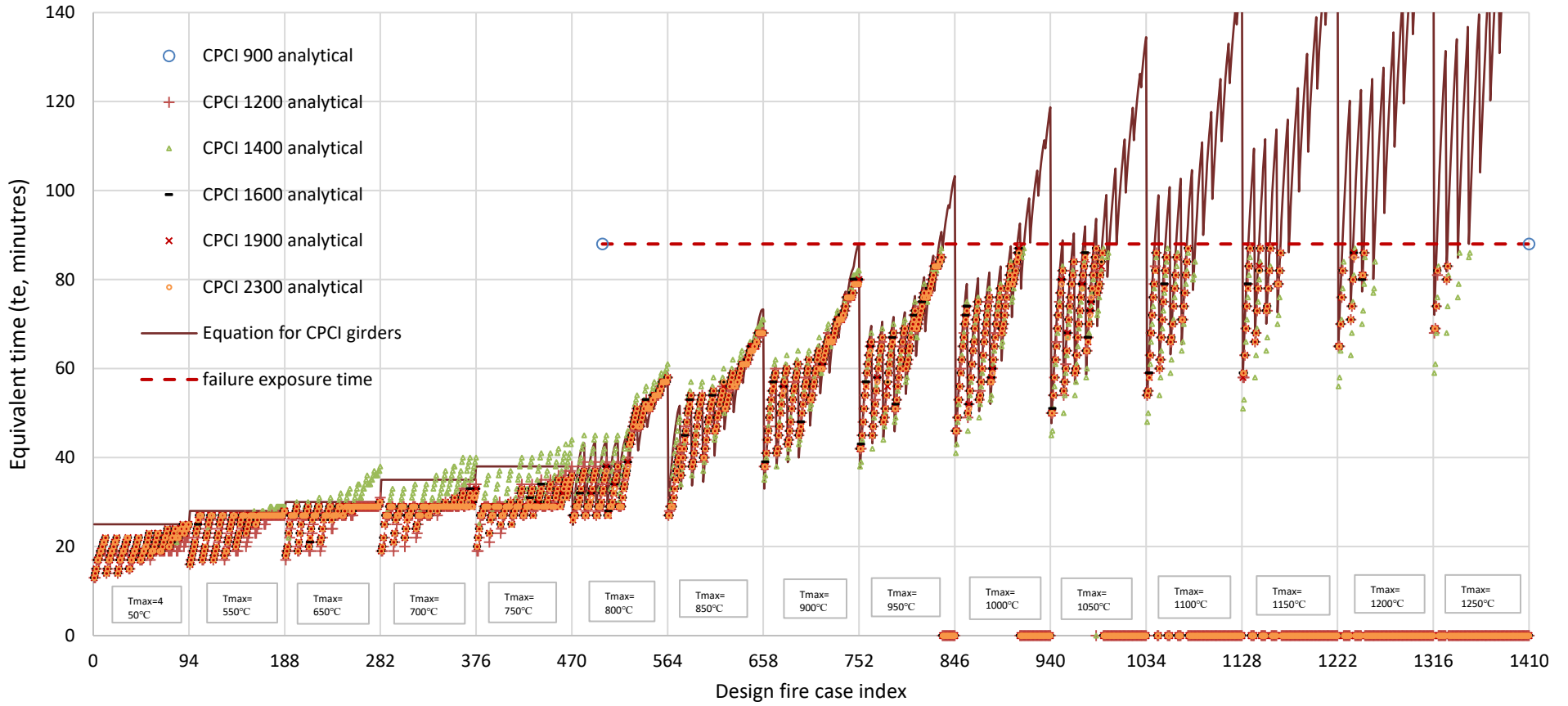


Figure 4.13 Comparison between the equivalent time predicted by the equation versus that by the numerical study

4.8 Summary and Conclusions

To apply the numerical model developed in Chapter 3 for the analysis of prestress girders exposed to natural fires, a time equivalent methodology is adopted in this chapter. The duration t_e of a standard fire resulting in the same thermal distribution within the section is evaluated. The chapter is the first to account for the effect of concrete spalling and section shape on t_e .

A benchmark section (width \times height = 250 \times 500mm) is first analyzed. The section was exposed to 1410 natural fires at its bottom and sides. For each fire, the profiles of the maximum temperatures at different heights were recorded. These profiles were then compared with those for standard fire considering different durations. The duration leading to the minimum average error between the profiles for the natural and standard fires defined t_e . The use of t_e was found to lead to high error values in the layers directly exposed to the fire. However, these layers are not critical for structural calculations as concrete in tension will be ignored and they are in the cover and do not affect the accuracy of estimating the temperature of the strands. Based on regression analysis, a simple equation was proposed to estimate t_e . The equation was found to provide better accuracy for fires with a maximum temperature higher than 700 °C. Application of the developed equation is limited to the examined cases.

Sections with bigger dimensions were then examined. As the variable temperature region was found to be near the bottom exposed surface, increasing the section height reduces t_e and increases the error of the exposed layers. Thus, it was proposed to use the same equation developed for a 250 mm by 500 mm section for sections with bigger heights. Regarding the section width, t_e values considering widths ranging from 300 mm to 800 mm were estimated. The effect of the width was found to be apparent for fires with a maximum temperature of less than 850°C. A width adjustment factor was proposed to correct the t_e values for a width of 250 mm.

The chapter then examines the application of the t_e concept on CPCI standard girders, which are widely used in Canadian highway bridges. The thermal analysis results showed that the t_e values for different sizes of these girders are similar. A regression equation was developed to estimate the t_e for these girders.

4.9 Reference

ASTM. E119-20. *Standard Test Methods for Fire Tests of Building Construction and Materials*. American Society for Testing and Materials, West Conshohocken, PA, USA. 2020

Buchanan. *Structural Design for Fire Safety*, 2nd ed. ISBN: 978-0470972892. Wiley, 2001

CPCI. *CPCI design manual*. Canadian Precast Prestressed Concrete Institute. Ottawa Ontario, Canada, 2017.

El-Fitiany and Youssef. *Assessing the Flexural and Axial Behaviour of Reinforced Concrete Members at Elevated Temperatures Using Sectional Analysis*. Fire Safety Journal. vol. 44, no. 5, 2009, pp. 691-703. 2009

EN 1991-1-2. *Eurocode 1: Actions on Structures - Part 1-2: Actions on Structures Exposed to Fire*. European Committee for Standardization. Brussels, Belgium. 2002

Harada, Kogure, Matsuyama, and Wakamtsu. *Equivalent Fire Duration Based on Time-Heat Flux Area*. 4th Asia-Oceania Symposium on Fire Science and Technology, Ottawa, Canada, 1994. Fire Safety Science, pp. 513-524, 2000.

Harmathy and Mehaffey. *The Normalized Heat Load Concept and Its Use*. Fire Safety Journal. vol. 12, no. 1, pp. 75-81, 1987.

Ingberg. *Tests on the Severity of Building Fires*. Quarterly of the National Fire Protection Association. vol. 22, pp. 43-61, 1928.

ISO 834-11:2014. *Fire resistance tests — Elements of building construction*. International Organization for Standardization, Geneva, Switzerland. 2014

Kodur, Pakala, and Dwaikat. *Energy Based Time Equivalent Approach for Evaluating Fire resistance of Reinforced Concrete Beams*. Fire Safety Journal, vol. 45, no. 4, pp. 211-220, 2010.

Kuehnen. *Performance-Based Design of Fire-Exposed Reinforced Concrete Elements using an Equivalent Standard Fire*. Thesis for Master of Engineering Science. Western University, ON, CANADA. 2019.

Law, M. *A Relationship Between Fire Grading and Building Design and Contents*. Fire Research Note no. 877, Building Research Establishment. UK, 1971.

Lennon. *Results and Observations from Full-Scale Fire Test at BRE Cardington*. Building Research Establishment, no. 215-741. Cardington, UK, 2004

Ministry of Transportation, Ontario. *MTO Structural Manual*. ISBN 978-1-4606-8646-1. MTO, 2016

Nyman. *Equivalent Fire Resistance Ratings of Construction Elements Exposed to Realistic Fires*. MS. Department of Civil Engineering, University of Canterbury. Canterbury, NZ, 2002

Pettersson. *The Connection Between a Real Fire Exposure and the Heating Conditions According to Standard Fire-Resistance Tests - With Special Application to Steel Structures*. Bulletin no. 39, Lund Institute of Technology. Lund, Sweden, 1975

Purkiss. *Fire Safety Engineering, Design of Structures*. ISBN: 978-1466585478. Elsevier Ltd, 2007

Schneider, Kersken-Bradley, and U. Max. *Recalculation of the heat extraction factors for DINV 18230: Part 1 - Structural fire protection in industrial construction*. Fraunhofer IRB Verlag. Stuttgart, Germany, 1990

Wickstrom. *A very simple method for estimating temperature in fire exposed concrete structures*. Swedish National Testing Institute. Fire Technology Technical Report SP-RAPP 1986

Chapter 5 Structural fire performance of HSC prestressed sections

5.1 Introduction

In this chapter, a parametric study is conducted to evaluate the influence of the design parameters on the structural performance of prestressed HSC sections exposed to fire. The section behaviour is defined using its moment-curvature diagram ($M-\Psi$ curves). The parametric study results are then examined using regression analysis to develop a methodology to estimate the moment at zero curvature, the moment of yielding, and the ultimate moment of the section during fire exposure.

5.2 Parametric study

The parametric study compares the structural performance of four sections that have different designs during exposure to fire. Details of the sections are given in Figure 5.1 and Table 5.1. The sections were chosen to represent a CPCI standard section (G1) and different sizes of rectangular sections (G2, G3, and G4). All sections are assumed to have a topping slab with the dimensions shown in Figure 5.1. Four values for the ambient concrete compressive strength are examined, $f_{c20}' = 35, 60, 75, \text{ and } 90$ MPa. All sections were exposed to the standard fire of ISO 834 at the bottom face and sides of the girder and the bottom face of the concrete slab. The sections are assumed to be prestressed using low relaxation 7-wire strands with a strength of 1860 MPa. Figure 5.2 shows the moment-curvature diagrams of the four sections at ambient temperature considering concrete compressive strength of 75 MPa. Three of the sections were chosen to have similar behaviour. The fourth section has a capacity of about 50% of that of the three other sections. Table 5.2 shows the layout of the parametric study, which examined the variation of the concrete strength of the girder and the topping slab, and the section's shape. For each of the considered cases, the moment-curvature ($M-\Psi$) diagrams were obtained considering fire duration of 0, 30, 45, 60, 70, 80, 90, and 120 minutes.

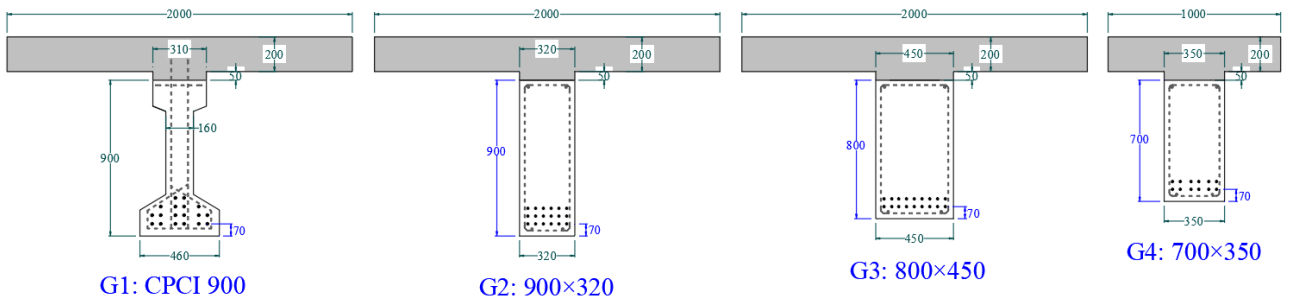


Figure 5.1 Girder sections for the parametric study

Table 5.1 Details of the girder sections

Sections	G1	G2	G3	G4
Girder size	CPCI 900	900×320 mm	800×450 mm	700×350 mm
Slab size	2000×200 mm			1000×200 mm
Strands	18 Φ 15mm			12 Φ 15mm
Prestressing Stress	Initial = 1116 MPa, effective = 1003 MPa			
Strand spacing	To bottom: 70 mm, to side: 45~50 mm, between strand: 45~50 mm			
400 MPa rebars	bottom: 4-M15, top: 4-M20, slab bottom: 4-M20			
Rebar concrete cover	50 mm			

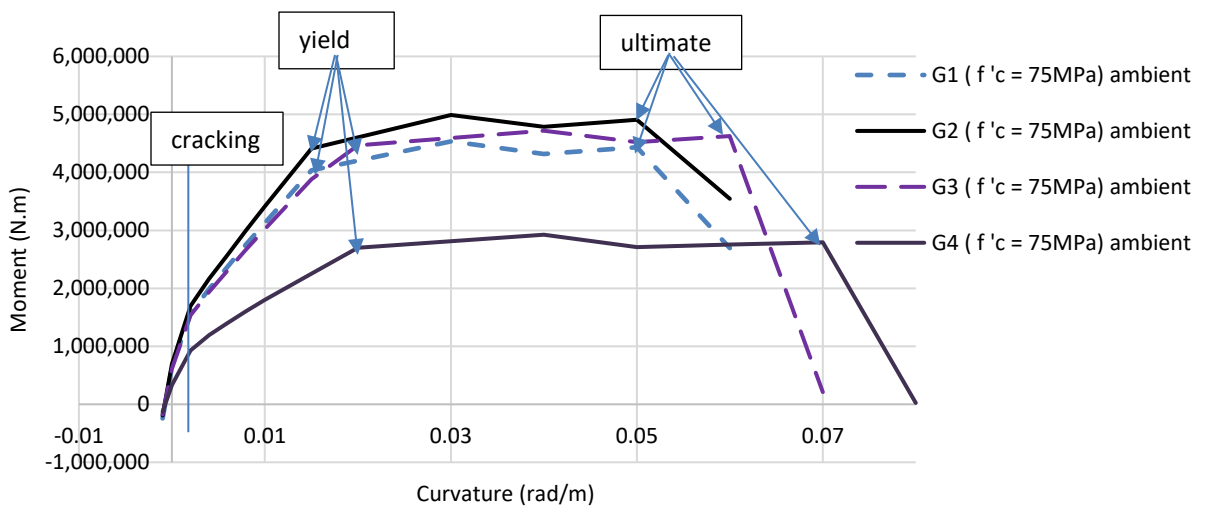


Figure 5.2 $M-\Psi$ curves at ambient temperature

Table 5.2 Parametric study layout

Parameter	Girders	Girder concrete strength (MPa)	Slab concrete strength (MPa)	Section number
Concrete strength of the section	G1	35, 60, 75, 90	35	5.2.1
Concrete strength of the section and the topping slab	G2	35, 60, 75, 90	35, 60, 75, 90	5.2.2
Girder section	G1, G2, G3, G4	75	75	5.2.3

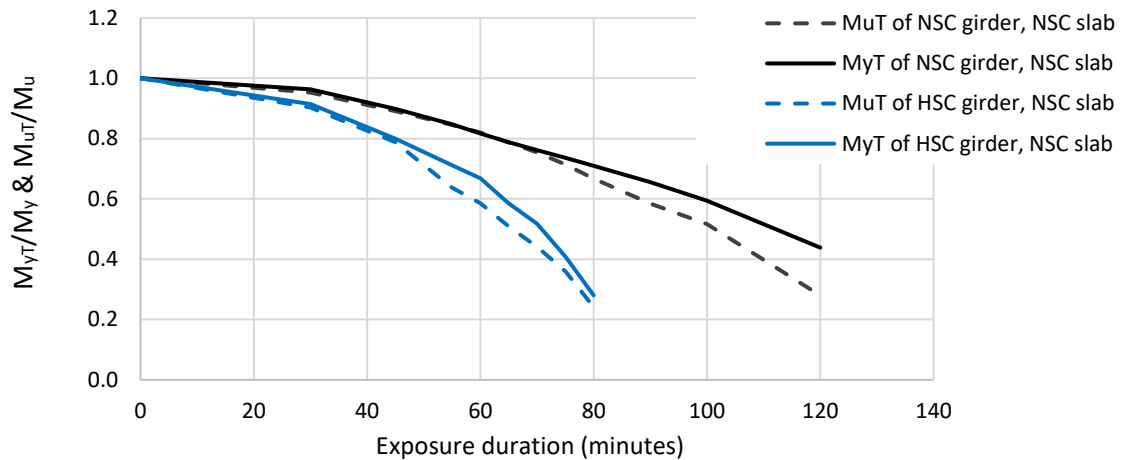
5.2.1 Influence of the concrete strength of the girder

The effect of the concrete compressive strength of the girder on its structural performance during fire exposure was examined in this section. Four concrete compressive strengths were considered (35, 60, 75, and 90 MPa). Explosive spalling was assumed to affect concrete with a compressive strength of 60 MPa or higher. The program developed in Chapter 3 was utilized to establish the $M-\Psi$ curves at different fire durations. Table 5.3 shows values of the yield (M_y or M_{yT}) and ultimate moments (M_u or M_{uT}) at ambient temperature and after 70 minutes of fire exposure. It also shows the fire duration at which the yield moment falls below 50% of the ambient value. Values of concrete compressive strength of 60, 75, and 90 MPa resulted in almost the same reduction in the yield and ultimate moments at all fire durations. The reduction when using a compressive strength of 35 MPa was much less. Figure 5.3 compares the yield and ultimate moments for NSC (35 MPa) and HSC (90 MPa) at different fire exposure durations. The figure shows that the deterioration in the yield moment for HSC is higher than for NSC. However, the difference between the deterioration of NSC and HSC is smaller when examining the ultimate strength. Differences in the analysis results were observed to be related to the effect of explosive spalling on the heat distribution within the section.

This parametric study shows that using HSC significantly reduces the moment capacity during fire exposure. However, the strength of HSC does not affect the reduction to the moment capacity.

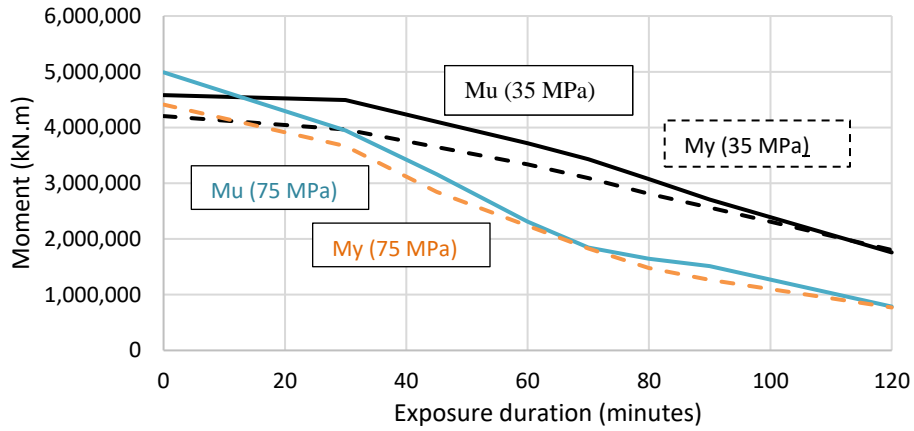
Table 5.3 Yield and ultimate moments of G1 considering different concrete strength

Concrete compressive strength of G1 (MPa)	M_y ambient (kN·m)	M_u ambient (kN·m)	M_{yT} at fire duration of 70 minutes (kN·m)	M_{uT} at fire duration of 70 minutes (kN·m)	Time when $M_{yT} < 50\% M_y$ (minutes)
35	3849	4395	2932	3137	> 100
60	3849	4395	1993	2127	70
75	3849	4395	1993	2127	70
90	3849	4395	1993	2127	70

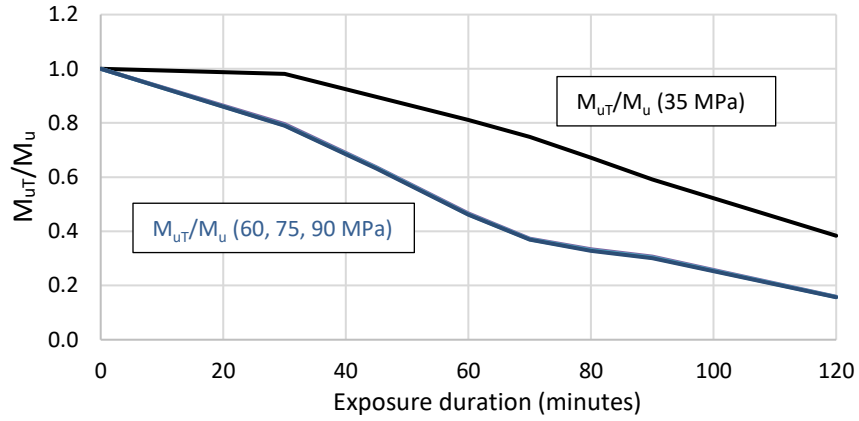
Figure 5.3 Comparison of M_{yT} and M_{uT} of G1 with different concrete strength

5.2.2 Influence of concrete strength of the girder and the topping slab

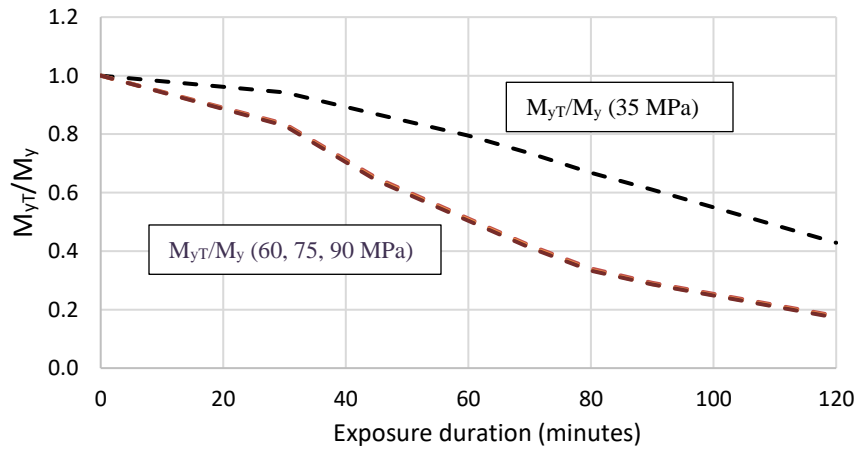
Figure 5.4 (a) tracks the yield and ultimate moments during fire exposure. It is clear from the figure that the use of HSC increases the capacity at ambient temperature. However, this higher capacity is quickly lost during fire exposure to be lower than the capacity provided by the NSC section. Another observation from the figure is that fire exposure eliminates the difference between the ultimate and yield moments. Figures 5.4 (b) and (c) show the variation of M_{uT}/M_u and M_{yT}/M_y during the fire exposure. The figures show that the trend for the reduction for both M_{uT} and M_{yT} is similar. They also show that deterioration is similar for HSC (60, 75, and 90 MPa) sections and is much higher than the NSC (35 MPa) section.



(a) M_y and M_u considering concrete compressive strength of 35 and 75 MPa



(b) M_{uT}/M_u for different concrete compressive strength



(c) M_{yT}/M_y for different concrete compressive strength

Figure 5.4 Yield and ultimate moments of section G2 at different fire durations

5.2.3 Influence of section shape

In this section, the effect of the section shape on the strength deterioration during fire exposure is examined. Figure 5.5 tracks the deterioration in M_{yT} and M_{uT} of the four considered girders during fire exposure.

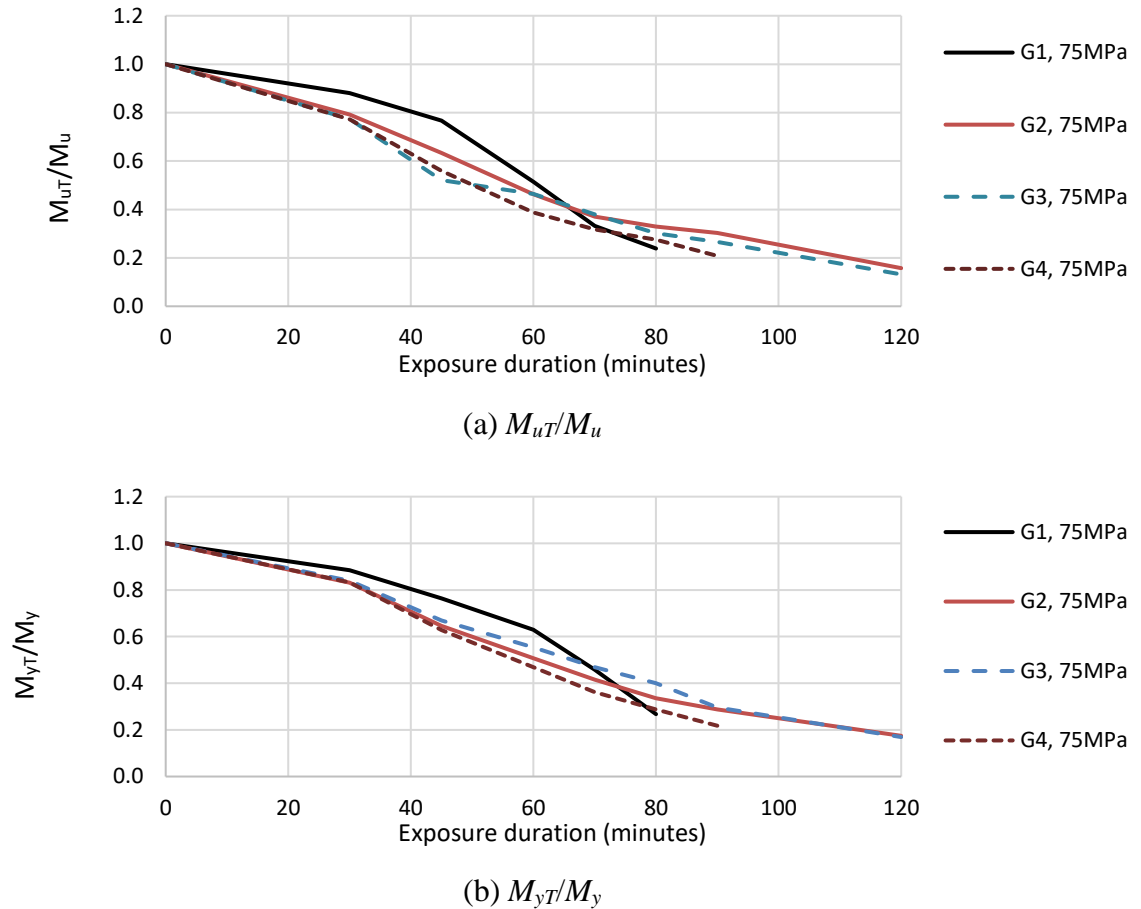


Figure 5.5 Yield and ultimate moments for sections G1, G2, G3, and G4 ($f'_c = 75$ MPa)

The CPCI 900 girder (G1) had a relatively slower capacity deterioration at the start of the fire, up to an exposure duration of about 30 minutes. Then, the rate of its capacity deterioration increases reaching a higher rate than other sections at about 60 minutes of fire exposure. Its capacity reached 50% of ambient capacity at about 65 minutes. At 80 minutes, the ratio reduced to 25% and the girder failed in shear. The rectangular girders (G2, G3, and G4) experienced similar rates of capacity deterioration at the start of the fire, then the

deterioration was more significant for smaller sections. The smallest girder G4 reached 50% of its ambient capacity at about 50 minutes and 25% at about 80 minutes. The larger sections (G2 and G3) reached 50% of the ambient capacity at about 70 minutes and 25% at about 90 minutes.

5.2.4 Moment-curvature diagrams

Fig. 5.6 shows an example of the obtained moment-curvature ($M-\Psi$) diagrams for girder G2 with concrete compressive strength of 75 MPa at different fire durations. The curvatures corresponding to the yield point have minor changes during fire exposure as the yield point is controlled by the strand properties. On the other hand, fire exposure has significantly reduced the ultimate curvature. For all the studied sections, it was found that the ultimate curvatures during fire exposure decrease at an accelerating rate. This reduction in the ultimate curvature can be explained by the reduction in the ultimate strand strain with fire exposure and the effects of the thermal strains on the concrete mechanical strains. The curvature at failure during fire exposure is higher than that at ambient temperature due to the transient strains experienced at elevated temperatures.

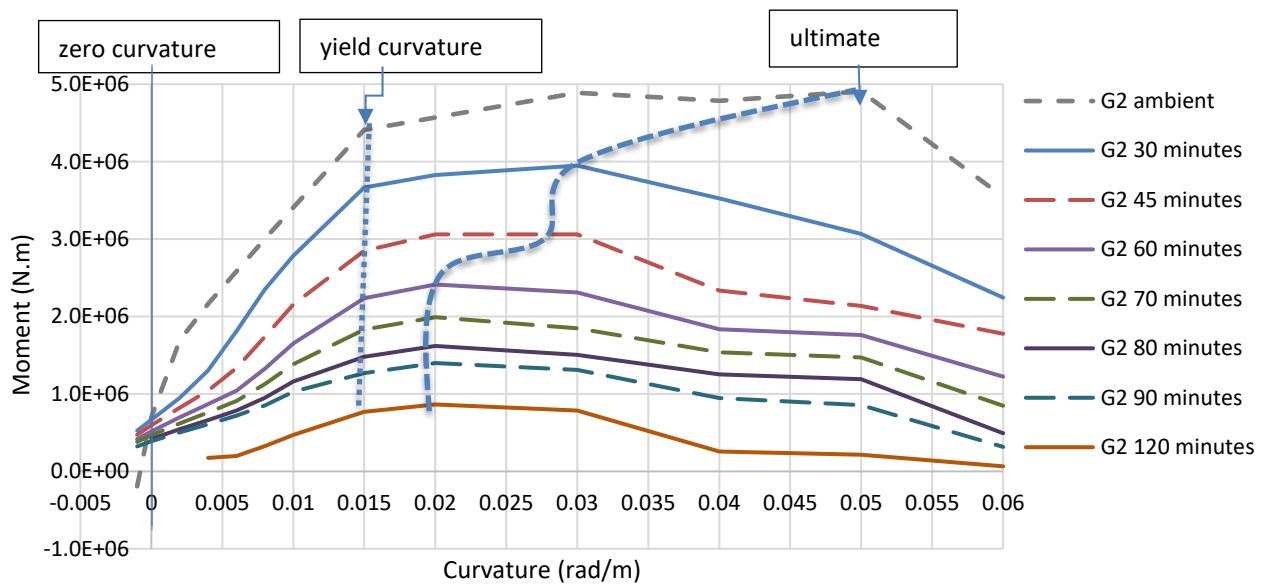


Figure 5.6 $M-\Psi$ curves at elevated temperatures for Section G2

5.3 Proposed expressions of the capacity adjustment factor

Equations that can be used to predict the moment-curvature diagram for the examined sections during fire exposure are presented in this section. The obtained curvature diagrams are simplified as trilinear curves, similar to Fig. 5.7. Three points, which correspond to zero curvature ($0, M_z$), yield (Ψ_y, M_y), and ultimate (Ψ_u, M_u), are identified on these diagrams. These points are then examined using regression analysis. The yield curvature during fire exposure was found to be declining as a linear function of the fire duration. The decline for the ultimate curvature was found to be following a polynomial function. Regarding M_{zt} , M_{yt} , and M_{ut} , it was found that they deteriorate during fire exposure following polynomial functions. The resulting equation, to estimate the moment and curvature values, is Eq. 5.1 with its coefficients given in Table 5.4. Predictions of the equation are closely correlated to the numerical results with a coefficient of determination (R^2) > 0.99.

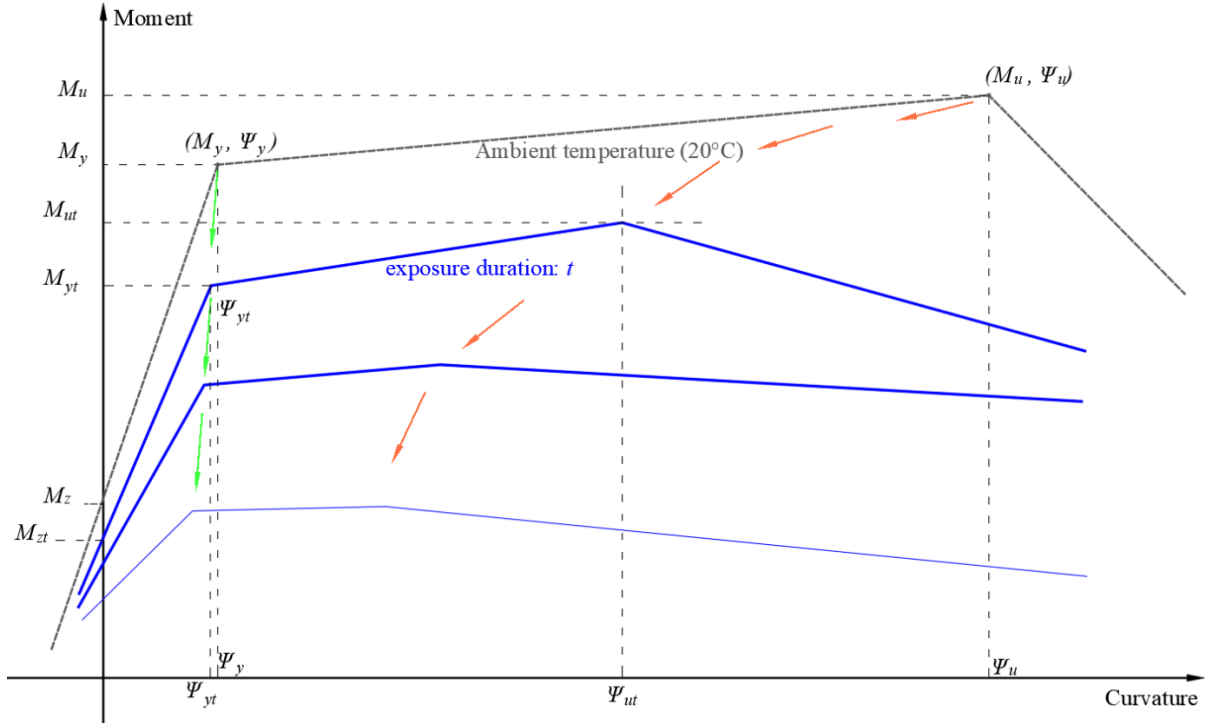


Figure 5.7 Idealized moment-curvature curves

$$\begin{cases} M_{zt} = \alpha_z \cdot M_z \\ M_{yt} = \alpha_y \cdot M_y \\ M_{ut} = \alpha_u \cdot M_u \\ \Psi_{yt} = \beta_y \cdot \Psi_y \\ \Psi_{ut} = \beta_u \cdot \Psi_u \end{cases} \quad \text{Eq. 5.1 (a)}$$

$$\alpha_z = Z_0 + Z_1 t + Z_2 t^2 \quad \text{Eq. 5.1 (b)}$$

$$\alpha_y = Y_0 + Y_1 t + Y_2 t^2 + Y_3 t^3 \quad \text{Eq. 5.1 (c)}$$

$$\alpha_u = U_0 + U_1 t + U_2 t^2 + U_3 t^3 \quad \text{Eq. 5.1 (d)}$$

$$\beta_y = 1 - 0.0042 \cdot t \quad \text{Eq. 5.1 (e)}$$

$$\beta_u = 1 + 2.8 \times 10^{-3} t - 4 \times 10^{-4} t^2 + 4 \times 10^{-6} t^3 \quad \text{Eq. 5.1 (f)}$$

where: t is the standard fire exposure duration in minutes ($10 \leq t \leq 120$)

Table 5.4 Coefficients to determine the moment capacity deterioration

coefficient	Girder G1	Girder G2	Girder G3	Girder G4
Z_0	0.999	1.014	0.993	1.004
Z_1	3.80×10^{-3}	-2.00×10^{-3}	1.00×10^{-3}	-40.0×10^{-3}
Z_2	-1.00×10^{-4}	-40.0×10^{-6}	-70.0×10^{-6}	-80.0×10^{-6}
Y_0	0.994	1.055	1.003	1.002
Y_1	0.30×10^{-3}	-3.90×10^{-3}	-3.70×10^{-3}	-0.30×10^{-3}
Y_2	-0.10×10^{-3}	-0.10×10^{-3}	-0.10×10^{-3}	-20.0×10^{-3}
Y_3	0.00	0.80×10^{-6}	0.60×10^{-6}	2.00×10^{-6}
U_0	1.012	1.00	1.002	0.999
U_1	1.20×10^{-3}	-7.80×10^{-3}	-10.2×10^{-3}	-8.00×10^{-3}
U_2	-0.10×10^{-3}	-30.0×10^{-6}	10.0×10^{-6}	-60.0×10^{-6}
U_3	0.00	0.30×10^{-6}	0.10×10^{-6}	0.60×10^{-6}

5.5 Summary and Conclusions

In this chapter, a study is conducted on the influence of prestressed girder design on the structural fire performance of HSC sections. A parametric study is first conducted to compare the moment-curvature behaviour for four different sections during exposure to a standard fire. HSC sections were found to experience higher deterioration in their capacity as compared to NSC sections due to explosive spalling. However, the concrete compressive strength of the HSC did not affect the strength deterioration experienced during fire exposure. It was also found that the yield curvature decreased slightly during fire exposure. However, the reduction in the ultimate curvature was significant. Regression analysis is then conducted and equations to predict the moment-curvature diagram for the examined sections are developed.

5.6 Reference

Alwis et. al., *Trilinear Moment-Curvature Relationship for Reinforced Concrete Beams*, ACI Structural Journal, Volume: 87, Issue: 3, pages(s): 276-283, 1990

Aurélie et. al., *Influence of cracked inertia and moment-curvature curve idealization on pushover analysis*, 15th World Conference on Earthquake Engineering (15WCEE). Lisbon, Portugal, 2012

CPCI. *CPCI design manual*. Canadian Precast Prestressed Concrete Institute. Ottawa Ontario, Canada, 2017.

Kwak et. al., *Nonlinear analysis of RC beams based on moment–curvature relation*, Computers and Structures, 80 (2002) 615–628, 2002

Ministry of Transportation, Ontario. *MTO Structural Manual*. ISBN 978-1-4606-8646-1. MTO, 2016

Youssef, *Lecture notes of “CEE9628, Prestressed Concrete”*, University of Western Ontario, London, ON, Canada, 2020

Chapter 6 Summary and Conclusions

The thesis presents the first simplified numerical model that can estimate the behaviour of prestressed high-strength concrete (HSC) girders during exposure to standard fire. The model allows users to understand the behaviour, and thus eliminate the mistakes associated with black box solutions. The thesis starts by presenting a literature review summarizing research related to the examined topic. It then provides details of the numerical model and its extension to cover natural fire incidents. Finally, it utilizes the model to understand the structural behaviour of prestressed HC sections. The following sections give details about the thesis content, conclusions, and recommended research related to the thesis topic.

6.1 Literature Review

Chapter 2 summarizes the existing literature related to high-strength concrete and fire exposure. The current prescribed design provisions for fire resistance and the relatively new objective and performance-based design are discussed. The fire development and the difference between standard fire, which has a prescribed temperature history, and natural fire, which represents a realistic fire scenario, are explained. The use of an equivalent duration of a standard fire to model a natural fire is reviewed. The chapter also presents a review of the thermal and mechanical behaviour of HSC sections including the effect of fire on the thermal and mechanical properties of steel bars, strands, and HSC, and the use of sectional analysis to simulate the behaviour of concrete elements exposed to fire.

6.2 Simplified Modeling of Prestressed Concrete Girders during Fire Exposure

Chapter 3 presents the development of the simplified model, which can predict the behaviour of prestressed HC sections. In addition to being the first simplified model, it is also the first to account for explosive spalling in the heat transfer stage and to model sections of any shape. The model estimates the concrete surface temperature from the fire

temperature and uses this temperature for the heat transfer stage to calculate the temperature distribution within the concrete section. Explosive spalling is modelled by excluding parts of the section, which reached temperatures higher than 350 °C. The extent of spalling is assumed to be limited to the concrete cover as the core concrete is protected by the stirrups. The model then utilizes the evaluated temperature values to analyze the section and evaluate its moment-curvature ($M-\Psi$) relationship. The analysis accounts for the developed thermal-induced strains, which are required to maintain the concept of “plane section remains plane”. A solution strategy is developed for both the thermal and mechanical stages of the model. The method used to predict the deformations of a concrete element based on the $M-\Psi$ relationship is explained. The chapter ends by presenting the validation of the numerical model.

6.3 Equivalent standard Fire Duration for Prestressed Concrete Girders Exposed to Natural Fire

Chapter 4 provides equations to estimate the equivalent duration (t_e) of a standard fire that can represent a natural fire. The concept of achieving a similar internal temperature within the HSC girder section was utilized. The methodology used to develop the equations is the first to account for explosive spalling while evaluating t_e . Also, it covers both rectangular and I-shaped sections. The methodology involves conducting an extensive parametric study using 1410 natural fires, then analyzing the results using a non-linear regression method to develop equations to predict t_e based on the natural fire characteristics. The use of t_e extends the validity of the model, developed in Chapter 3, to cover natural fire incidents.

6.4 Structural behaviour of prestressed HC sections exposed to fire

Chapter 5 presents a parametric study that examines the structural behaviour of four different prestressed concrete sections exposed to standard fire. Different concrete compressive strength values were examined. The model, developed in Chapter 3, is used

to predict the moment-curvature relationships of the four girders. It was concluded that HC increases the section's flexural capacity at ambient temperature. However, this increase is lost quickly during fire exposure. A nonlinear regression method is used to find equations that can model the $M-\Psi$ relationships of the examined sections during standard fire exposure.

6.5 Limitations of this research

The developed model can only apply to simply supported prestressed HSC beams. Only the case of bonded tendons was considered. A perfect bond is assumed between the concrete and the strands. The equations developed by regression analysis in the thesis are limited to the cases considered.

6.6 Recommendations for Future Work

Although the objectives of this study were achieved; further research is needed to better understand and model the behaviour of HC prestressed beams. Potential topics are:

1. Development of a universal model of HSC spalling, which can predict spalling based on pore water pressure.
2. Accounting for tensile cracking while conducting thermal analysis of HSC elements.
3. Explicit modelling of transient creep strains in HSC.
4. Understanding the behaviour of prestressed beams under fire exposure considering dynamic loading conditions.

Curriculum Vitae

Name: Yi Mao

Post-secondary Education and Degrees: Concordia University
Montreal, Quebec, Canada
2002-2006 B.Eng.

Honours and Awards: Concordia University Engineering Faculty Dean's List
2005
Graduate with Distinction on Academic Accomplishment
2006

Related Work Experience: Assistant Project Engineer,
The Mayaguana Company
2006-2008
Engineer in Training
Westmar Consultant
2008-2009

Engineering Inspector
Key-Tech
2009-2020

Teaching Assistant
The University of Western Ontario
2021-2022

Publications:

Mao, Y., M.A. Youssef, S. El-Fitiany. "*Simplified Model to Estimate Behaviour of Bonded Prestressed High Strength Concrete Sections during Exposure to Fire.*" 11th International Conference on Short and Medium Span Bridges, Toronto, Ontario, Canada, July 19 – 22, 2022.